SYNTHESIS AND ELECTROCHEMICAL CHARACTERIZATION OF HIGHLY MONODISPERSE DENDRIMER-TEMPLATED MONOLAYER PROTECTED CLUSTERS

A Dissertation

by

YONG-GU KIM

Submitted to the Office of Graduate Studies of
Texas A&M University
in partial fulfillment of the requirements for the degree of

DOCTOR OF PHILOSOPHY

December 2005

Major Subject: Chemistry

SYNTHESIS AND ELECTROCHEMICAL CHARACTERIZATION OF HIGHLY MONODISPERSE DENDRIMER-TEMPLATED MONOLAYER PROTECTED CLUSTERS

A Dissertation

by

YONG-GU KIM

Submitted to the Office of Graduate Studies of
Texas A&M University
in partial fulfillment of the requirements for the degree of

DOCTOR OF PHILOSOPHY

Approved by:

Chair of Committee, Richard M. Crooks
Committee Members, Paul S. Cremer
Raymond E. Schaak
Roger J. Morgan
Head of Department, Emile A. Schweikert

December 2005

Major Subject: Chemistry

ABSTRACT

Synthesis and Electrochemical Characterization of Highly Monodisperse Dendrimer-Templated Monolayer Protected. Clusters (December 2005)

Yong-Gu Kim, B.S.; M.S.,

Ajou University, Suwon, South Korea

Chair of Advisory Committee: Dr. Richard M. Crooks

We described the synthesis of multilayer organic thin films prepared by sequential vapor-phase coupling of monomers. The reactions were carried out at room temperature and atmospheric pressure. Films prepared using up to six sequential coupling reactions are reported. Homobifunctionalized monomers, such as hexamethylenediamine, react primarily via a single endgroup rather than cross coupling to the reactive surface via both reactive groups.

We synthesized bifunctionalized polyamidoamine (PAMAM) dendrimers having both quaternary ammonium groups and primary amines on their periphery were prepared. The high positive charge on the surface of these dendrimers prevents agglomeration, and the unquanternized amine groups provide a reactive handle for immobilizing the dendrimer-encapsulated nanoparticles onto surfaces.

We prepared highly monodisperse, 1-2 nm diameter Au nanoparticles using bifunctionalized PAMAM dendrimers as templates. The synthesis is carried out in water, takes less than 30 min, and requires no subsequent purification. The high monodispersity is a function of the template synthesis, which avoids size variations arising from random nucleation and growth phenomena, and the use of magic number equivalent ratios of $AuCl_4^-$/dendrimer.

We investigated the electrochemical properties of Au, Pd and PdAu monolayer-protected clusters (MPCs), prepared by dendrimer-templating and subsequent extraction, are described. Purification of the extracted Au, Pd and PdAu nanoparticles was not required to obtain well-defined differential pulse voltammetry peaks arising from quantized double-layer charging. The calculated sizes of the nanoparticles were essentially identical to those determined from the electrochemical data. The capacitance of the particles was independent of the composition of core metal.

To my parents

and my brothers

for believing in me.

ACKNOWLEDGEMENTS

I would like to thank my research advisor, Professor. Richard M. Crooks, for his consistent guidance and support over the years. He was always there when I was disappointed and I needed his help. He advised and encouraged me to conduct meaningful scientific research. Without his help the achievements of this work would not be possible. I would also like to thank Professor Paul S. Cremer, Professor Raymond E. Schaak, and Professor Roger J. Morgan for their willingness to serve on my committee.

I have had the pleasure of working with many post-docs and graduate students in the group over the years and have learned something valuable from each of them. Specifically, I would like to thank Lane Baker, Gregory Perez, Li Sun, Sang-Keun Oh, Gi-Hun Sung, Jinseok Heo, Joaquin Garcia-Martinez, Robert Scott, Orla Wilson, each of whom educated and enlightened me. I would like to thank my parents for their belief and support. Financial support of this work from the National Science Foundation (NSF) is also greatly acknowledged.

TABLE OF CONTENTS

CHAPTER Page

LIST OF TABLES

LIST OF FIGURES

FIGURE Page

FIGURE Page

FIGURE Page

FIGURE Page

FIGURE Page

FIGURE Page

CHAPTER I

INTRODUCTION

1.1 Main Goals

The main objectives of this work are the preparation of highly monodisperse metal nanoparticles within dendrimer templates and the characterization of the electrochemical properties of these metal nanoparticles. The dendrimer-templating approach is a versatile method for preparing monodisperse metal nanoparticles with diameters of <2 nm. A dendrimer has a uniform structure (with predictable size and number of peripheral groups) with a dense outer layer and a less dense core. The internal functional groups of a dendrimer can attract metal ions, and the void in the interior of the dendrimer can accommodate nanoparticles. However, further applications require better characterization methods for these small nanoparticles, and in this work, electrochemical and conventional methods were used to characterize metal nanoparticles. Electrochemical

---

This dissertation follows the style and format of *Langmuir*.

methods make it possible to precisely calculate both the nanoparticle sizes and the size-dependent HOMO-LUMO gap energy.

The results of this work are described as follows. Chapter III represents a preliminary project unrelated to dendrimers, and instead it describes a methodology for preparing organic thin films in the absence of solvents. The preparation of highly monodisperse Au dendrimer encapsulated nanoparticles (DENs)(Figure 1.1a) within quaternized dendrimers is discussed in Chapters IV and V. Finally, the electrochemical properties of monometallic (Au and Pd) DENs) and bimetallic Pd-Au DENs are discussed in Chapter VI and Chapter VII, respectively.

1.2 Motivation and Objectives

There are potential advantages in the preparation of multilayer organic thin films by the vapor-phase reactions compared to traditional solution-phase reactions. For example, first, the interferences of solvent on the formation of multilayer films or spectroscopic measurements can be eliminated. Second, H-bonding or acid-base interactions, which are weak when a solvent is used, can be studied. Third, sequential reaction can be carried out

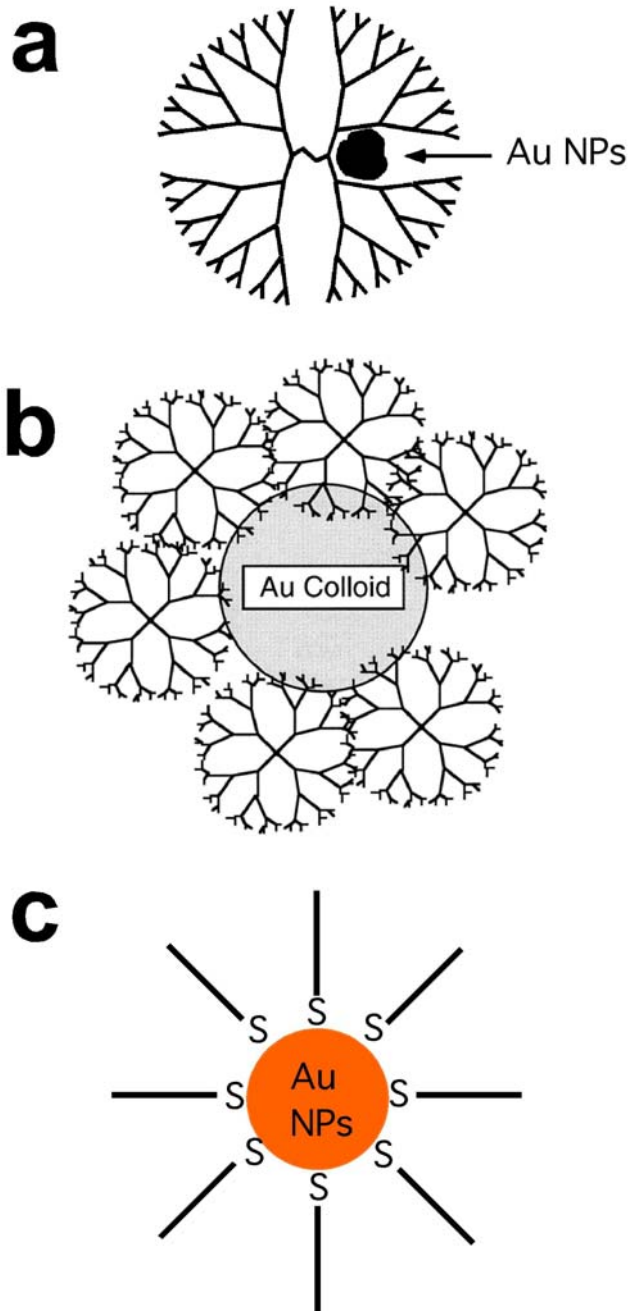

Figure 1.1. (a) dendrimer-encapsulated nanoparticles (NPs) (b) dendrimer-stabilized nanoparticles (c) Monolayer protected clusters. (Reprinted with permission from Garcia, M. E.; Baker, L. A.; Crooks, R. M. *Anal. Chem.* **1999**, *71*, 256-258 copyright 2005 American Chemical Society.)

without repositioning of the substrate. Fourth, chemical reactions can be performed with high-energy organic surfaces without the interference of impurities. Fifth, vapor-phase reactions provides a way to link the ultra high vacuum(UHV) and condensed liquid-phase reaction in studying of the formation mechanism of multilayer organic thin films.[1-3]

I show that multilayer organic thin films consisting of six-layers can be synthesized via vapor-phase reactions using bifunctional amines and acid chlorides in this dissertation without a vacuum and at the room temperature. This is significant because previously vapor-phase reaction carried out in a vacuum and/or high temperature and mostly, the thickness of multilayer organic thin films, which can be prepared by vapor-phase reaction, was limited to bi- or tri-layer.

DENs have been prepared using hydroxyl-terminated dendrimers because metal ions strongly complex with peripheral amines of amine-terminated dendrimers and it results in the formation of dendrimer-stabilized nanoparticles (Figure 1.1b) however it is difficult to covalently attach hydroxyl-terminated dendrimers to a substrate. Therefore, quaternized dendrimers in which half

of the peripheral amines were modified with ammonium chloride were prepared to prevent metal-ion complexations and consequential agglomerations. Peripheral ammonium chloride of quaternized dendrimers prevents the formation of largely aggregated particles, and dendrimer can be covalently attached to the substrate using unquaternized amine functional groups. For studying the size-dependent characteristics of DENs, highly size-monodisperse Au DENs with a size of 1-2 nm were prepared using quaternized dendrimers as templates, and the measured particle sizes agreed well with theoretical values. The monodispersity was further improved by using "magic number" ratios of metal ion/dendrimer. Preparation of DENs in this way provides a condition that lets us study the size-dependent properties of DENs in which size-monodispersity is very important.

DENs have been characterized mostly by transmission electron microscopy (TEM) and UV-vis spectroscopy; however, neither technique satisfies the precise measurement of 1-2 nm diameter metal nanoparticles that this dissertation addresses. Therefore in this dissertation, electrochemical methods were used as a new way of characterizing DENs. Actually, the electrochemical properties of dendrimer-

templated monolayer protected clusters (MPCs) (Figure 1.1c) have been studied instead of DENs, because DENs themselves are generally electroinactive. Dendrimer-templated MPCs are prepared by extracting the nanoparticles from dendrimer templates. Importantly the nanoparticle size and size-monodispersity are retained after extraction. Small MPCs (1-2 nm) act as tiny capacitors, and quantized double-layer (QDL) charging behavior can be observed as peaks in the plots of current vs. voltage. The average peak interval is a function of nanoparticle size, and the nanoparticle size can be calculated from the average peak spacing. The size of Au MPCs calculated by electrochemical method is identical to the values calculated from the number of atoms present in each particle.

The electrochemical properties of Au MPCs have been extensively studied, whereas MPCs other than Au have rarely been examined. Pd and Pd-Au alloy DENs were characterized by this method, and the calculated nanoparticle sizes agree well with theoretical values. The electrochemical methods have some advantages over the TEM method for particle size measurement. For example, small nanoparticles whose sizes are comparable to the TEM resolution cannot be precisely measured, especially for the nanoparticles consisting of

atoms with a small number of electrons, because the contrast of these particles is low. Moreover, the focus can also affect particle sizes during the measurement, and sometimes the particle boundary is not clear. In summary, highly monodisperse dendrimer-templated Au, Pd, and Pd-Au alloy MPCs could be prepared and characterized by electrochemical methods. This is a new way to characterize DENs.

1.3 Vapor-phase deposition

A vapor-phase reaction has been used as an alternative of condensed-phase reaction.[2,4,5] Usually, vapor-phase deposition requires a vacuum and/or high temperatures,[5] but our study shows that it is possible to synthesize multilayer films at room temperature and without a vacuum. In this approach, vapor-phase molecules are introduced into a chamber in which substrates are positioned with N_2 carrier gas, and airborne molecules are deposited on the substrate or react with thin films on the substrate.[6,7] Multilayer thin films could be prepared with this method, however, this method was limited to the tri-layer film previously described by our group.[7]

1.4 Dendrimer-encapsulated nanoparticles (DENs)

Chemical structure and properties of dendrimers.

Poly(amidoamine) (PAMAM) dendrimers are star-shaped polymers highly branched from NH_3 or ethylenediamine (EDA) cores by repeating the Michael addition of methyl acrylate and amidation of EDA.[8,9] The size of the dendrimer increases in a linear manner, and the number of peripheral groups increases exponentially as the generation increases. Therefore, apart from generation 0-2, the dendrimers have a void in their interior. The chemical structure of a second generation hydroxyl-terminated dendrimer (G2-OH) is shown in Figure 1.2.

Synthesis and characterization of DENs. Dendrimers have dense peripheries and a void at the core, and this unique structure makes them ideal candidates for templating and stabilizing nanoparticles.[10-12] When an aqueous dendrimer solution is mixed with aqueous metal ions, the metal ions are extracted into the dendrimer interiors by either complexation[10-12] or electrostatic interactions.[13,14] In the case of complexation, the number of metal ions that can be extracted by one dendrimer is limited by the number of functional groups at the interior of a dendrimer. For

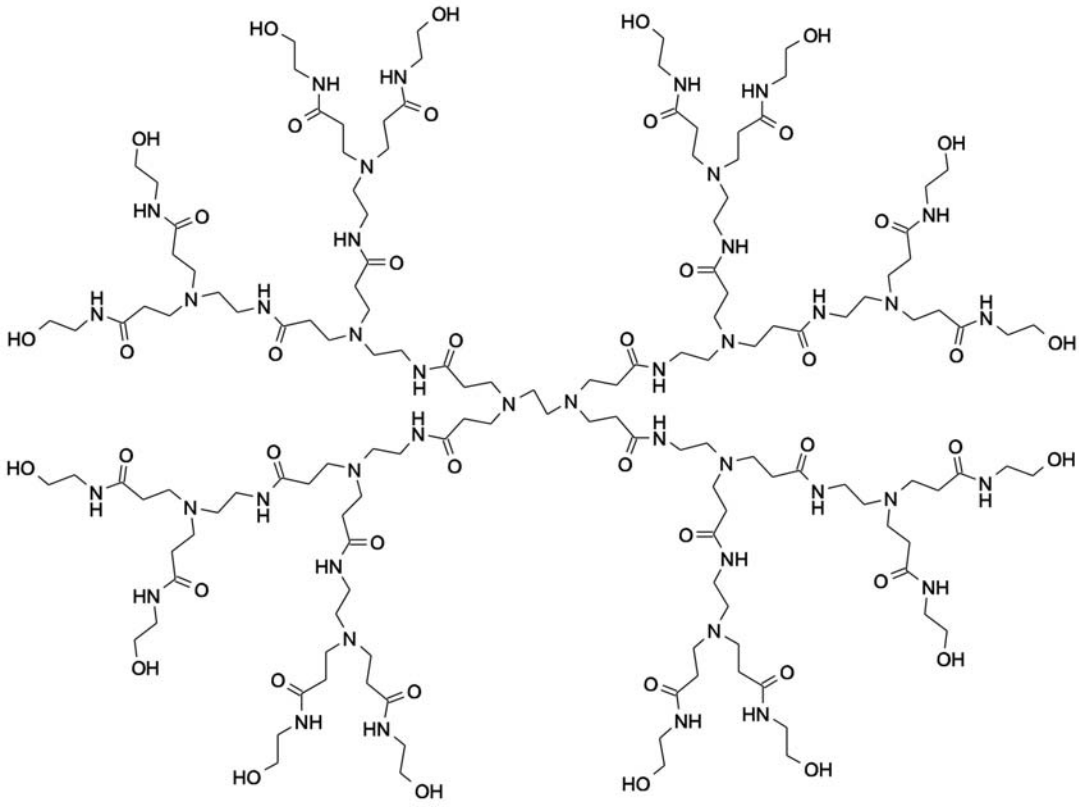

Figure 1.2. Structure of a second-generation, hydroxyl-terminated PAMAM dendrimer (G2-OH).

example, a previous titration study revealed that G4-OH dendrimers can accommodate 16 Cu^{2+}, meaning that Cu^{2+} coordinate with four amines in the interior of the dendrimer; however, CPK models suggest that the configuration of the inner amine groups is not conducive to complexation with Cu^{2+} ions, and therefore it seems that the outer two amines are involved in complexation with Cu^{2+}. Metal ions (such as Au or Ag), which do not strongly react with amines, are extracted into the dendrimer interior by the difference in the dielectric strength between dendrimer interiors and the solvent. Extracted metal ions are chemically reduced by $NaBH_4$, and DENs are formed by the coalescence of zero valent metal ions.

Bimetallic DENs have been prepared and studied because of their synergistic effect on the catalytic reaction and their structure-dependent properties.[15-19] For example, Pd-Pt alloy bimetallic DENs prepared by co-complexation showed an enhanced catalytic effect in the hydrogenation reaction of allyl alcohol, compared to Pd-only DENs or a physical mixture of Pd and Pt DENs.[15]

It is possible to control the structure of bimetallic DENs by choosing different preparation methods such as co-complexation or sequential loading. The preparation of Pd-

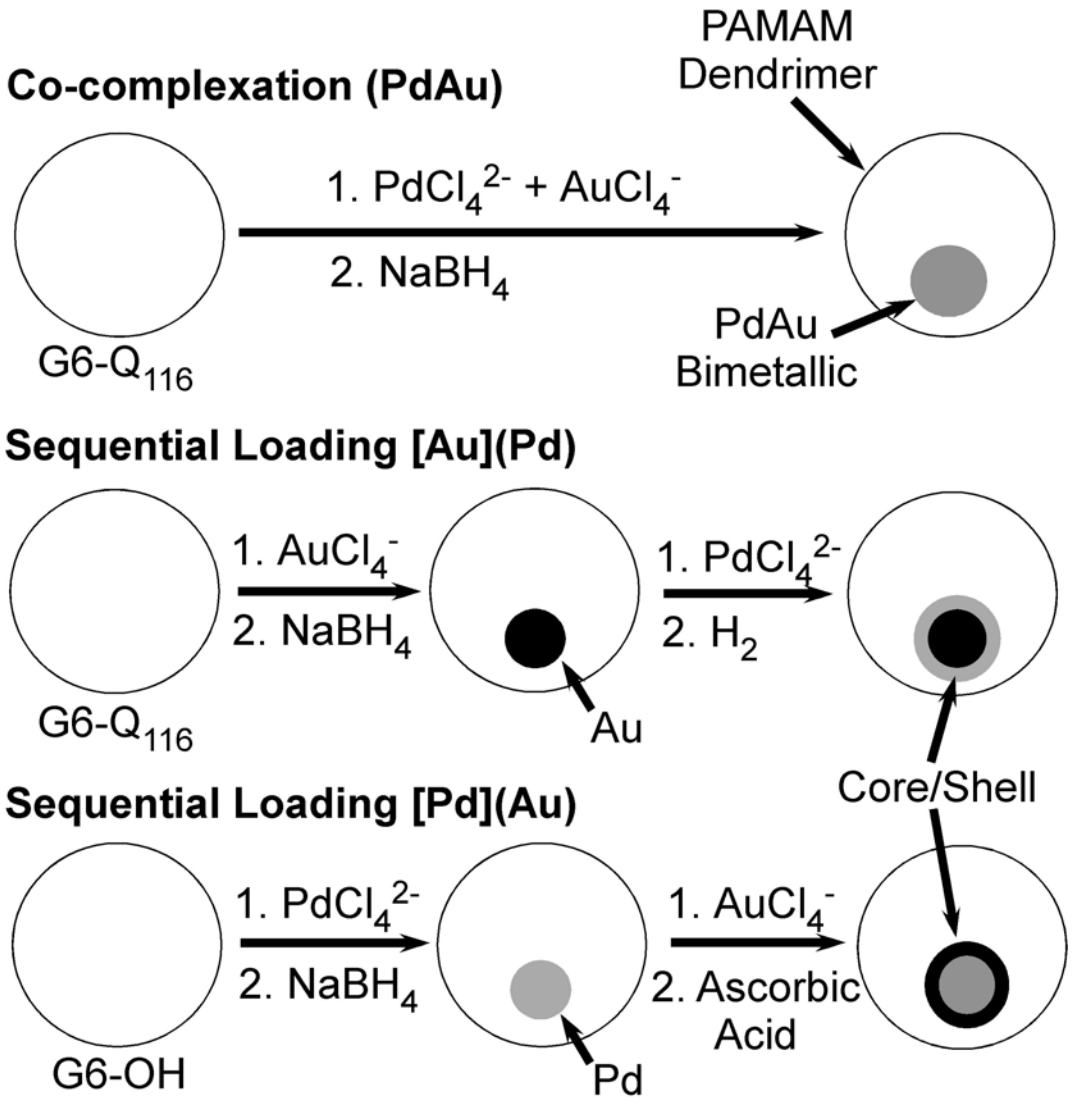

Figure 1.3. Schemes for alloy or core shell Pd-Au bimetallic DENs formation. (Reprinted with permission from Scott, R. W. J.; Wilson, O. M.; Oh, S.-K.; Kenik, E. A.; Crooks, R. M. *J. Am. Chem. Soc.* **2004**, *126*, 15583-15591. copyright 2005 American Chemical Society.)

Au alloy or core-shell DENs have been reported (Figure 1.3). Pd-Au core-shell DENs (G6-OH[Pd](Au), brackets indicate the core metal, and parentheses indicate the shell metal) have been synthesized by sequential loading in which Au ions are introduced to the Pd DEN solution and reduced at the surface of Pd DENs. Pd-Au bimetallic DENs showed structure-dependent optical properties. G6-OH[Pd_{55}](Au_{255}) showed a plasmon band at 520 nm in the UV-vis spectrum due to the Au shell. For comparison, G6-OH($Pd_{55}Au_{255}$) alloy DENs were prepared by co-complexation in which Pd and Au ions were extracted into the dendrimer and reduced at the same time. In contrast to the G6-OH[Pd_{55}](Au_{255}) DENs, G6-OH($Pd_{55}Au_{255}$) DENs did not exhibit a plasmon band even though Au_{255} shows a plasmon band at 525 nm.

The structure-dependent optical properties were observed from UV-vis spectroscopy of Au-Ag bimetallic DENs synthesized by the same methods.[19] The position of plasmon band of Au-Ag alloy DENs shifted in a linear manner from 390 nm to 520 nm as the Au composition of the DENs increased. Core-shell DENs (G6-OH[Au_{55}](Ag_n) and G6-OH[$Au_{27.5}Ag_{27.5}$](Au_n)) were prepared by sequential loading. These bimetallic DENs showed optical properties different from monometallic or alloy DENs. For example, G6-

OH[Au_{55}](Ag_n) showed two plasmon bands due to Au and Ag, even though Au_{55} DEN did not show a plasmon band due to its small size. The plasmon band of Au-shell DENs (G6-OH[$Au_{27.5}Ag_{27.5}$](Au_n)) shifted to 520 nm as the Au shell thickness increased. In summary, the structure-dependent spectral changes of bimetallic DENs, which differ from monometallic DENs, indicates the successful formation of bimetallic DENs and also shows that the structure of bimetallic DENs can be controlled by preparation methods (sequential loading or co-complexation).

Extraction. Pd and Au nanoparticles can be extracted from dendrimer interiors into organic phases by *n*-alkanethiols. The extraction is carried out by mixing aqueous-phase DENs and *n*-alkanethiols in the organic phase (Figure 1.4).[20,21] The physical and chemical properties of nanoparticles are preserved before and after the extraction.[21] Previous studies showed that at least a 10-fold excess of *n*-alkanethiols to DENs is required to avoid changes in nanoparticle sizes after extraction. When lower concentration of *n*-alkanethiols were used, MPCs with sizes larger than those of the DENs were obtained. Generally, the chain length of the *n*-alkanethiols was not important, but bulky thiols could not extract nanoparticles from high

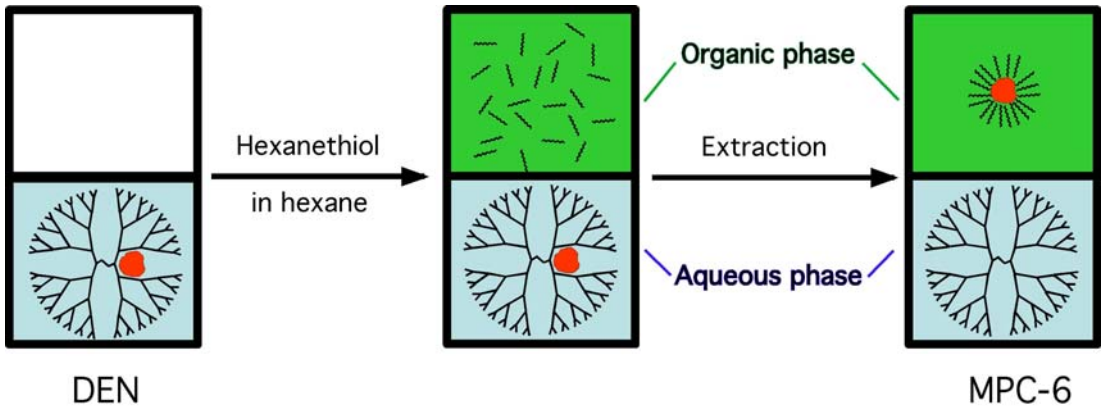

Figure 1.4. Schematic illustration of the extraction procedure.

generation dendrimers (such as G8-OH). The extraction method was also applied to the separation of DENs and the characterization of the structure of core-shell DENs. It was possible to extract selectively Ag DENs from a mixture of Ag and Au DENs with *n*-alkanoic acid, which can extract only Ag DENs. In other applications, the structure of Au-Ag core-shell DENs could also be characterized using selective extraction.[19] The *n*-alkanoic acid could extract G6-OH[Au_m](Ag_n) and Au-Ag alloy DENs, which were more than 75% Ag. In contrast, G6-OH[Ag_m](Au_n) could not be extracted by *n*-alkanoic acid.

1.5 Monolayer Protected Clusters (MPCs)

Since the development of the two-phase synthesis of MPCs (Figure 1.1c), MPCs have been employed for studying the size-dependent optical and electronic properties of nanoparticles. MPCs are stable during repeated dissolution and isolation. In addition, MPCs can be handled as simple chemicals because they are stable in air. With the two-phase synthesis method, small MPCs (<5 nm) can be prepared in large quantities using a relatively simple method.[22,23]

Synthesis and characterization of MPCs. MPCs are prepared as follows. First, an aqueous solution of $HAuCl_4$

is mixed with a phase-transfer salt. An organic phase containing thiol ligands is also prepared. Finally the two phase are mixed and MPCs are formed by adding an aqueous solution of $NaBH_4$.[23-25] The organic phase is separated from the mixture, and MPCs are obtained by the evaporation after solvent. Ag,[26] Cu,[27] Pd,[28,29] and alloy MPCs[30,31] can be prepared by this same method. The crude MPCs are polydispersed in size, because MPCs are prepared by random nucleation and growth. However, the monodispersity can be improved by HPLC,[32] annealing,[33] and fractional precipitation.[34,35] Previous studies have shown that MPC sizes can be controlled by adjusting the [ligand]:[$HAuCl_4^-$] ratio, or reaction time.[36] It was reported that the average particle size gradually increases during the first 60 h before leveling off.

MPC sizes and corresponding size distributions can be precisely measured by TEM.[34] TEM is responsive to the metal core, and the protecting ligands remain transparent. In addition, MPC shapes can be determined with TEM. Mass spectrometry reveals both the number of atoms that a cluster contains as well as the relative abundance of particular particle masses.[23,34,37,38] The structure of protecting ligands of MPCs can be characterized by

thermogravimetric analysis (TGA), differential scanning calorimetry (DSC), infrared (IR) spectroscopy, and nuclear magnetic resonance (NMR) spectroscopy. These techniques are useful in determining the weight percentage of protecting ligands and the structure-changes of the protecting monolayer as a function of the cluster size.[23, 37]

Electrochemical properties. The electrochemical properties of Au MPCs larger than 1.1 nm are similar to those of metallic capacitors, and quantized double-layer (QDL) charging of MPCs can be observed as peaks in voltammetric experiments.[22,33,39] The peak spacing (ΔV) is inversely proportional to the nanoparticle capacitance (C_{CLU}) by the following equation:

$$\Delta V = e/C_{CLU} \quad (1)$$

where e is the electronic charge(1.602×10^{-19} C) and C_{CLU} is the capacitance of the nanoparticle.[39] The capacitance is related to the properties of the nanoparticles and the surrounding dielectric medium by the following equation:

$$C_{CLU} = 4\pi\varepsilon\varepsilon_0(r/d)(r+d) \quad (2)$$

where ε is the monolayer dielectric constant (~3 for alkanethiols), ε_0 is the vacuum permittivity (8.854×10^{-12} $C^2/J \cdot m$), r is the radius of the nanoparticle, and d is the monolayer thickness (d = 0.77 for hexanethiol).[35] If all of these assumptions are valid, it is possible to calculate the particle size from peak intervals using eq 1 and 2.

Core size effect. MPCs act as tiny capacitors, and QDL charging behavior can be observed in the voltammograms at room temperature due to their very small capacitance (~aF). As mentioned earlier, the capacitance of MPCs is a function of cluster size (eq 2).[22] Cluster size effects on voltammetric responses were studied with C4 - C6 alkylthiol-stabilized Au MPCs whose mass varied from 8 kD to 38 kD corresponding to 1.1 nm- and 1.9 nm-diameter Au clusters. The QDL charging behavior of MPCs was observed as a peak in the voltammogram, and the average peak intervals changed with MPC size. The 22 kD – 38 kD MPCs acted as simple metal capacitors and showed regularly-spaced peaks in the corresponding voltammograms. However, the electrochemical responses of small MPCs (8 kD – 14 kD) were different from those of large MPCs, and irregularly-spaced peaks were observed. Of particular interest, a

large peak spacing was observed around Z_{PZC} (PZC: potential of zero charge). This molecule-like behavior of small MPCs originates from the opening of the HOMO-LUMO gap. The spacing between the -1/0 and 0/+1 charge state of MPCs includes the HOMO-LUMO gap energy in addition to the energy needed to change the MPC charge states. In summary, the electrochemical study of Au MPCs showed the possibility of measuring particle size by using electrochemical methods.

Monolayer-thickness effect. The QDL charging of 1.6 nm-diameter Au MPCs stabilized by different lengths of monolayer (C4 – C16-SH) was studied.[35] The capacitance of these MPCs was found to be a function of the monolayer length (eq 2) and is inversely proportional to the chain length of the protecting alkanethiol. Therefore, it is expected that the voltammetric peak intervals will increase as the alkanethiol chain length increases. The results show that the capacitance of MPCs stabilized by C4-, C6-, C10-, C12- and C16-SH were 0.59, 0.57, 0.47, 0.40, and 0.39 aF, respectively. It is clear from the results that the capacitance of MPCs is a function of the monolayer-thickness and, as a result, peak intervals are changed as the protecting monolayer length changes.

Solvent and electrolyte effect. Solvent and electrolytes mostly influence the effective dielectric constant of the protecting monolayer by penetrating into the monolayer or by electrostatic pairing with MPCs.[40] The penetration of the solvent into the protecting monolayer is more pronounced for arenethiol-protected MPCs than alkylthiol-protected MPCs because of the low packing density of the former. Therefore, the solvent effect is more apparent for the arenethiol-protected MPCs than for the alkylthiol-protected MPCs. Hydrophobic electrolytes can intercalate with the monolayer and lower the dielectric constant of the protecting monolayer more effectively than hydrophilic ions. The effect of the intercalation of hydrophobic electrolytes is greater for the MPCs protected by short ligands because the penetration of electrolytes is more favorable.

Molecule-like behavior. Regarding the cluster size effects on the voltammograms, small Au MPCs (~1.1 nm) showed different properties than large MPCs.[41-43] The differential pulse voltammetry (DPV) of $Au_{38}(PhC_2S)_{24}$, shown in Figure 1.5, has irregularly-spaced peaks, with a large central gap at around Z_{PZC}.[41] This molecule-like behavior does not agree with the simple metal capacitor model in

which peaks are spaced regularly. The large peak spacing (1.62 eV) between the first oxidation and reduction peaks of MPCs was observed, and this includes both the HOMO-LUMO gap energy and the charging energy. The calculated HOMO-LUMO gap energy, obtained by subtracting charging energy (0.29 eV) from the peak spacing (1.62 eV), is 1.33 eV, and this value is consistent with the values obtained from UV-vis spectroscopy and photoluminescence spectroscopy.

The electrochemical properties of *n*-hexanethiol-protected Au_{38} MPC were also tested to study the effect of the protecting ligand on the HOMO-LUMO gap energy.[42,43] The observed peak spacing between the -1/0 and 0/+1 MPC charge state was close to the value obtained from arenethiol-protected Au_{38}. This result indicates that the HOMO-LUMO gap energy is not measurably affected by the properties of the protecting ligands. However, there is some discrepancy in the HOMO-LUMO gap energy. Quinn and co-workers reported the HOMO-LUMO gap energy as 0.9 eV from the DPV of $Au_{38}(C6S)_{24}$.[43] It is possible that the discrepancy can originate from different electrolyte used for the voltammetry or the divergence in the level of the presence of impurities on the cluster. However there is not clear explanation for the difference in HOMO-LUMO gap energy.

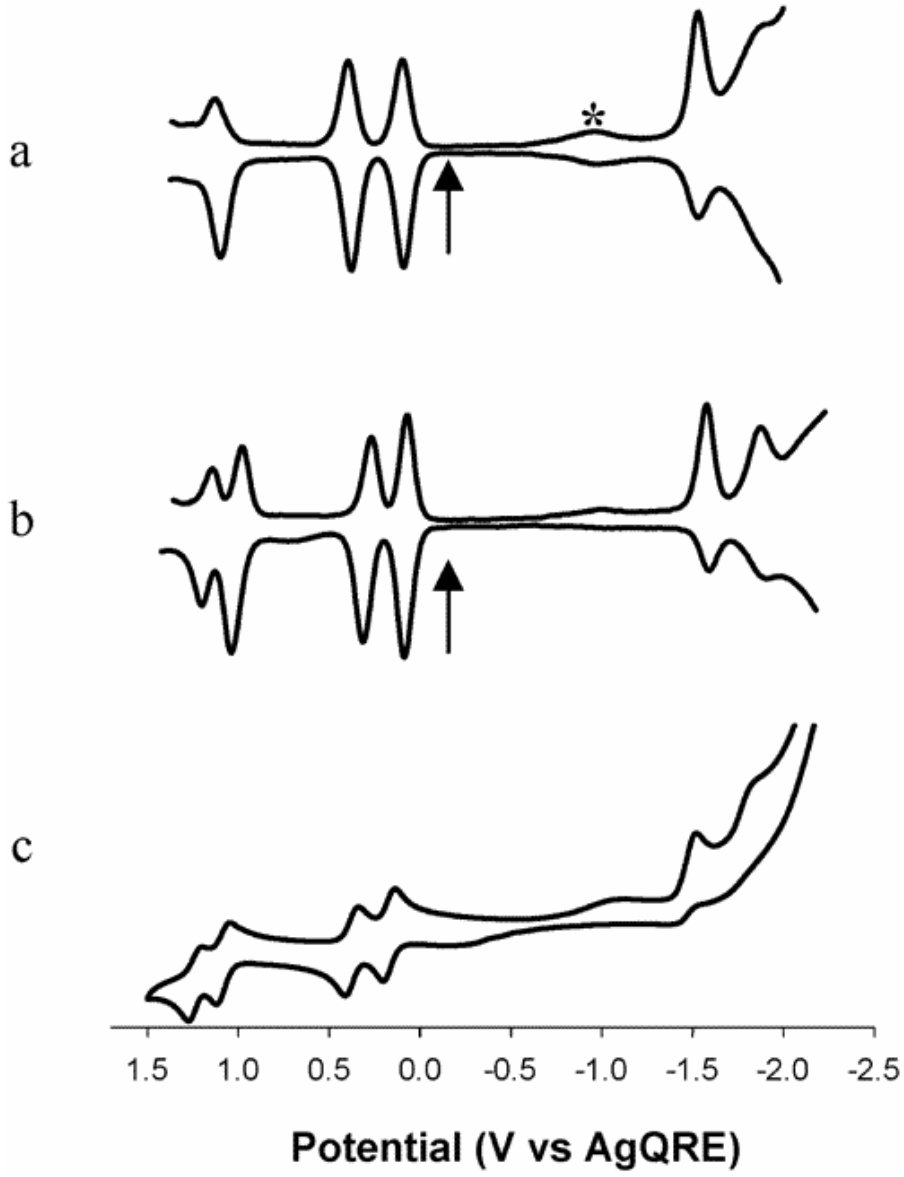

Figure 1.5. DPV responses for MPC solutions $Au_{38}(PhC_2S)_{24}$ showing a HOMO-LUMO gap at (a) 25 °C and (b) -70 °C (The arrow indicates the potential of zero charge, and * indicates peak from residual oxygen). (c) Cyclic voltammogram of $Au_{38}(PhC_2S)_{24}$ measured at -70 °C. (Reprint with permission from Lee, D.; Donkers, R. L.; Wang, G.; Harper, A. S.; Murray, R. W. ***J. Am. Chem. Soc.*** **2004**, *126*, 6193-6199. copyright 2005 American Chemical Society.)

Pd MPCs. MPCs with core metals other than Au are rarely reported because of the relatively low stability during preparation and purification.[27-29] The DPV of Pd MPCs is not resolved as well as for Au MPCs and the particle sizes calculated from peak intervals in the DPV are not consistent with TEM results. For example, the DPV of C6-SH stabilized Pd MPCs was studied by Zamborini and co-workers and the average peak spacing of 450 mV, corresponding to a particle size of 1.2 nm, is not consistent with the size measured from TEM (2.2 nm).[29] The authors rationalized this discrepancy as follows: 1) the size of MPCs which respond to the voltammogram is smaller than average particle size measured from TEM. 2) the ε value of Pd MPC is different from that of Au MPC (ε = ~3).

The inconsistency between MPC size calculated from DPV and the size measured from TEM was also reported by Chen and co-workers.[28] The average peak spacing in the DPV of Pd MPCs was 210 mV and this peak spacing corresponds to a particle size of 2.0 nm. However, this value is different from the size measured by TEM (2.5 m). The authors explained that this can originate from the lower ε (2.1) of Pd MPCs compared to Au MPCs (~3).

In summary, previous studies have shown that the Pd MPC particle size calculated from the electrochemical method is different from MPC size measured from TEM.

1.6 Summary and Accomplishments

In the first part of this dissertation, I will discuss the formation of organic multilayer thin films in the absence of a solvent. Specifically I will show:

- The multilayer film can be synthesized via amidation by utilizing bifunctional molecules in the absence of a solvent.
- The multilayer film having up to six layers can be prepared by vapor-phase deposition.

These studies are important because they provide a way to automate the synthesis of multilayer thin films.

In the second part of this dissertation, I will describe the preparation of highly monodisperse Au nanoparticles. Specifically I will show:

- Highly monodisperse Au nanoparticles can be prepared using quaternized dendrimer-templates.
- Au DEN size can be precisely controlled by adjusting the [$HAuCl_4$] to [dendrimer] ratio.

The development of a method to prepare highly monodisperse metal nanoparticles is important because size-monodispersity makes it possible to study the size-dependent electrochemical and optical properties of nanoparticles.

In the final part of this dissertation I will discuss the characterization of the electrochemical properties of Pd, Au, and Pd-Au DENs. Specifically I will show:

- Pd, Au, and Pd-Au DENs can be extracted from dendrimer interiors by *n*-hexanethiols as MPCs without altering the nanoparticle properties.
- Pd, Au, and Pd-Au MPCs are sufficiently size-monodisperse to show QDL charging behavior in the voltammograms without purification.
- Nanoparticle size can be precisely calculated by electrochemical methods.

These studies are important because the electrochemical method provides a new approach to precisely calculating the nanoparticle size.

CHAPTER II

EXPERIMENTAL SECTION

2.1 Dendrimers

Poly(amidoamine) (PAMAM) Dendrimers. Fourth- and sixth-generation hydroxyl-terminated PAMAM dendrimers (G4-OH and G6-OH, respectively) were obtained as 10-25% aqueous solutions from Dendritech, Inc. (Midland, MI). Partially quaternized dendrimers were synthesized from forth or sixth-generation, amine-terminated PAMAM dendrimers as described in Figure 2.1a.[44] These materials are referred to as G*n*-Q*p* where *n* is the dendrimer generation and *p* is the number of peripheral amine groups that have been quaternized (Figure 2.1b).

2.2 Preparation of DENs

Generally, DENs are prepared as follows: First, an aqueous solution of dendrimer is mixed with an aqueous solution of metal salts. The mixture is vigorously stirred and metal ions are extracted into the dendrimer interior. Finally the metal ions are reduced and coalesce into zero-valent metal nanoparticles by addition of an excess amount

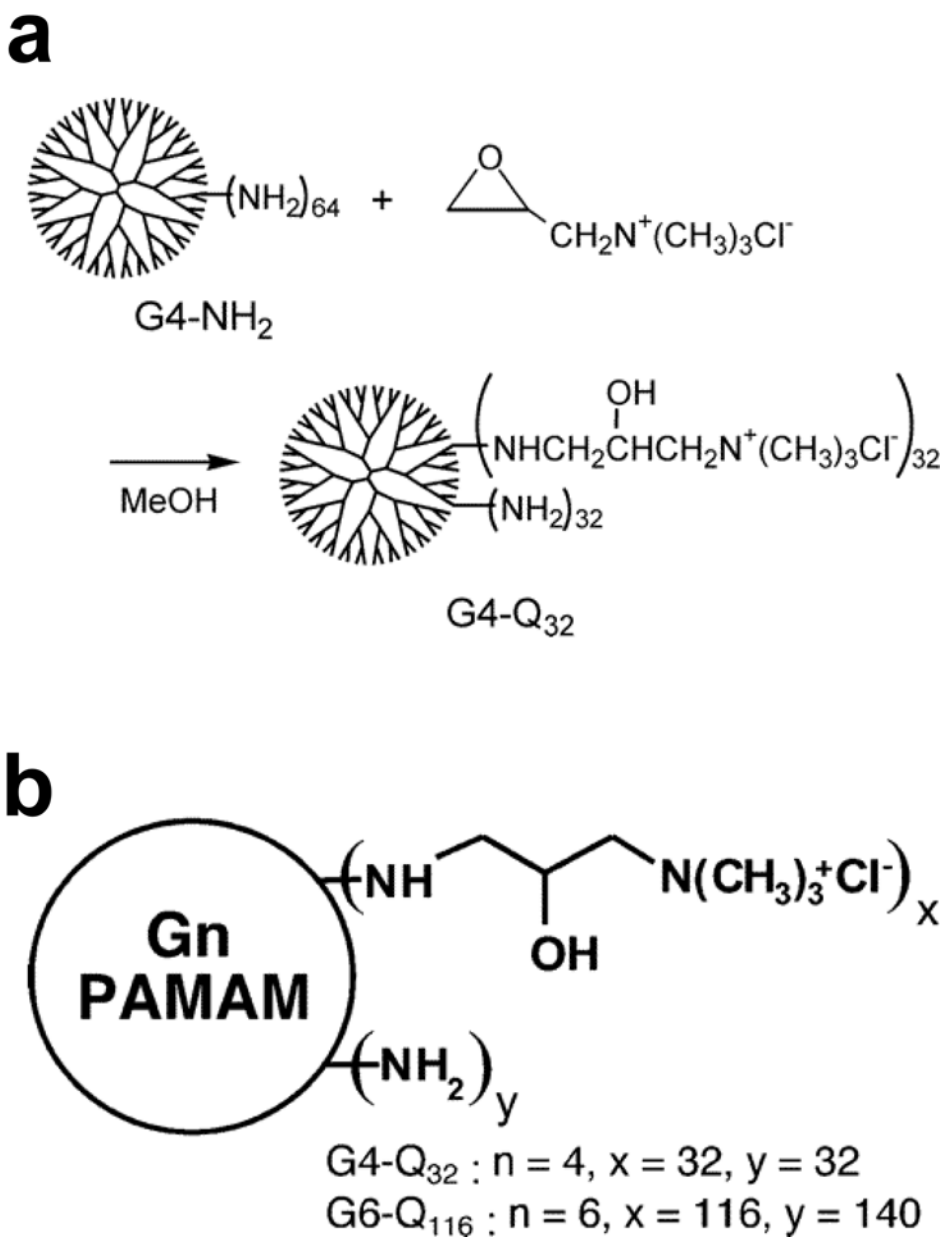

Figure 2.1. (a) Quaternized dendrimers are synthesized by reaction between amine terminated dendrimers and glycidyltrimethylammonium chlorides (b) Structures of generation 4 and 6 quaternized PAMAM dendrimers. (adapted from ref. 47 and 48)

of $NaBH_4$ to the mixture (Figure 2.2).[10-12] More detailed procedures of the preparation of Au, Pd and Pd-Au DENs are described below.

Preparation of Au DENs. 0.50 mL of a 10.0 μM G4-Q_{32} or G6-Q_{116} aqueous solution and 55, 100, 140, 225 or 300 equiv. aqueous solution of 2 mM $HAuCl_4$ were mixed.[45,46] This pale yellow solution was vigorously stirred for 20 min to provide enough time for $AuCl_4^-$ to be extracted into the dendrimer interior. A 5-fold molar excess of $NaBH_4$ in 0.30 M NaOH was quickly added to this solution with stirring to reduce the Au complex to zerovalent Au, and immediately the color changed from yellow to brown. $NaBH_4$ was dissolved in 0.30 M NaOH, which helps to control the rate of reduction. Following the synthesis, the total solution volume was 5 mL and the final concentration of DENs was 1 μM. For the electrochemical experiment, 100 mL of DEN solution was prepared according to the procedure described above.

Preparation of Pd DENs. Slight deviations from this procedure were required to prepare Pd DENs.[46] Specifically, 6.25 mL of an aqueous solution containing 0.10 mM G4-OH or G6-OH was mixed with 40, 80, or 140 equiv of an aqueous 5.00 mM K_2PdCl_4 solution. The solution was vigorously

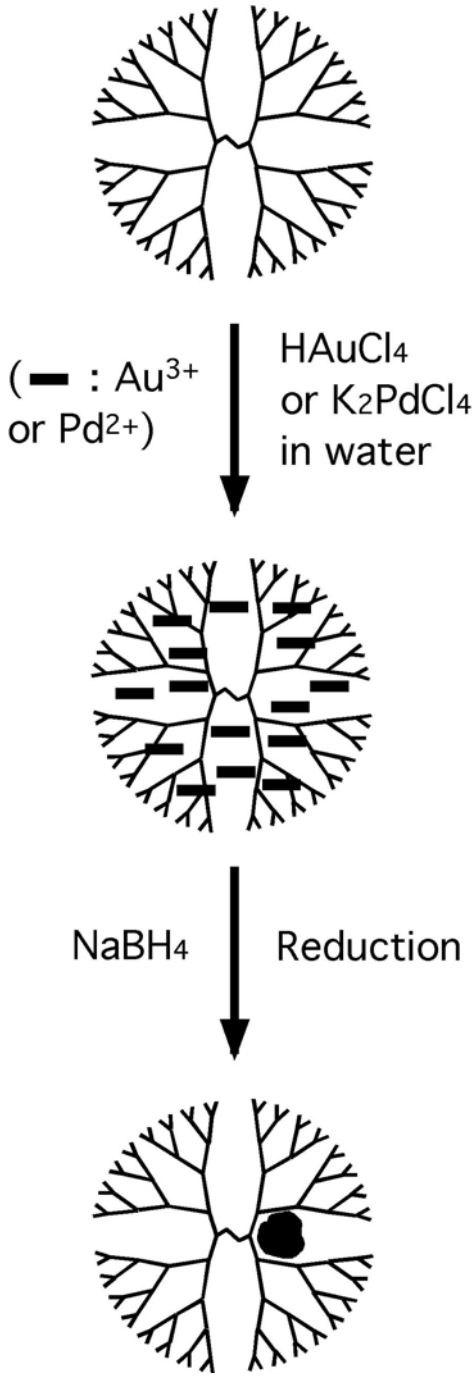

Figure 2.2. General procedure of Au and Pd DEN synthesis.

stirred for 5 min, and then a 10-fold molar excess of an aqueous $NaBH_4$ solution was added to yield G4-OH(Pd_{40}), G6-OH(Pd_{80}) or G6-OH(Pd_{140}), respectively.

Preparation of Pd-Au Bimetabllic DENs. Pd-Au bimetallic DENs were prepared by following the method used for the preparation of Au DENs with slight modifications.[16] 10.0 mL of a 10.0 μM G6-Q_{116} aqueous solution was mixed with 19 or 70 equiv. of a 2.00 mM K_2PdCl_4 aqueous solution. 19 or 70 equiv. of a 2.00 mM $HAuCl_4$ aqueous solution was added to the mixture after 30 min with vigorous stirring. The mixture was additionally stirred for 10 min, and 10-fold molar excess $NaBH_4$ was subsequently added to yield G6-Q_{116}($Pd_{19}Au_{19}$) or G6-Q_{116}($Pd_{70}Au_{70}$).

Extraction. The Au, Pd and Pd-Au DENs were extracted as MPCs as reported previously, but a short summary of the basic procedure follows.[20,21] The extraction was carried out by mixing together 10.0 mL of either an Au, Pd or Pd-Au DEN aqueous solution and 10.0 mL of a hexane or toluene solution containing 50.0 mM *n*-hexanethiol. A 150-fold molar excess of $NaBH_4$ was added to the mixture and the vial was shaken. After settling, the hexane layer containing the *n*-hexanethiol-coated MPCs (MPC-6(Au_n), MPC-6(Pd_n), or

MPC-6(Pd_nAu_n) where n is number of metal atoms) was transferred to a round-bottom flask and the solvent and excess *n*-hexanethiol were removed by evaporation under vacuum at 23 ± 2 °C. The dried MPCs were used for subsequent experiments without further purification.

Spectroscopic characterization. UV-vis spectroscopy has played an important role in the study of metal nanoparticles because the peak position and the intensity of absorption bands in spectra are closely related to the size, shape, and composition of the nanoparticles. For example, Au nanoparticles show a characteristic band attributed to surface plasmon at 525 nm and the intensity of this band is related to the nanoparticle size. This absorption band becomes weak or not observable with a decrease in particle size and the surface plasmon band is absent when the Au nanoparticle size is less than 2 nm.[45] UV-vis absorbance spectra were obtained at 23 ± 2 °C using quartz cells and a Hewlett-Packard model 8453 UV-vis spectrophotometer system (Hewlett-Packard, Wilmington, DE).

Microscopic characterization. In the transmission electron microscopy (TEM) measurement, a beam of highly energetic electrons is used to determine the shape, size,

and size distribution of DENs and MPCs. When a beam of electrons passes through the sample on a grid, the degree of transmission of the beam is related the electron density of samples. Therefore, only nanoparticles which have high density of electrons can be observed by TEM while dendrimers remain transparent in TEM measurement unless they are stained. TEM was performed using a JEOL 2010 electron microscope (JEOL USA Inc., Peabody, MA) with 0.19 nm point-to-point resolution. A diagram of the cross section of a TEM is shown in the Figure 2.3.

2.3 Electrochemical Measurements

Differential pulse voltammetry (DPV) has been widely used to study QDL charging behavior of MPCs because the peaks are well resolved compared to other voltammetry techniques. The potential wave of DPV consists of small pulses which are superimposed upon a staircase wave form (Figure 2.4). Current is sampled before and at the end of the pulse and the difference between these two current values is recorded. A voltammogram is a plot of current difference versus the base potential. Therefore the effect

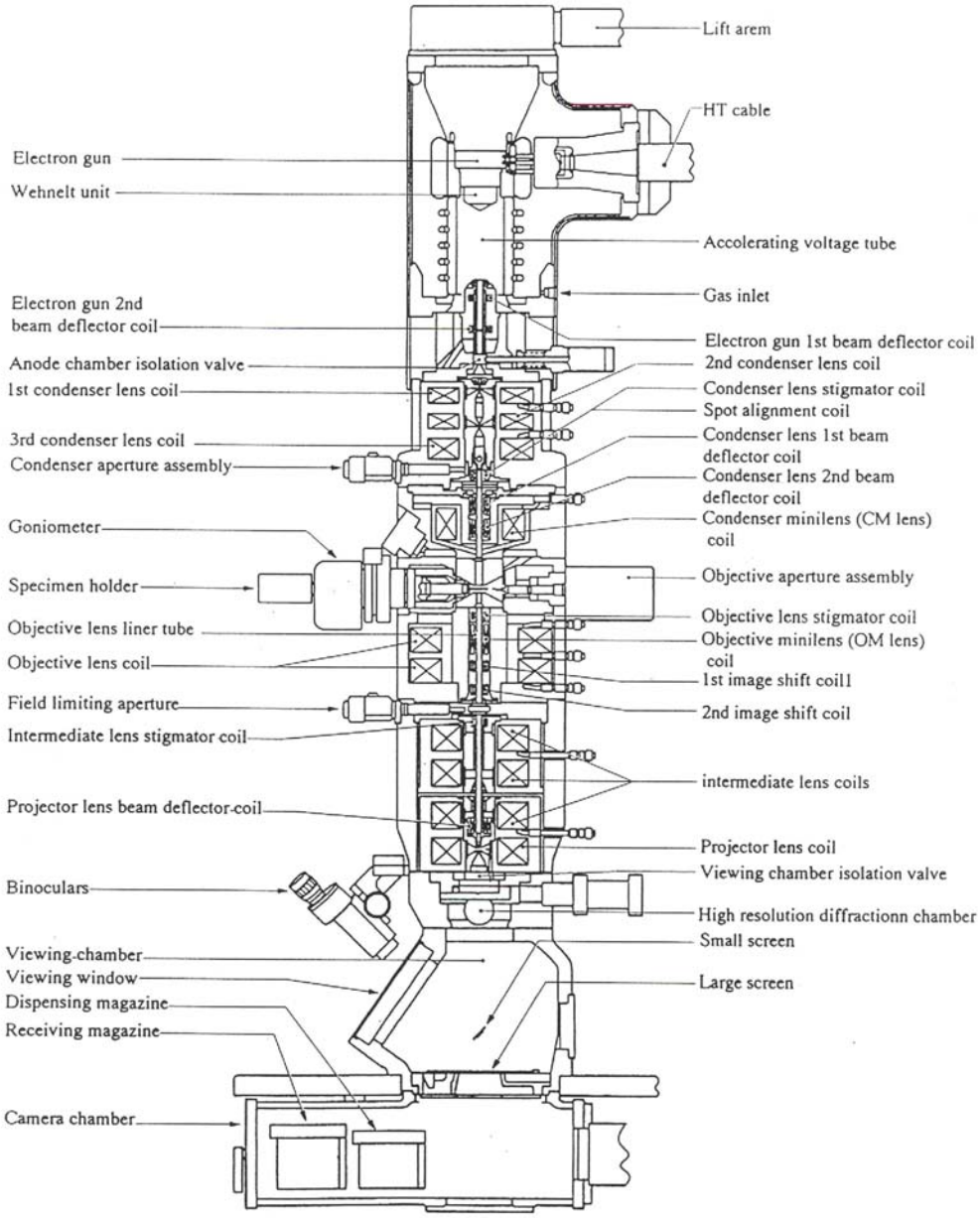

Figure 2.3. Cross section of TEM column. (taken from JEOL 2010 electron microscopy manual)

of charging current on a voltammogram can be reduced and DPV shows a higher sensitivity than CV. The voltammetric response from DPV can be controlled by adjusting the parameters used for DPV. For example, the scan rate cannot be controlled directly, however it is possible to control the scan rate by changing step E and pulse period because the scan rate is step E/pulse period. The pulse period must be at least twice the pulse width for the measurement and generally the signal to noise ratio increases as the sample period increases.

DPV was performed in a 2 mL, single-compartment glass cell configured with a 1.0 mm-diameter Au disk working electrode, a Pt wire counter electrode, and a Ag wire quasi-reference electrode (QRE). The Au working electrode was successively polished with 1.00, 0.30, 0.05 μm alumina (Buehler, Lake Bluff, IL) and sonicated in Milli-Q water and ethanol. The counter electrode and QRE were cleaned in piranha solution (3:1 H_2SO_4/H_2O_2; caution: piranha reacts violently with organics and should be used with care) before use, and the QRE was additionally soaked in HNO_3 for 5 min. Dichloromethane was purified by refluxing over P_2O_5 for 3 h and then distilled. Tetrabutylammonium

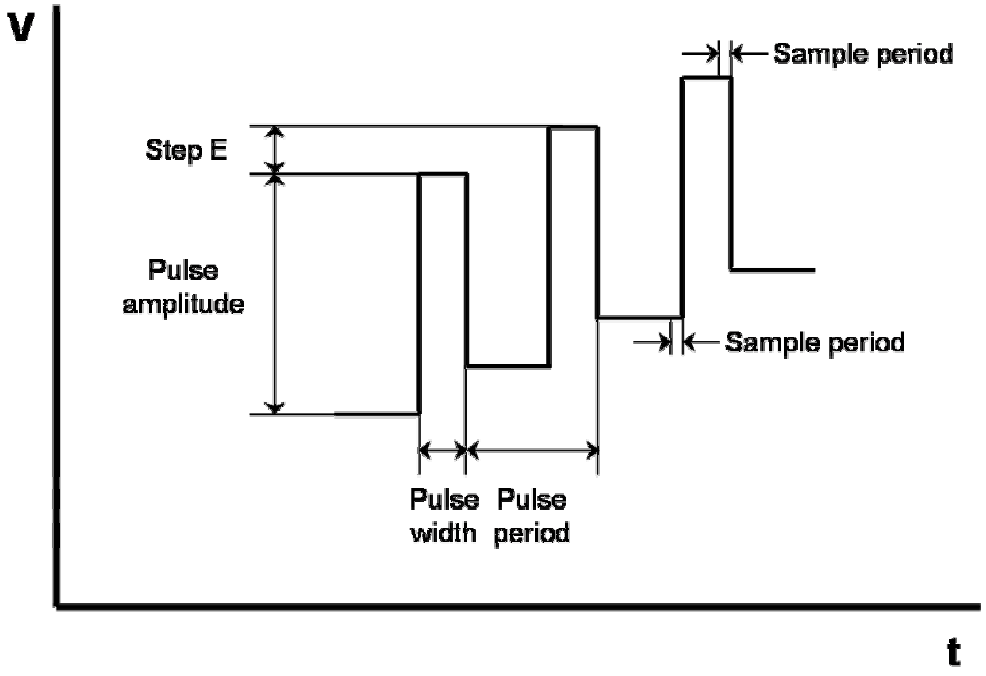

Figure 2.4. Potential wave form for DPV.

hexafluorophospate (Bu_4NPF_6) was used as received and stored in a N_2-purged drybox. The electrolyte solutions were prepared by dissolving Bu_4NPF_6 in dichloromethane in an Ar-purged vinyl bag. The background of voltammogram was improved by using a hydrophobic salt (bis(triphenylphosphoranylidene) ammoniumtetrakis (pentafluorophenyl)borate).[43] This salt is prepared by metathesis between lithium tetrakis(pentafluorophenyl) borate etherate ($LiB(C_6F_5)_4O(CH_2CH_3)$, Boulder Scientific Co., Mead, CO) and bis(triphenylphosphoranylidene)ammonium chloride ($(C_6H5)_3P=N(Cl)=P(C_6H_5)_3$, Aldrich Chemical CO., Milwaukee, WI). The solution was prepared by dissolving the salts in a 1:2 water/methanol solution. The mixing of equimolar quantities of each solution results in the formation of a white precipitate. This white precipitate was filtered and recrystallized. The crystals were dried in the oven at 130 °C for overnight and stored in the drybox. All DPV experiments were performed in the N_2-purged drybox. A model 760B electrochemical workstation (CH Instruments, Austin, TX) was used for all DPV experiments. The parameters used for DPV were: step E, 4 mV; pulse amplitude, 50 mV; pulse width, 50 ms; pulse period, 200 ms; and sample period 17 ms.

2.4 Additional Techniques

Vapor-phase surface modification. The configuration of the apparatus for vapor phase reaction is described in Figure 2.5a and the picture of the actual arrangement of the apparatus is shown in Figure 2.5b. The clean Au substrate is placed in a chamber made by connecting clean borosilicate glass vials fitted with teflon/silicone septa. This chamber is purged with dry N_2 for at least 30 min before dosing vapor phase reactants. Reactants were stored in the vial fitted with septa or pear shaped two neck flasks (ACE Glass, Vineland, NJ) with screwed cap mininert valve (VWR Scientific Products, Suwanee, GA)(Figure 2.5C). Vapor-phase reactants were generated by passing dried N_2 at 0.5 L/min over the head space of a vial or a pear shaped flask.

Fourier transformation infrared-external reflection spectroscopy (FTIR-ERS). FTIR-ERS provides information about molecular structures on the surface. When p-polarized light radiated at high incident angle, vibration modes that have dipoles normal to the surface strongly interact with the electric field and are selectively excited by following the surface selection rule. Therefore

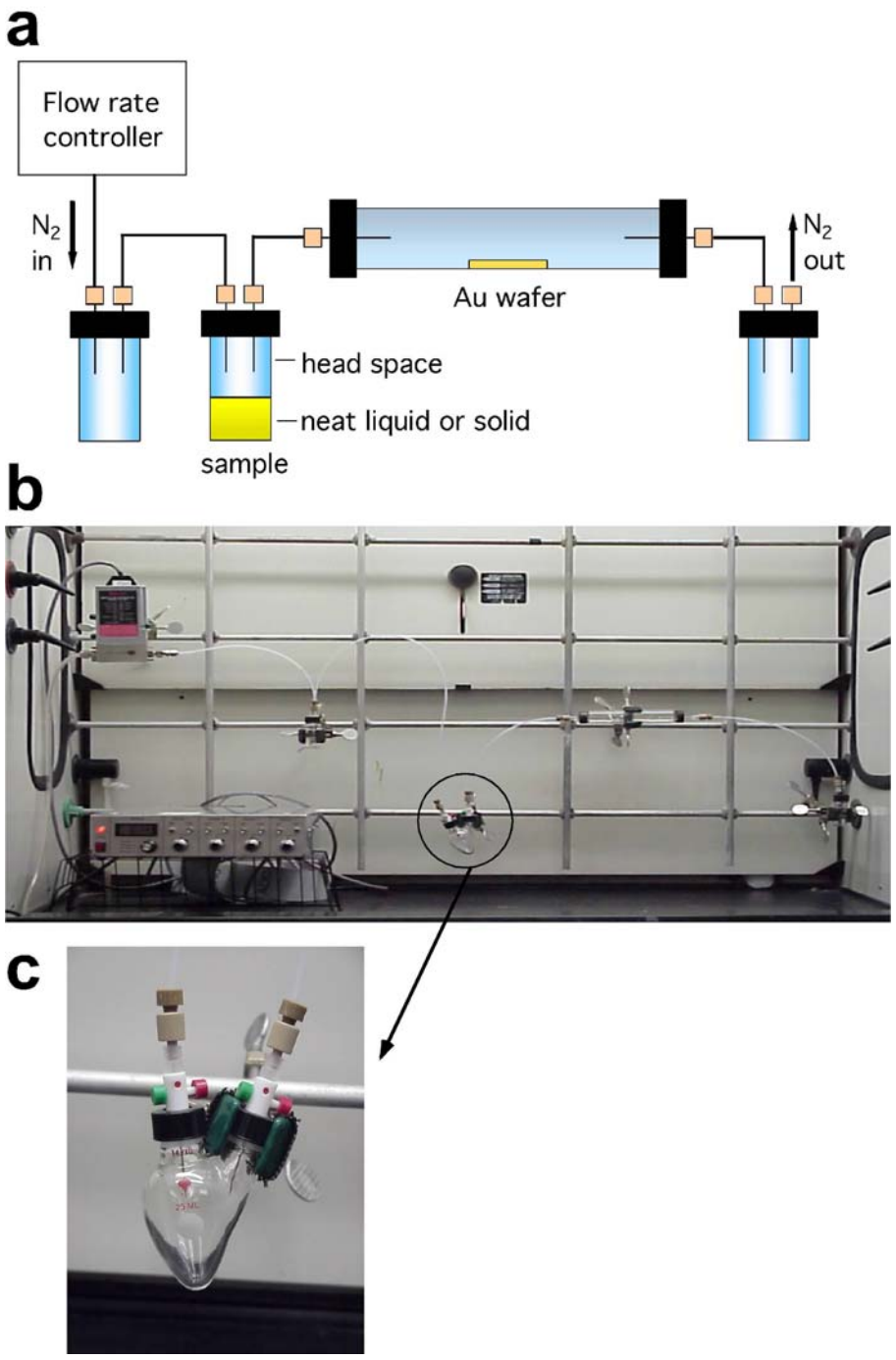

Figure 2.5. (a) Diagram of vapor phase deposition apparatus (b) corresponding picture of an arrangement of vapor phase deposition apparatus (c) pear-shaped flask with mininert valve.

FTIR-ERS allows detailed information about the orientation and interactions of molecules on the surface.

FTIR-ERS measurements were carried out using an FTS-6000 spectrometer (Bio-Rad, Cambridge, MA) equipped with a Harrick Scientific Seagull reflection accessory. The *p*-polarized light at 84° incident angle with respect to the Au substrate was used as a light source. The FTIR-ERS reflected beam depends on the optical properties of thin film on the surface and substrate.

Ellipsometric thickness. When the film thickness is changed, the reflection properties of light on the surface also changed. Ellipsometry measures the changes in polarization state of light reflected from the surface. When the two components of light (P- and S-polarized) are reflected from the surface, the phase difference (Δ) and relative amplitude differences (Ψ) are changed in different ways. The refractive index and the film thickness can be calculated from resulting elliptically polarized light. However since it is difficult to precisely calculate both the refractive index and the thickness in thin films, we used a value of 1.46 for the refractive index of the organic thin film to determine film thickness.[6,7,47] The

ellipsometer, made by Gaertner Scientific (model L2W26D, Chicago, IL), was used for film thickness measurement. 632.8 nm laser light with 70.00 ± 0.02° incident angle was used as a light source and the film refractive index (n_f) was assumed as 1.46.

CHAPTER III

SYNTHESIS AND CHARACTERIZATION OF COVALENTLY LINKED MULTILAYER FILMS PREPARED IN THE ABSENCE OF SOLVENT*

3.1 Introduction

In this chapter, we report the synthesis of multilayer organic thin films prepared via multiple, sequential chemical reactions at the vapor/solid interface. Specifically, small aliphatic and aromatic molecules bifunctionalized with either primary amines or acid chloride groups were found to undergo coupling reactions at surfaces at room temperature and atmospheric pressure in the absence of solvent (Figures 3.1 and 3.2). Using this approach, it is possible to prepare partially organized thin films up to six molecular layers in thickness. This result is significant because multilayer organic thin films are normally prepared in liquids, or by vapor-phase reaction in vacuum[5,48-50] or at high temperature.[48-50] The objectives of this study are the development of a better understanding of the types of reactions that proceed in the

---

absence of solvents and optimization of conditions for carrying them out.

There are some potential advantages associated with synthesizing organic thin films in the absence of solvents that have motivated this research. First, vapor-phase reactions eliminate the effects of solvent and impurities (especially water) on the structure and properties of the films. Second, vapor-phase reactions are more easily automated than those requiring solvents. Third, certain types of intermolecular interactions, such as hydrogen bonding and electrostatic interactions, which are weak in many solvents, are strong in their absence. Fourth, reactions carried out at the vapor/solid interface at atmospheric pressure provide a valuable link between UHV and condensed-phase studies.[1-3]

We previously showed that several different types of intermolecular interactions can be used to prepare simple bilayer films via vapor-phase reactions. For example, when a 4-mercaptophenol-modified Au substrate is exposed to chlorodimethyloctylsilane vapor a siloxane bond between the two layers results.[2,4] In addition to covalent bonds, noncovalent interactions, such as acid-base[3,51,52] and H-bonding interactions,[53] are also useful for preparing

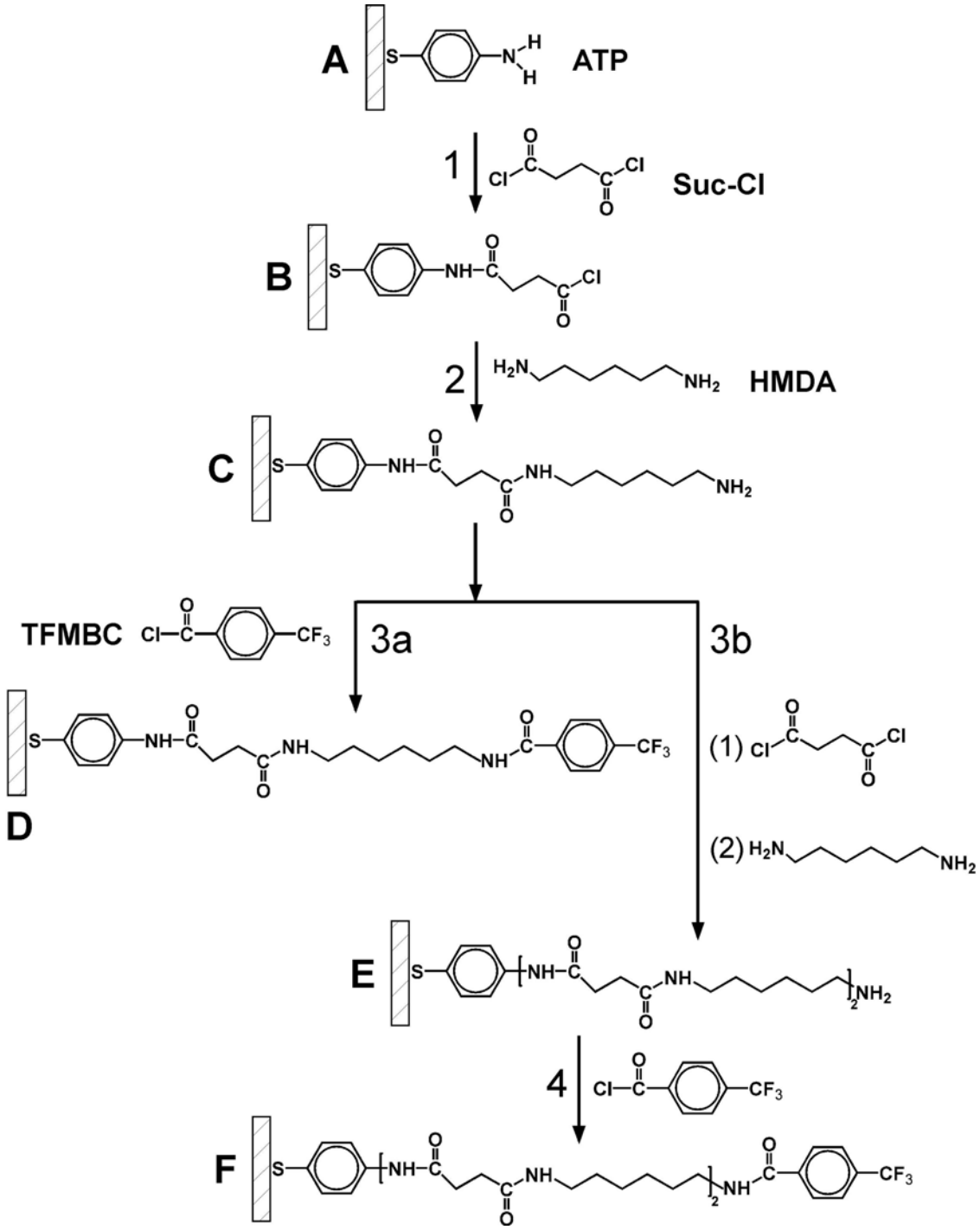

Figure 3.1. Schematic diagram of the preparation of multilayer film via sequential reaction of an aniline-modified Au surface with bifunctional acid chlorides and amines.

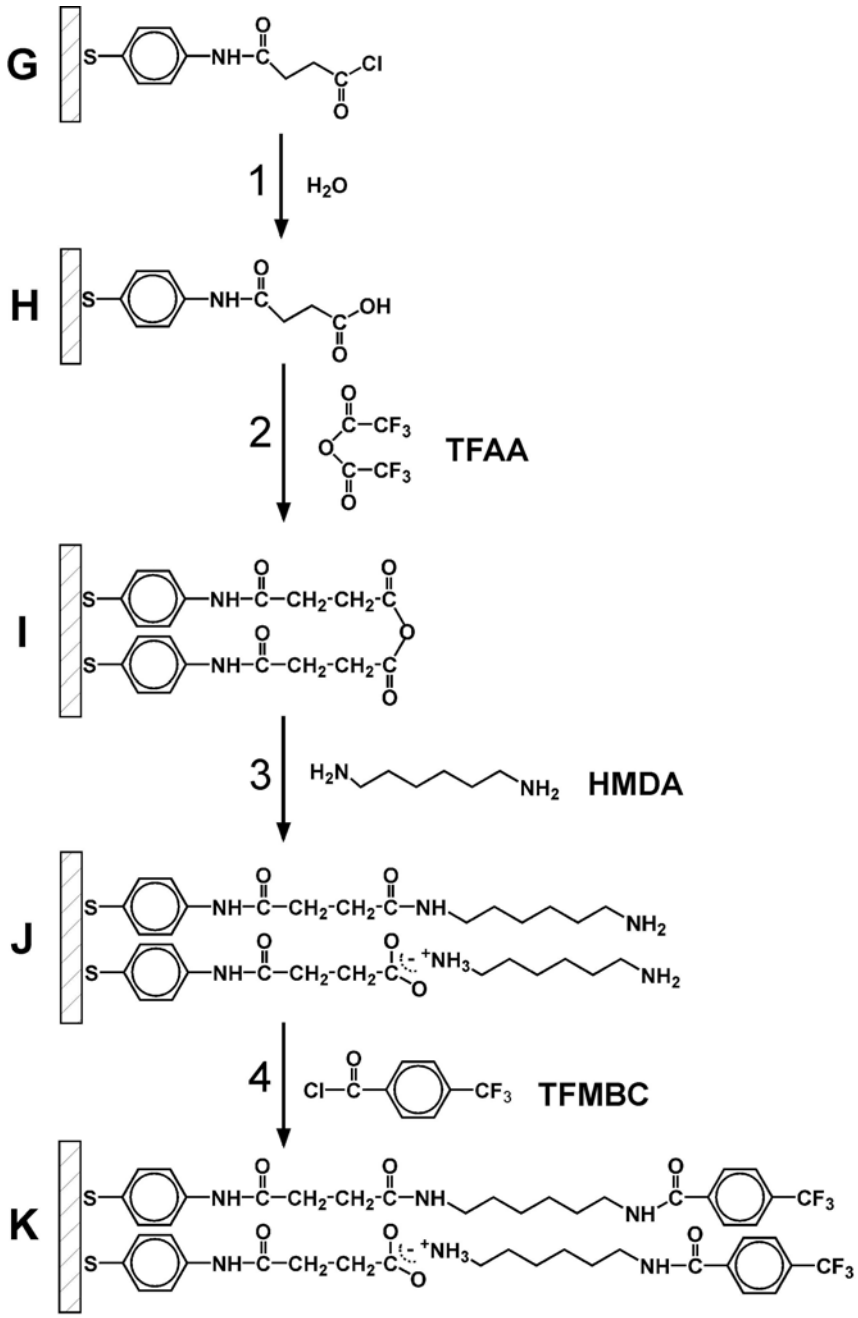

Figure 3.2. Schematic diagram of the preparation of multilayer film via the reaction of an acid-chloride-modified Au surface with water to form the acid, activation of the acid to an anhydride, coupling with a bifunctional amine.

bilayer films in the absence of solvents. Finally, we have also shown that trilayer thin films can be prepared via vapor-phase coupling of active anhydrides, amines, and acid chlorides.[7]

Other groups have also explored the viability and scope of vapor/solid reactions, but most of these have been carried out under vacuum[5,48-50] and/or at high temperature.[48-50] For example, the reactivity of hydroxyl- and acid-terminated monolayers have been examined under UHV conditions,[5] hydrogen-bonded electrooptic thin films have been prepared,[48] and fluorosilane monolayer assemblies have been reported.[3] Recently, the Morris group synthesized a well-ordered bilayer film by exposing a Au substrate modified with a hydroxyl-terminated alkylthiol monolayer to a vapor-phase alkyl isocyanate at 40 °C at atmospheric pressure. These conditions resulted in formation of a carbamate linkage.[50]

In this paper we expand upon our previous findings by showing that multilayer films having up to six layers can be prepared by vapor-phase reactions. Two distinctly different approaches were used to demonstrate generality. Figure 3.1 shows the strategy for preparing covalently linked multilayer films via sequential reaction of an

aniline-modified Au surface with bifunctional acid chlorides and amines. The method shown in Figure 3.2 involves reaction of an acid-chloride-modified Au surface with water to form the acid, activation of the acid to an anhydride, coupling with a bifunctional amine, and then capping with a second acid chloride. The results of ellipsometric, infrared spectroscopic, and contact-angle measurements indicate that these types of reactions result in partially organized thin films.

3.2 Experimental Section

Chemicals. Aminothiophenol (ATP, 90%), succinyl chloride (Suc-Cl, 95%), *n*-octylamine (OA, 99%), hexamethylenediamine (HMDA, 98%), trifluoroacetic anhydride (TFAA, 99+%), and 4-(trifluoromethyl)benzoyl chloride (TFMBC, 97%) were purchased from the Aldrich Chemical Co. (Milwaukee, WI) and except for ATP were used as received. ATP was purified by vacuum sublimation. Dichloromethane (99.5+%) was purchased from EM Science (Darmstadt, Germany) and dried with molecular sieves just before use. Absolute ethanol was purchased from Aaper Alcohol & Chemical Co. (Shelbyville,

KY). N_2 gas (99.995%) was used as the carrier for vapor-phase reactants. Traces of water were removed by passing it over a Drierite gas purifier (Hammond 26800, Fisher Scientific Co. Pittsburgh, PA).

Substrate preparation. Au-coated substrates were prepared by electron-beam deposition of 200 nm of Au onto Ti primed (10 nm) Si(100) wafers (Lance Goddard Associates, Foster City, CA). Prior to use the wafers were diced into 2.6 x 1.3 cm pieces. These substrates were cleaned in a low-energy ozone cleaner for 15 min (Boekel Industries, Inc.,model 135500) and rinsed with ethanol before placing them into the vapor-phase reaction chamber.

Vapor-phase surface modification. The reaction chamber consisted of a borosilicate glass tube fitted at each end with caps that exposed only PTFE/silicone liners (Alltech, Deerfield, IL) to the reactive vapors. After placing the Au substrate in this chamber, it was purged with dry N_2 for at least 30 min before dosing with reactants. N_2 gas was purified by passing it through the Drierite (W.A. Hammond Drierite CO. LTD, Xenia, OH) and activated carbon filters (Whatman, Florham Park, NJ). The reactants were stored in vials and capped with septa or in pear-shaped, two-necked flasks (ACE Glass, Vineland, NJ)

fitted with Mininert syringe valves (VWR Scientific Products, Suwannee, GA). The vapor-phase reactant streams were generated by passing N_2 gas (0.5 L/min) over the head space of a vial or pear-shaped flask containing the neat solids or liquids. The resulting vapor was passed through TFE tubing (3.2 mm OD and 2.5 mm ID) and into the reaction chamber for 10 - 60 min. The chamber was purged with N_2 between each reaction step to remove excess reactants.

Liquid-phase surface modification. In some cases, ATP monolayers were prepared on Au surfaces using ethanol as the solvent. In this case, the Au substrate was placed in a 1 mM ethanolic ATP solution for 24 h, sonicated for 30 s in ethanol, and rinsed with ethanol prior to characterization. An ATP-TFMBC bilayer was prepared by immersing the ATP-modified substrate in dry dichloromethane containing 1 mM TFMBC for 9 h. This film was also sonicated and thoroughly rinsed with dichloromethane prior to characterization.

Fourier transformation infrared-external reflection spectroscopy (FTIR-ERS). All FTIR-ERS measurements were performed using a N_2-purged FTS 6000 spectrometer (Bio-Rad, Cambridge, MA) equipped with a Harrick Scientific Seagull reflection accessory (Ossining, NY) and a liquid-nitrogen-

cooled, narrow-band mercury-cadmium-telluride (MCT) detector. Spectra were obtained at 4 cm^{-1} resolution using *p*-polarized light incident on the substrate at 84° with respect to the substrate normal. The reported spectra consisted of 256 - 512 summed individual spectra from which a background spectrum, obtained using a freshly cleaned Au surface, was subtracted.

Ellipsometric thickness and contact-angle measurements. A Gaertner Scientific (model L2W26D, Chicago, IL) ellipsometer was used for film thickness measurements. The light source was a 632.8 nm laser incident on the substrate at an angle of 70.00 ± 0.02° relative to the surface normal. The refractive index (n_f) of the film was assumed to be 1.46.[6,7,47] The thickness of each film was measured at five different locations, and the average of these values is reported. The contact angle was measured using a goniometer (Rame-Hart Inc., Mountain Lake, NJ). The reported contact angles are the average of five independent measurements made on different locations on the substrate surface.

3.3 Results and Discussion

Layer-by-layer vapor-phase synthesis of amide-linked multilayer organic thin films. Figure 3.3 shows FTIR-ERS spectra of monolayer and bilayer films corresponding to structures A and B in Figure 3.1. Figure 3.3a was obtained after vapor-phase dosing of an Au substrate with ATP. The peaks at 1590 cm^{-1} and 1487 cm^{-1} are characteristic of the quadrant stretching and semicircle stretching modes of the ATP ring system.[54,55]

Suc-Cl was coupled to the distal amine functional group of ATP via a vapor-phase amidation reaction (Step 1, Figure 3.1). This results in a new IR band at 1526 cm^{-1} (amide II band, Figure 3.3b) that corresponds to the presence of the amide bond.[6,7,56-59] Note, however, that the amide I band, usually present in the range of 1640 - 1675 cm^{-1}, is absent. This is probably a consequence of the orientation of the bond relative to the substrate. The amide I band correlates most closely with the carbonyl stretch and the amide II band corresponds to the N-H bending and C-N stretching modes. Therefore, the absence of a well-defined amide I band suggests that the C=O bond is oriented parallel to the substrate surface (as drawn in Figure 3.1).[60]

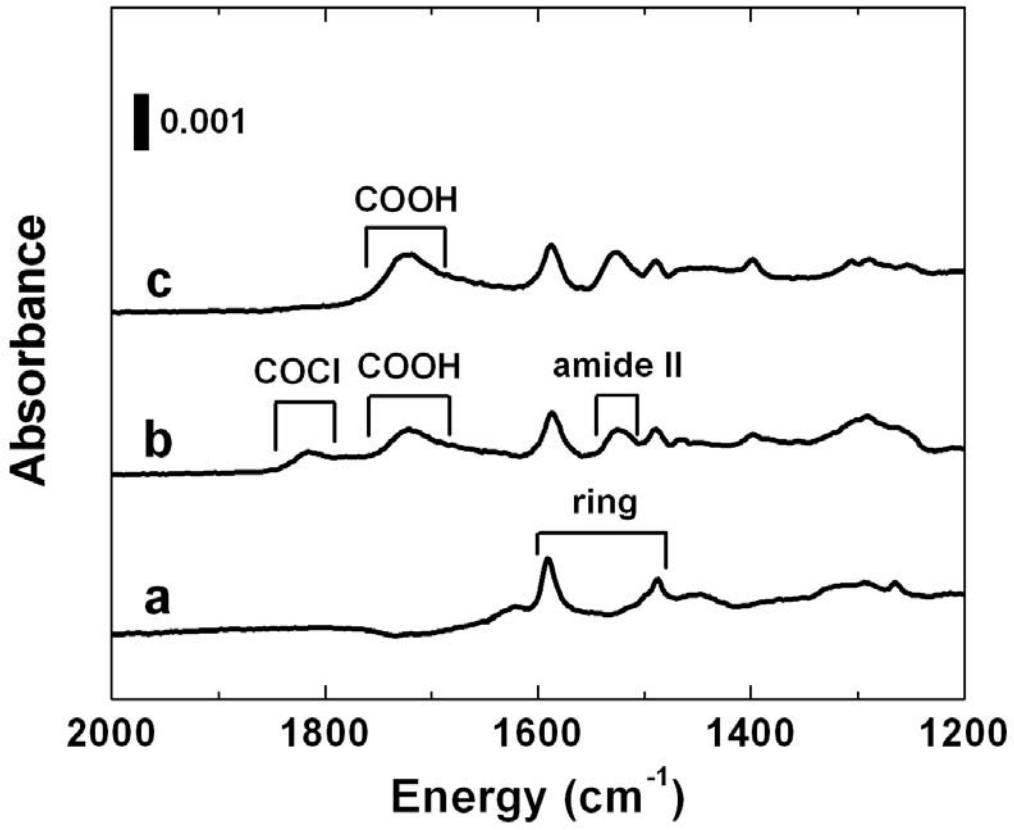

Figure 3.3. FTIR-ERS spectra of the thin films shown in Figure 3.1. Spectra (a) and (b) correspond to structures A and B in Figure 3.1. Spectrum (c) was obtained from a film corresponding to structure B after exposure to air for two weeks.

The new band at 1815 cm^{-1} in Figure 3.3b is attributable to the carbonyl stretching mode of the acid chloride. The band at 1721 cm^{-1} probably corresponds to partial hydrolysis of the acid chloride surface, which would likely occur when the substrate is removed from the reaction chamber and transferred to the FTIR for spectral analysis.[47,53] This supposition was confirmed by exposing an acid chloride-terminated surface (structure B, Figure 3.1) to air for two weeks and then obtaining Figure 3.3c. Here, the acid chloride band at 1815 cm^{-1} has been replaced with a more intense acid carbonyl stretch at 1721 cm^{-1}. As a consequence of this finding, subsequent reactions on acid chloride-terminated surfaces were carried out in the absence of air. That is, no intermediate IR spectra of acid chloride-terminated surfaces were obtained for the remainder of the films discussed herein.

The ellipsometric thickness of the ATP layer was found to be 0.7 nm, and this value increased to 1.1 nm after coupling with the acid chloride (all calculated and experimental film thicknesses are provided in Table 3.1). Taken together, the IR and ellipsometric data confirm vapor-phase coupling of Suc-Cl to ATP via amide bond formation. At this point, however, it is not possible to

Table 3.1. The ellipsometric thickness and contact-angle data for the films prepared by vapor phase reactions.

Au/Monolayer	Calculated thickness (nm)[a]	Thickness (nm)[b]	Contact angle (deg)[c]
A	0.6	0.7 ± 0.2	51 ± 3
B	1.2	1.1 ± 0.1	[d]
C	2.1	1.8 ± 0.2	42 ± 4
C(OA capped)	2.2	2.0 ± 0.6	59 ± 3
D	2.7	2.4 ± 0.4	73 ± 2
E	3.6	2.8 ± 0.4	[d]
F	4.2	3.2 ± 0.3	70 ± 3
I	1.1	0.9 ± 0.2	[d]
J	2.1	2.2 ± 0.4	[d]
K	2.7	2.6 ± 0.4	[d]

(a) Thicknesses were calculated by assuming the films are oriented perpendicular to the substrate. Molecular dimensions were estimated using CS Chem3D Ultra (Cambridgesoft, Cambridge, MA, 2002). (b) Average of five ellipsometric thickness measurements made at five different locations on each of two independently prepared substrates. (c) Average of five static water contact-angle measurements made on each of two independently prepared substrates. (d) Not determined.

say with certainty whether just one end of Suc-Cl couples to ATP or whether it cross couples and lays flat on the ATP surface. This latter issue was addressed by carrying out a third coupling reaction that relies on the presence of a free acid chloride group on the surface. Specifically, a bilayer film prepared by vapor-phase reaction of ATP with Suc-Cl, but without exposing the acid chloride-functionalized surface to air, was reacted with HMDA vapor to yield a trilayer film (structure C, Figure 3.1). This reaction resulted in a change in the ellipsometric thickness from 1.1 nm to 1.8 nm. The height of the amide II band also increased by ~30% after reaction with HMDA (Figure 3.4a). New bands are present in the spectrum of the three-layer film at 3220, 3132, 2929, and 2857 cm^{-1}. The bands at 3220 and 3132 cm^{-1} are attributed to the asymmetric and symmetric N-H stretching modes, respectively, and the bands at 2929 and 2857 cm^{-1} correspond to the methylene stretching modes.[2,47,53,54,61,62] Also present in the high-frequency region are two very small shoulders at 3030 and 2961 cm^{-1}. We are not able to assign these with confidence at the present time. These spectral changes and the increase in film thickness are fully consistent with

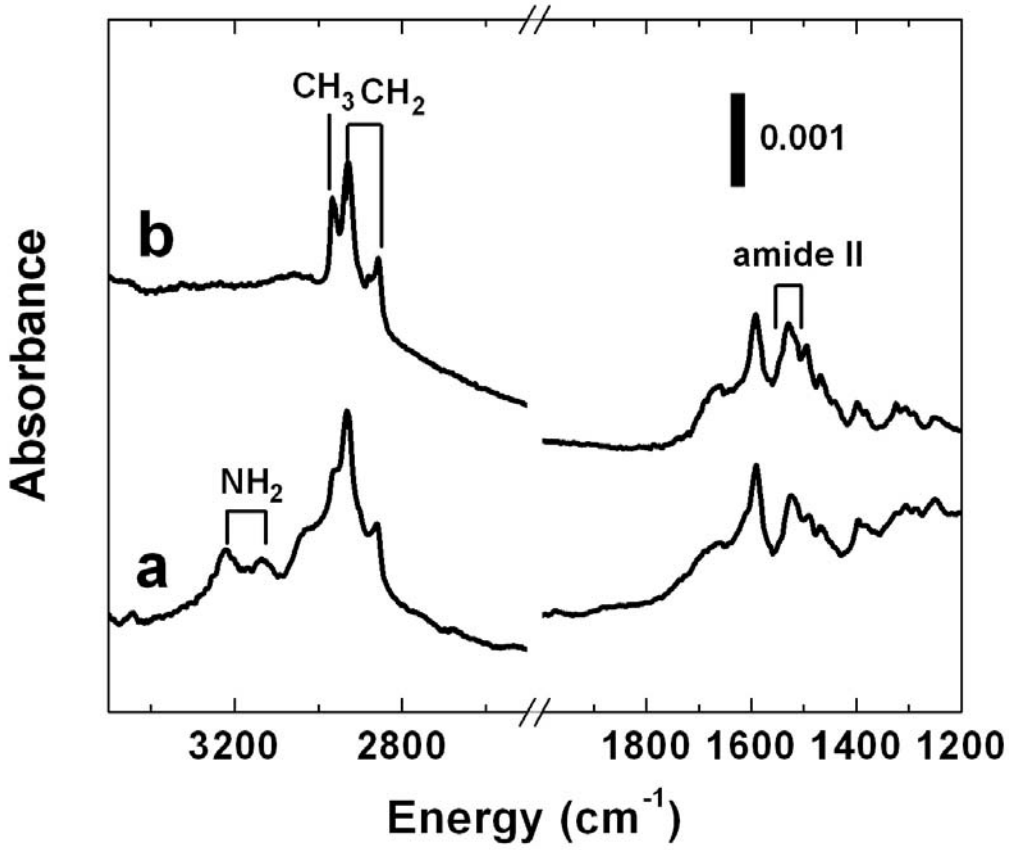

Figure 3.4. FTIR-ERS spectra of trilayer films corresponding to (a) structure C in Figure 3.1 and (b) the corresponding film prepared by reaction of structure B with monofunctionalized octylamine rather than HMDA.

bilayer film prepared by vapor-phase reaction of ATP with Suc-Cl, but without exposing the acid chloride-functionalized surface to air, was reacted with HMDA vapor to yield a trilayer film (structure C, Figure 3.1). This reaction resulted in a change in the ellipsometric thickness from 1.1 nm to 1.8 nm. The height of the amide II band also increased by ~30% after reaction with HMDA (Figure 3.4a). New bands are present in the spectrum of the three-layer film at 3220, 3132, 2929, and 2857 cm^{-1}. The bands at 3220 and 3132 cm^{-1} are attributed to the asymmetric and symmetric N-H stretching modes, respectively, and the bands at 2929 and 2857 cm^{-1} correspond to the methylene stretching modes.[2,47,53,54,61,62] Also present in the high-frequency region are two very small shoulders at 3030 and 2961 cm^{-1}. We are not able to assign these with confidence at the present time. These spectral changes and the increase in film thickness are fully consistent with Structure C in Figure 3.1.

The just-described spectral features conclusively prove that a substantial fraction of the acid chloride groups of the two layer film are available for further reaction with HMDA; that is, they are not cross-coupled to the original ATP surface. However, at this stage of the

film growth it was necessary to address the possibility of HMDA cross coupling to the acid chloride surface by confirming that the peaks at 3220 and 3132 cm^{-1} correspond to the free amine. This issue was addressed by coupling structure B (Figure 3.1) to monofunctionalized *n*-octylamine (OA) instead of to HMDA. This experiment resulted in a film having a thickness of 2.0 nm, which compares favorably to the 1.8 nm-thick HMDA-coupled film. Moreover, the OA-terminated film exhibited a significantly higher static contact angle than the HMDA-terminated trilayer (59° vs. 42°, respectively).

The spectrum of the OA-capped film (Figure 3.4b) was similar to that of the HMDA-modified trilayer in the region from 1400-1600 cm^{-1}, but a new band at 2967 cm^{-1} arising from the distal methyl group is also apparent.[2,51] Importantly, however, the bands at 3220 and 3132 cm^{-1}, previously attributed to the peripheral amine group of the HMDA-capped film, are absent. Because the only difference between the two films represented by the spectra in Figure 3.4 is this amine group, it is reasonable to conclude that the assignment is correct and that this is a free amine ready for additional synthetic elaboration.

The amine-terminated trilayer film was exposed to vapor-phase TFMBC to yield a covalently linked, four-layer film capped with a trifluoromethyl group (structure D, Figure 3.1). Evidence for the presence of TFMBC on the surface comes from the very strong absorption band at 1328 cm^{-1} (Figure 3.5b), which corresponds to the CF_3 symmetric stretching mode.[7,57,63] Other important features of Figure 3.5b include slight increases (10 – 22%) in the aromatic ring bands (1589 cm^{-1} and 1489 cm^{-1}) and the amide II band (compare with the spectrum of the trilayer film, Figure 3.5a). After reaction with TFMBC, the thickness of the film increased from 1.8 nm to 2.4 nm. The change in contact angle from 42° to 73° is also fully consistent with the presence of CF_3 surface functional groups.

A six-layer film was prepared by successively dosing the three-layer film (structure C in Figure 3.1) with Suc-Cl, HMDA, and TFMBC vapors (Steps 3b and 4, Figure 3.1). Addition of the final three layers resulted in an increase in the film thickness from 1.8 to 3.2 nm. Increases in the magnitudes of the ring modes at 1589 cm^{-1} and 1487 cm^{-1}, and the amide II band at 1526 cm^{-1} (Figure 3.5c), are also consistent with formation of the thicker film (compare to

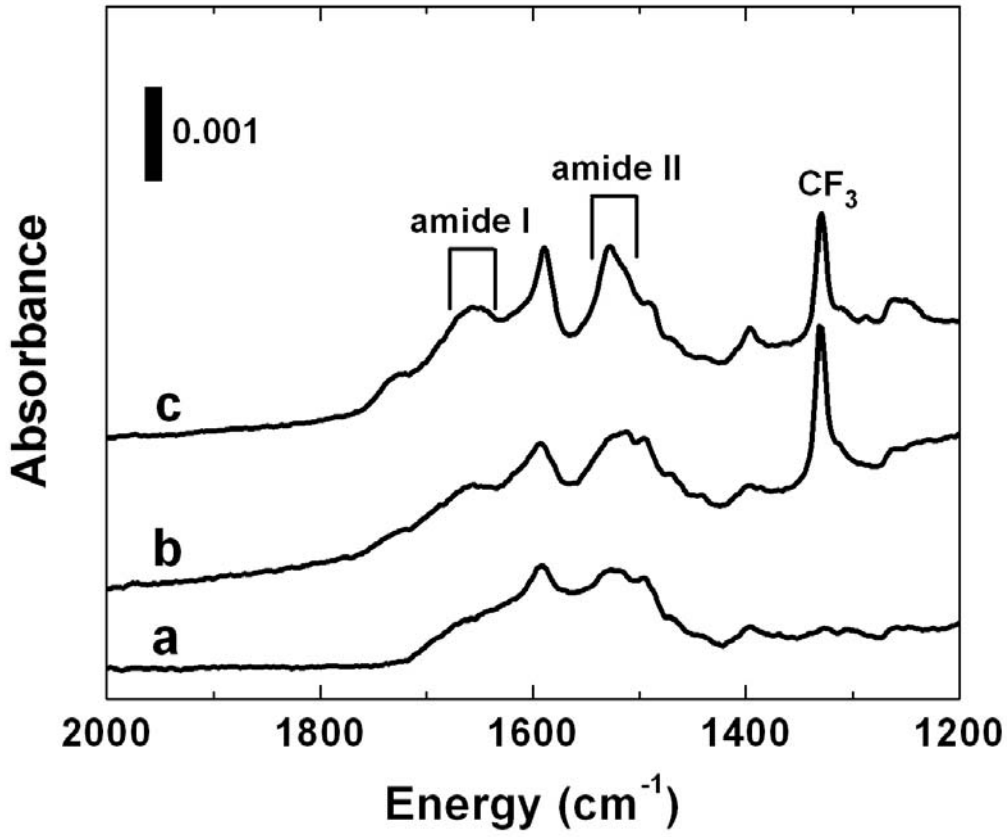

Figure 3.5. FTIR-ERS spectra corresponding to (a) structure C, (b) structure D, and (c) structure F.

Figures 3.5a and 3.5b). However the intensity of CF_3 band at 1328 cm^{-1} is lower than that of the four-layer film by 22%. We attribute this finding to a gradual reduction in the density of the growing film, which is probably related to the accumulation of defects that accompanies the growth of each successive layer. However, it is also possible that this decrease is due to a thickness-dependent orientational change in the film structure; specifically, a more significant tilt of the film away from the surface normal. Evidence for this possibility comes from the appearance of an amide I band at 1656 cm^{-1}, which would be enhanced if the film cants away from the surface normal.[6, 7, 64, 65] The main point, however, is that the spectroscopic, ellipsometric, and contact-angle measurements are all consistent with a six-layer film prepared by successive vapor-phase dosing experiments.

Vapor-phase synthesis of anhydride-based multilayer organic thin films. In this section we describe the synthesis of multilayer films prepared using anhydride intermediates. This study commenced with the preparation of an acid chloride-terminated bilayer film (structure G in Figure 3.2) prepared using the procedure described in the previous section. Figure 3.6a was obtained after dosing

this bilayer with water (Step 1, Figure 3.2). The presence of the carbonyl band at 1710 cm^{-1} is consistent with conversion of the acid chloride to the corresponding acid. Note the absence of the acid chloride band at 1815 cm^{-1} observed in Figure 3.3b.

The acid-terminated bilayer film was activated by exposing it to TFAA vapor (Step 2, Figure 3.2). This results in the C=O stretching band at 1710 cm^{-1} being replaced with two bands at 1807 cm^{-1} and 1735 cm^{-1}, which are characteristic of a carboxylic anhydride (Figure 3.6b).[56, 66, 67] No other changes are observed in the FTIR spectrum, and no change was observed in the ellipsometric thickness of the bilayer after this reaction. These results are consistent with the reaction going to completion.

Structure I (Figure 3.2) was reacted with HMDA vapor to yield a trilayer film (structure J). The reaction between the surface-confined anhydride groups and HMDA is more complicated than those discussed thus far, because the anhydride can undergo two types of reactions with primary amines. As discussed in the previous section, and as represented in Figure 3.2, HMDA should react with the surface principally via a single amine group. If this is

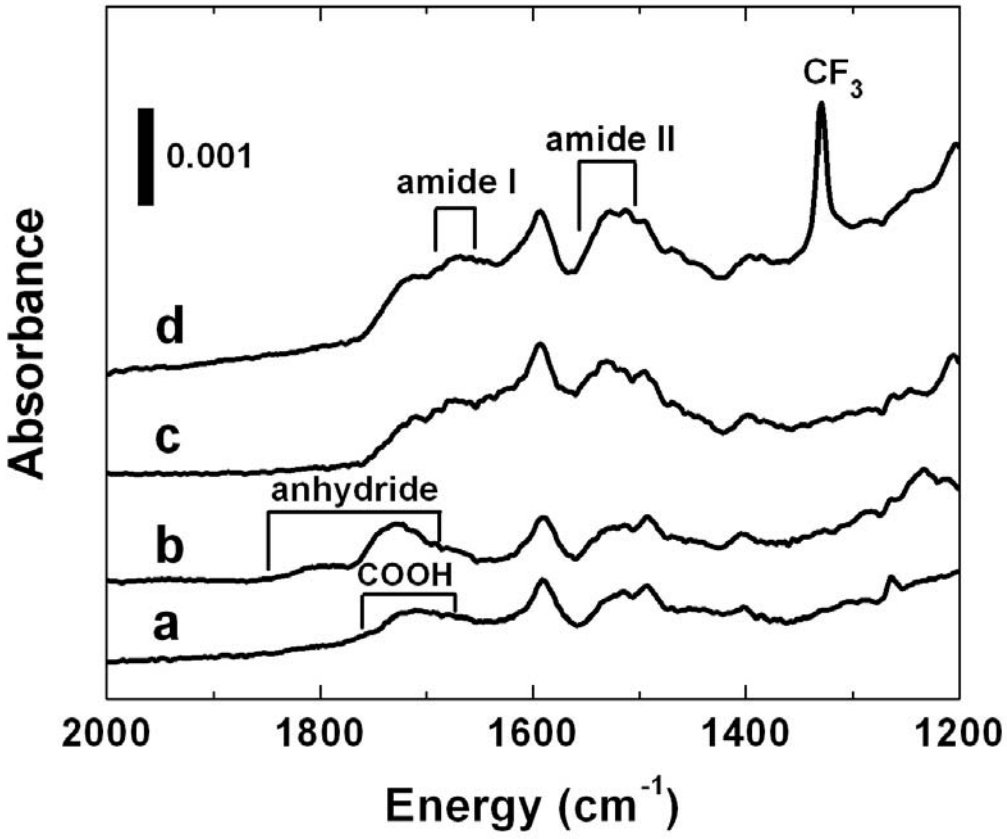

Figure 3.6. FTIR-ERS spectra of (a) structure H, (b) structure I), (c) structure J, and (d) structure K.

true, then half of the HMDA should react with the surface anhydride to form an amide bond and the other half should be immobilized on the surface via an electrostatic interaction with COO^-. The intensity of the amide II band at 1528 cm^{-1} Figure 3.6c) increases by 25% compared to the anhydride-terminated film (Figure 3.6b), and the presence of a broad amide I band can just be detected at 1670 cm^{-1}. The ellipsometric results are also consistent with reaction of the third layer with the surface: the thickness of the film increased from 0.9 nm to 2.2 nm after reaction with HMDA.

The HMDA-modified film was exposed to TFMBC vapor to yield a covalently attached four-layer film (structure K, Figure 3.2). This reaction resulted in a change in the ellipsometric thickness from 2.2 nm to 2.6 nm and increases in the magnitude of aromatic ring and amide II mode by 20 – 25% (Figure 3.6d). The new band at 1329 cm^{-1} arising from the CF_3 group of TFMBC is also apparent after the coupling reaction.

Coverages of the vapor-phase reactions. To determine the coverages (yield) of the four- and six-layer TFMBC-terminated films, we prepared a two-layer film capped with TFMBC using a reliable liquid-phase synthesis (details are

provided in the Experimental Section). If we assume that this film represents 100% coverage of TFMBC, then by comparing the magnitude of the CF_3 IR bands of this film with those prepared via vapor-phase synthesis it is possible to estimate the coverage of the films represented by structures D, F, and K.[7]

The FTIR-ERS spectrum of the bilayer film prepared by liquid-phase reaction is shown in Figure 3.7a. The strong band at 1332 cm^{-1} arises from the symmetric CF_3 stretching mode. The corresponding bands associated with structures D, F, and K (Parts d, c, and b of Figure 3.7, respectively) have relative heights of 46%, 36%, and 38%. These values can be correlated to the coverage of the films prepared by vapor-phase synthesis if two conditions are met. First, the orientation of the CF_3 group relative to the substrate must be the same for all four films, because small differences can affect the magnitude of this band.[7] This condition is satisfied, because the absorbance of the asymmetric CF_3 modes, present at 1177 and 1145 cm^{-1},[63] is very small and nearly constant. This observation is consistent with the axis of the symmetric mode being oriented nearly normal to the substrate surface for all

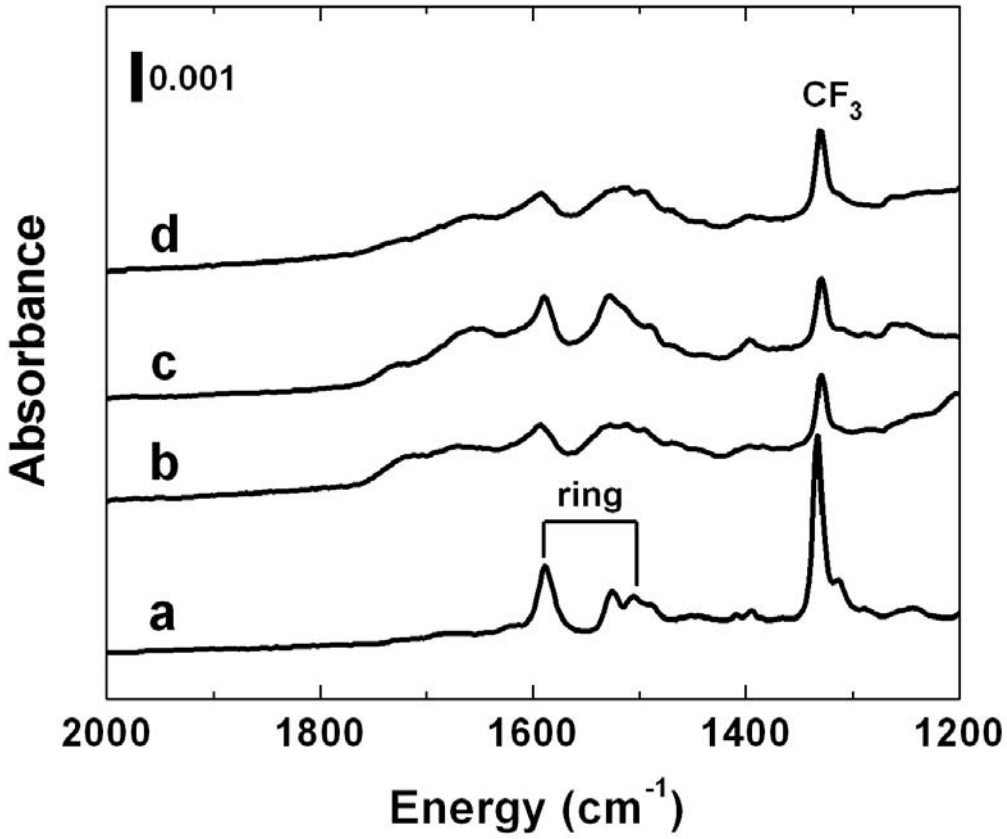

Figure 3.7. FTIR-ERS spectra comparing relative magnitudes of the symmetric CF_3 stretching mode. (a) a trifluoromethyl-terminated bilayer prepared by liquid-phase reaction. (b) Structure K, (c) structure F, and (d) structure D.

films.[63] Second, we must assume that reactions between the films and TFMBC take place with ~100% yield, because otherwise the CF_3 IR signature will not correctly report back the yield of previous reactions.

It is also possible to estimate the extent of the surface reactions using the ellipsometric thickness data shown in Table 1. In this case, it is also necessary to make a number of assumptions. First, the individual oligomers comprising the films must have a known orientation with respect to the surface; from the IR data we know this condition is satisfied. Second, only the oligomers that comprise the films and void space may be present on the surface. The presence of water within the films (recall that the ellipsometric thicknesses were measured in air) will change the effective medium approximation[68] and distort the linear correlation between film thickness and extent of reaction upon which this analysis relies. Third, it is necessary to assume a single index of refraction (1.46 in this case) for all of the films. With these three caveats, the thickness data give estimated yields for films D, F, and K of 89%, 76%, and 96%, respectively. Clearly these values are substantially higher than those estimated from the spectroscopic results.

There is only one reasonable situation that is consistent with both the IR and ellipsometry data. If all of the reactions, except for the final CF_3 capping reaction, go to completion, then the film thickness will be consistent with the calculated values but the IR data, which relies on the presence of the CF_3 group, will indicate a low yield. We view this scenario as possible but improbable given that TFMBC couples to the amine-terminated film via the same chemistry that is responsible for the other coupling reactions. On the basis of previous results,[7] therefore, we tend to have more confidence in the IR data. Clearly, however, the results reported here show that it is difficult to measure the yields of surface reactions of this type with a high degree of accuracy.

3.4 Summary and Conclusions

Here we have shown that covalently linked films up to six monomer units in length can be prepared on a solid support using vapor-phase reactions. These films have surface coverages ranging from about one-third to one-half of full coverage, which is quite encouraging considering the number of synthetic steps that are involved and that error propagation limits the coverage of any film prepared

by sequential reaction. We have also shown that a number of reactions routinely used in liquid-phase synthesis are also effective for vapor-phase reactions. These include reactions between acid chlorides and both aliphatic and aromatic amine, hydrolysis reactions, anhydride activation, and reactions between anhydrides and primary amines. Finally, we demonstrated that homobifunctionalized monomers, such as HMDA, react primarily via a single functional group rather than cross coupling on the reactive surface.

This approach for preparing organic thin films may find use in some technological applications where the trade-off between film quality and convenience is positive.

CHAPTER IV

SYNTHESIS, CHARACTERIZATION, AND SURFACE IMMOBILIZATION OF METAL NANOPARTICLES ENCAPSULATED WITHIN BIFUNCTIONALIZED DENDRIMERS*

4.1 Introduction

Here, we report on the advantages of using partially quaternized poly(amidoamine) (PAMAM) dendrimers for preparing dendrimer–encapsulated nanoparticles (DENs) and for linking DENs to surfaces. Specifically, we have found that DENs prepared using amine-terminated PAMAM dendrimers that have been partially quaternized (Gn-Q_p, where n is the dendrimer generation and p is the number of the peripheral amine groups that have been quaternized) lead to formation of DENs having a significantly narrower size distribution than DENs prepared using commercially available, amine-terminated PAMAM dendrimers. Moreover, because the surface of Gn-Q_p bifunctional dendrimers is only partially quaternized, the remaining amine groups can be used to covalently link DENs to other polymers, biomolecules, or,

---

* Reprinted with permission from Oh, S.-K.; Kim, Y.-G.; Ye, H.; Crooks, R. M. *Langmuir* **2003**, *19*, 10420-10425: copyright 2003 American Chemical Society.

as we show here, monolithic solid surfaces.

Nanometer-scale metal and semiconductor particles sometimes exhibit unique physical or chemical properties that are interesting in their own right, but that also hold out the promise of technological advances in fields such as catalysis, sensors, electronics, and biotechnology.[23,69,70] Applications such as these require simple synthetic approaches for preparing highly uniform nanomaterials. A number of methods have been reported for preparing metal nanoparticles in the <3 nm size range,[71,72] but only a few of these result in materials having monodispersities in range of ± 20%.[73-75] In addition to uniformity, many technological applications also require that nanomaterials be linked to one-another or to monolithic solid supports.[76-78] Typical methods for immobilizing nanoparticles onto surfaces involve adsorption onto substrates coated with functional groups that induce electrostatic interactions[79-81] or covalent bonds[82-90] between the nanoparticle and the surface.

Dendrimers have been used as templates for preparing metallic, bimetallic, and semiconductor nanoparticles.[11,15,91] DENs are prepared in a two-step process. First, metal ions are sequestered within the dendrimer, and then the ions are reduced. Because the synthesis relies on a dendrimeric

template, the resulting metal nanoparticle (the replica) can be quite monodisperse in size. The ability of high-generation dendrimers to host metal nanoparticles is attributable to their spheroidal structure, which contains void spaces and functional groups that are able to complex with metal ions. Specifically, Cu, Pd, Pt, Ag, and Au DENs can be prepared within the interior of PAMAM dendrimers.[14,73,92-96] The structure of metal-dendrimer nanocomposites depends on the nature of the terminal groups of the dendrimers. For example, amine peripheral groups usually (but not always)[97] induce agglomeration and precipitation of large metal clusters of Pd and Pt. This is most likely because metal ions complex with the periphery of amine-terminated dendrimers, which typically results in rather large (>5 nm) metal clusters stabilized by multiple dendrimers.[98]

One approach for preventing metal-ion complexation is to selectively protonate peripheral primary amine groups.[99,100] However, this requires a restrictive pH window, which can be a nuisance for many applications. Accordingly, dendrimers having non-complexing functional groups on their periphery, such as hydroxyl-terminated PAMAM dendrimers, are most often used for preparing relatively small (<2 nm),

and in some cases nearly size-monodisperse, DENs. However, there are two drawbacks of using hydroxyl-terminated dendrimer for preparing DENs. First, hydroxyl groups themselves are fairly good reducing agents.[94,101] This makes it very difficult to prepare, for example, monodisperse Au DENs using hydroxyl-terminated dendrimers.[102] Second, hydroxyl groups are not very reactive, which makes it difficult to covalently link DENs prepared within such materials to other molecules or objects. Note, however, that such materials have been immobilized on solid surfaces by electrostatic interactions.[103-108]

This paper describes the use of dendrimers for templating, stabilizing, and immobilizing onto surfaces 1-2 nm metal nanoparticles having a narrow size distribution. Specifically, we found that partially quaternized PAMAM dendrimers, Gn-Q_p, are an attractive template for preparing highly monodisperse Pd and Pt nanoparticles because of the high positive charge at the dendrimer periphery, which prevents metal ion-induced interdendrimer agglomeration. In addition, Pd and Pt DENs can be immobilized onto Au surfaces via covalent amide bond formation between the unquaternized amine groups on the dendrimer periphery and anhydride-activated self-assembled monolayers (SAMs). In

this approach, the dendrimers act as a mediator for linking metal nanoparticles to monolithic solid surfaces. Covalent attachment was confirmed by investigating the stability of Pd and Pt DEN monolayers.

4.2 Experimental Section

Chemicals and materials. Fourth-generation poly(amidoamine) (PAMAM) dendrimers having amine terminal groups (G4-NH_2) were obtained from Dendritech, Inc. (Midland, MI) as a 17.3% wt/wt solution in methanol. The methanol was removed under vacuum prior to use. The following chemicals were used as received: Glycidyltrimethylammonium chloride (~90%, Fluka Chemie AG), K_2PdCl_4 (99.99%, Aldrich Chemical Co., Milwaukee, WI), K_2PtCl_4 (99.9%-Pt, Strem Chemicals, Inc., Newburyport, MA), $NaBH_4$ (99%, Aldrich), methanol (EM Science), mercaptoundecanoic acid (MUA) (95%, Aldrich), ethyl chloroformate (97%, Aldrich), 4-methylmorpholine (99%, Aldrich), and $CHCl_3$ (99.8%, EM Science). Cellulose dialysis sacks having a molecular weight cut off of 1.2 x 10^4 were purchased from Sigma Diagnostics, Inc. (St. Louis, MO). 18 MΩ·cm water (Milli-Q, Millipore, Bedford, MA) was

used to prepare aqueous solutions. Au-coated substrates were prepared by electron-beam evaporation of 10 nm of Ti followed by 200 nm of Au onto Si(100) wafers (Lance Goddard Associates, Foster City, CA). The wafers were subsequently diced into 2.6 cm x 1.3 cm pieces. Before each experiment all wafers were cleaned in a low-energy ozone cleaner for 10 min (Boekel Industries, Inc., model 135500).

Synthesis of polycationic dendrimers. Partially quaternized, fourth-generation PAMAM dendrimers (G4-Q_p) were prepared by reacting G4-NH_2, which carries 64 terminal primary amines, with 64 equiv of glycidyltrimethylammonium chloride. The synthetic procedure used is similar to one previously reported in the literature.[109] G4-NH_2 (0.39 g, 27.4 µmol) was dissolved in 10 mL of methanol and 0.27 g (1.75 mmol) of glycidyltrimethylammonium chloride was added dropwise with stirring. The reaction mixture was stirred for 2 days at 40 $^{\circ}$C, and then methanol was removed by rotary evaporation. The crude product was redissolved in 30 mL of water and the solution was purified by dialysis against water for 24 h. The final product was dried in vacuum to give 0.5 g (96% yield) of G4-Q_{32} as a white viscous solid. Using the same synthetic procedure, G6-Q_{116}

was prepared by reaction of G6-NH_2 with 256 equiv of glycidyltrimethylammonium chloride (97% yield). The chemical structures of G4-Q_{32} and G6-Q_{116} were confirmed by ^{1}H and ^{13}C NMR, and (for G4-Q_{32}) MALDI-MS spectra (see the Supporting Information).

Characterization and instrumentation. ^{1}H and ^{13}C NMR spectra were collected on a Varian Inova 500 MHz Spectrometer at 500.1 MHz and 125.8 MHz, respectively. CD_3OD was used as an internal standard for the NMR analyses. MALDI-MS were recorded on a Voyager Elite XL MALDI time-of-flight mass spectrometer outfitted with a 337 nm pulsed nitrogen laser. 2′,4′,6′-Trihydroxyacetophenone was used as the MALDI matrix. Complexation between aqueous metal ions and dendrimers was monitored with an HP8453 UV-vis absorption spectrophotometer. High-resolution transmission electron micrographs (HRTEM) were obtained using a JEOL-2010 transmission electron microscope having a point-to-point resolution of 0.19 nm. Samples were prepared by placing a drop of DEN solution on a carbon-coated Cu TEM grid (400 mesh, Electron Microscopy Science, Fort Washington, PA) and allowing the solvent to evaporate in air. FTIR-external reflection spectroscopy (FTIR-ERS) measurements were carried out using an FTS-6000

spectrometer (Bio-Rad, Cambridge, MA) equipped with a Harrick Scientific Seagull reflection accessory (Ossining, NY) and a liquid-N_2-cooled, narrow-band MCT detector. All spectra were obtained at 4 cm^{-1} resolution using *p*-polarized light at an 84° angle of incidence with respect to the substrate normal. Electrochemical experiments were performed in a single-compartment, glass cell using a standard three-electrode configuration with a Pt-gauze counter electrode and a Ag/AgCl (3 M NaCl) reference electrode (Bioanalytical Systems, West Lafayette, IN). Cyclic voltammetry was performed using a computer-controlled potentiostat (Model 660A, CH Instruments, Austin, TX) to monitor the stability of DENs on Au surfaces.

Preparation of dendrimer-encapsulated Pd and Pt nanoparticles. The preparation of G4-Q_{32}/Pd and G4-Q_{32}/Pt DENs followed procedures we have previously reported for preparing metal nanoparticles encapsulated within hydroxyl-terminated PAMAM dendrimers (G4-OH).[73,93,110] Briefly, to 8.9 mL of water was added 0.5 mL of a 1 mM G4-Q_{32} aqueous solution, and subsequently 0.2 mL of a 0.1 M K_2PdCl_4 (or 0.1 M K_2PtCl_4) aqueous solution. After stirring for 30 min (or 48 h in case of K_2PtCl_4), 0.4 mL of a 1.0 M $NaBH_4$ aqueous

solution was added. The resulting dark brown solution was purified by dialysis against water for 18 h to give G4-$Q_{32}(Pd_{40})$ (or G4-$Q_{32}(Pt_{40})$), which contain an average of 40 metal atoms per dendrimer.

Surface modification. Surface-immobilized DENs were prepared by covalently linking G4-$Q_{32}(Pd_{40})$ to a self-assembled mercaptoundecanoic acid (MUA) monolayer. The monolayer was prepared by immersing an ozone-cleaned Au substrate in a 1 mM ethanol solution of MUA for 6 h. The resulting MUA SAM was activated in a $CHCl_3$ solution containing 10 mM ethyl chloroformate and triethylamine for 1 h.[111, 112] DENs were covalently linked to the activated monolayer by soaking it in a 5 mM aqueous solution of G4-$Q_{32}(Pd_{40})$ for 6 h, followed by rinsing with water and ethanol, and then drying with N_2. As a control experiment to confirm covalent attachment of DENs, G4-$Q_{32}(Pd_{40})$ monolayers on MUA SAMs were prepared using the same procedure, but activation with ethyl chloroformate was omitted.

4.3 Results and Discussion

Synthesis of polycationic, bifunctionalized dendrimers. Our objective in this work was to develop a dendrimer that

could serve as a template for preparing DENs and also have a sufficiently reactive periphery that it could subsequently be covalently attached to solid surfaces, biomolecules, or other types of polymers. We reasoned that partial quaternization of amine-terminated PAMAM dendrimers would be the simplest way to achieve this goal for the following reasons. First, modification of the periphery should not change the desirable templating properties of the PAMAM interior. Second, partial quaternization of the periphery should prevent interdendrimer complexation of metal ions, because of the poor metal-ion complexing ability of quaternized amines[113,114] as well as the electrostatic repulsion between the positively charged dendrimers. Note that in the absence of quaternization, except over a fairly narrow pH range,[100] the surface of amine-terminated dendrimers has a strong affinity for metal ions. This leads to interdendrimer crosslinking and subsequent precipitation, and therefore it is not possible to prepare small, monodisperse DENs.[103] Third, the remaining unquaternized amines on the dendrimer surface should be sufficiently reactive to form covalent bonds under appropriate conditions.

To synthesize polycationic dendrimers, G4-NH_2 having 64 peripheral amine groups was reacted with glycidyltrimethylammonium chloride to yield pendant quaternary ammonium groups (Figure 4.1a). The product was characterized using ^{1}H and ^{13}C NMR and MALDI-MS analyses (Figures 4.1 – 4.3), and the extent of quaternization of the G4-NH_2 periphery was calculated from ^{1}H NMR integration. Comparison of the area of the methine proton (δ = 4.28 ppm) adjacent to the hydroxyl group (Figure 4.1) versus the area of the methylene protons (δ = 2.42 ppm) associated with the dendrimer backbone reveals that, on average, ~34 of the amine-terminal groups of G4-NH_2 are modified with quaternary ammonium groups (~53% functionalization). MALDI-MS of the functionalized dendrimer reveals the molecular ion peak at 18,735 m/z (Figure 4.3). This value corresponds to G4-NH_2 having ~30 quaternary ammonium groups (47% functionalization) on the periphery. We estimate the extent of surface functionalization at 50% by taking the average of the MALDI-MS and NMR data (here we denote the dendrimer as G4-Q_{32}). We also prepared the sixth-generation equivalent of G4-Q_{32}, G6-Q_p, and from NMR the extent of surface functionalization was estimated to be 45%. It is important to note that although 64 and 256 equiv of the

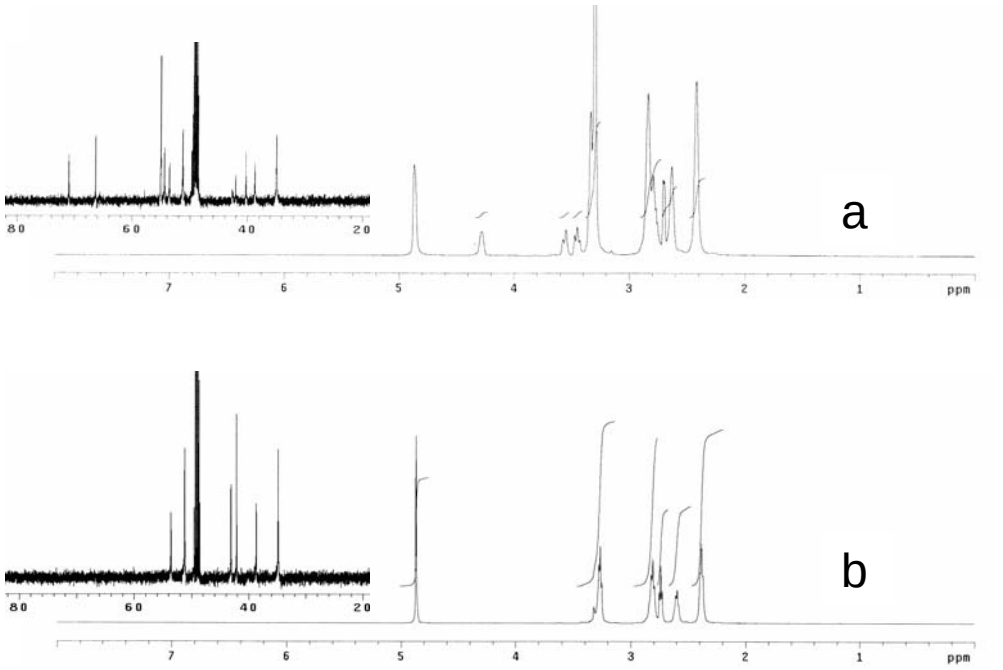

Figure 4.1. ^{1}H NMR (500 MHz, CD_3OD) spectra of (a) G4-Q_{32} and (b) G4-NH_2. The inset is the ^{13}C NMR spectrum of each compound. ^{1}H chemical shift assignments for G4-Q_{32}: δ 2.42 (-$\underline{CH_2}$-CONH-, protons within the dendrimer backbone), δ 2.70 (-NH-$\underline{CH_2}$-CH(-OH)-), δ 3.30 (-CH_2-N($\underline{CH_3}$)$_3$Cl, overlapped with protons within the dendrimer backbone), δ 3.45 and 3.55 (-$\underline{CH_2}$-N(CH_3)$_3$Cl), δ 4.28 (-NH-CH_2-$\underline{CH}$(-OH)-). The observed integration ratio between peaks at δ 2.42 and 4.28 is 248:34 (the calculated ratio for a fully functionalized dendrimer, G4-Q_{64}, is 248:64).

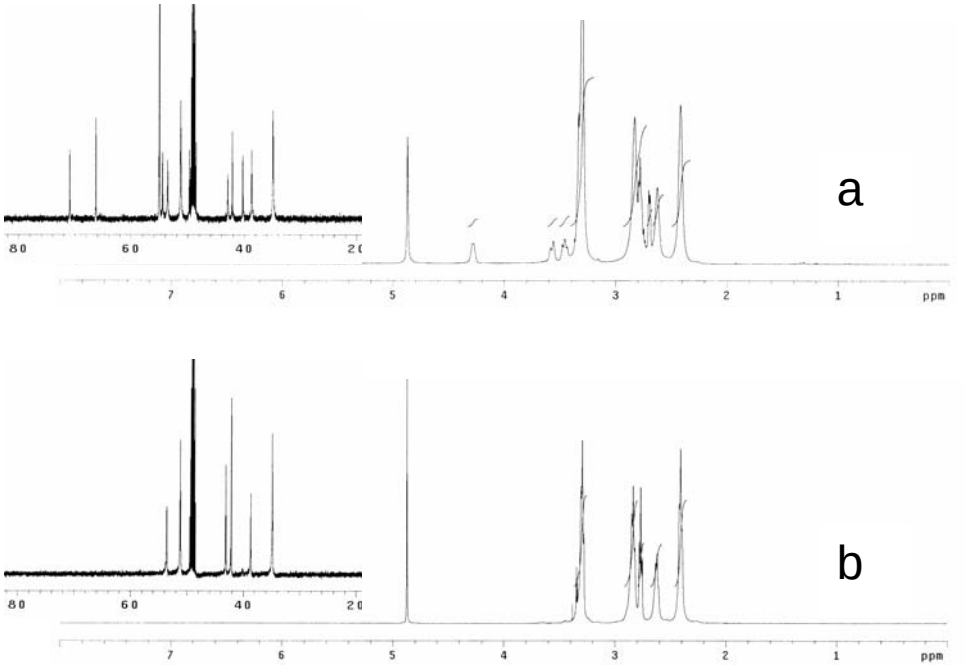

Figure 4.2. ^{1}H NMR (500 MHz, CD_3OD) spectra of (a) G6-Q_{116} and (b) G6-NH_2. The inset is the ^{13}C NMR spectrum of each compound. ^{1}H chemical shift assignments for G6-Q_{116}: δ 2.42 (-$\underline{CH_2}$-CONH-, protons within the dendrimer backbone), δ 2.70 (-NH-$\underline{CH_2}$-CH(-OH)-), δ 3.30 (-CH_2-N($\underline{CH_3}$)$_3$Cl, overlapped with protons within the dendrimer backbone), δ 3.46 and 3.56 (-$\underline{CH_2}$-N(CH_3)$_3$Cl), δ 4.28 (-NH-CH_2-$\underline{CH}$(-OH)-). The observed integration ratio between peaks at δ 2.42 and 4.28 is 1016:116 (the calculated ratio for a fully functionalized dendrimer, G6-Q_{256}, is 1016:256).

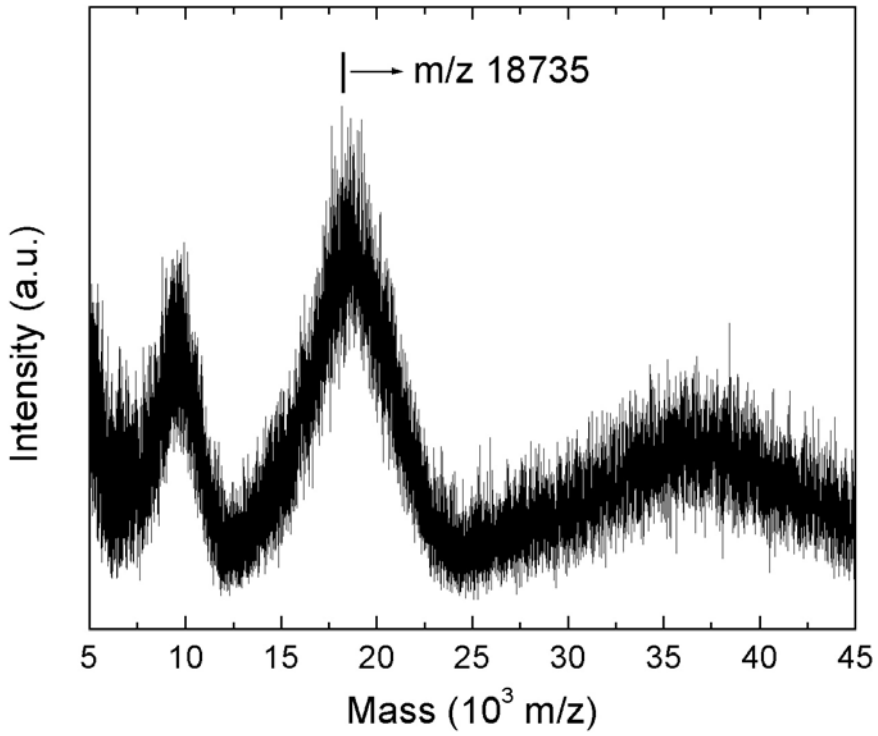

Figure 4.3. MALDI-MS of G4-Q_{32}. The spectrum was recorded on a Voyager Elite XL MALDI time-of-flight mass spectrometer outfitted with a 337 nm pulsed nitrogen laser. 2′,4′,6′-Trihydroxyacetophenone was used as the MALDI matrix. The calculated molecular weight for G4-Q_{32} is 19070.

epoxide derivative were used for the synthesis of G4-Q_p and G6-Q_p, respectively, the extent of functionalization was still only ~50%. Control experiments indicate that this is a consequence of reduced reactivity of the partially functionalized dendrimer, which is likely due to electrostatic repulsion between positively charged reactants in solution and the partially reacted, positively charged dendrimer surface. For example, the reaction of G4-NH_2 with 64 equiv of *t*-butyl glycidyl ether, which is an uncharged analog of glycidyltrimethylammonium chloride, results in 100% surface functionalization.

Preparation and characterization of polycationic, bifunctionalized DENs. The approach for preparing nanoparticles within polycationic dendrimers is similar to that used for hydoxyl-terminated PAMAM dendrimers.[73, 93, 110] Specifically, metal ions are extracted from solution into the dendrimer interior, and then the encapsulated metal ions are chemically reduced to yield an encapsulated, zerovalent nanoparticle. Figure 4.4 shows UV-vis absorbance spectra of aqueous solutions of dendrimers each containing, on average, 40 Pd^{2+} or Pt^{2+} ions (we denote all possible complex ions in solution and within the dendrimer as Pd^{2+} or Pt^{2+})[115] encapsulated within G4-Q_{32} before (G4-

$Q_{32}(Pd^{2+})_{40}$ and G4-$Q_{32}(Pt^{2+})_{40}$, respectively) and after (G4-$Q_{32}(Pd_{40})$ and G4-$Q_{32}(Pt_{40})$, respectively) reduction with BH_4^-. In the case of Pd^{2+} (Figure 4.4a), an absorption band, which corresponds to the ligand-to-metal charge transfer transition between Pd^{2+} and tertiary amine ligands within the dendrimer, is present at 225 nm prior to reduction. After chemical reduction, this band is greatly diminished and a featureless interband transition, corresponding to zerovalent Pd nanoparticles, is observed as a monotonically increasing absorption toward higher energy.[73,116] In addition, the color of the solution turns from pale yellow prior to reduction to dark brown after reduction. No sign of agglomeration or precipitation is observed. Taken together with previous reports of Pd DENs prepared within hydroxyl-terminated PAMAM dendrimers,[73] these results are indicative of encapsulation of Pd nanoparticles within individual dendrimers. Similar spectroscopic behavior (Figure 4.4b) is observed for G4-$Q_{32}(Pt^{2+})_{40}$ and G4-$Q_{32}(Pt_{40})$, except that the ligand-exchange reaction that leads to complexation between Pt^{2+} and the dendrimer is much slower. Control experiments performed under the same conditions, but using unquaternized G4-NH_2 PAMAM dendrimers, lead to immediate precipitation when the reducing agent is added.

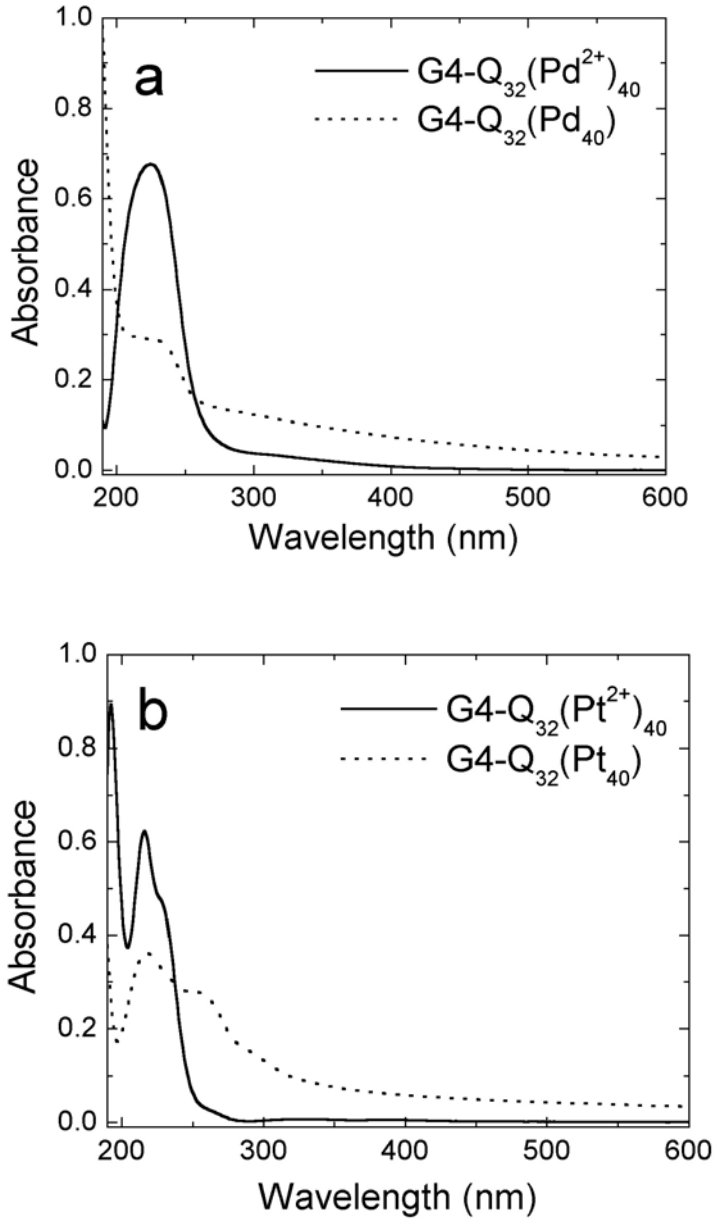

Figure 4.4. UV-vis absorption spectra of aqueous solutions containing (a) Pd^{2+} and (b) Pt^{2+} and G4-Q_{32} before (solid line) and after (dashed line) chemical reduction with $NaBH_4$. An aqueous solution of G4-Q_{32} was used to obtain the background spectrum.

These results strongly suggest that repulsive electrostatic interactions between positively charged dendrimers, along with the poor metal-ion complexing ability of quaternized amines, play an important role in preventing agglomeration of metal nanoparticles.[114]

Figure 4.5 presents HRTEM images and particle size distributions for Pd and Pt nanoparticles prepared within G4-Q_{32}. The images indicate that these particles are well separated, which is a likely consequence of the high electrostatic charge on the host dendrimers, and that they are nearly monodisperse in size. The mean diameters and standard deviations (1σ) for the G4-Q_{32}(Pd_{40}) (Figure 4.5b) and G4-Q_{32}(Pt_{40}) (Figure 4.5d) nanoparticles are both 1.7 ± 0.3 nm. Note that all these sizes are significantly larger than expected for a roughly spherical 40-atom metal particle (~1.1 nm), but the results are fully consistent with our previous results for Pt and Pd DENs prepared within fourth-generation hydroxyl-terminated PAMAM dendrimers (G4-OH).[73,93,110] Specifically, we found that the mean diameters for G4-OH(Pd_{40}) and G4-OH(Pt_{40}) are in the range of 1.3-1.7 nm and their standard deviations are ± 0.2-0.3 nm.[11]

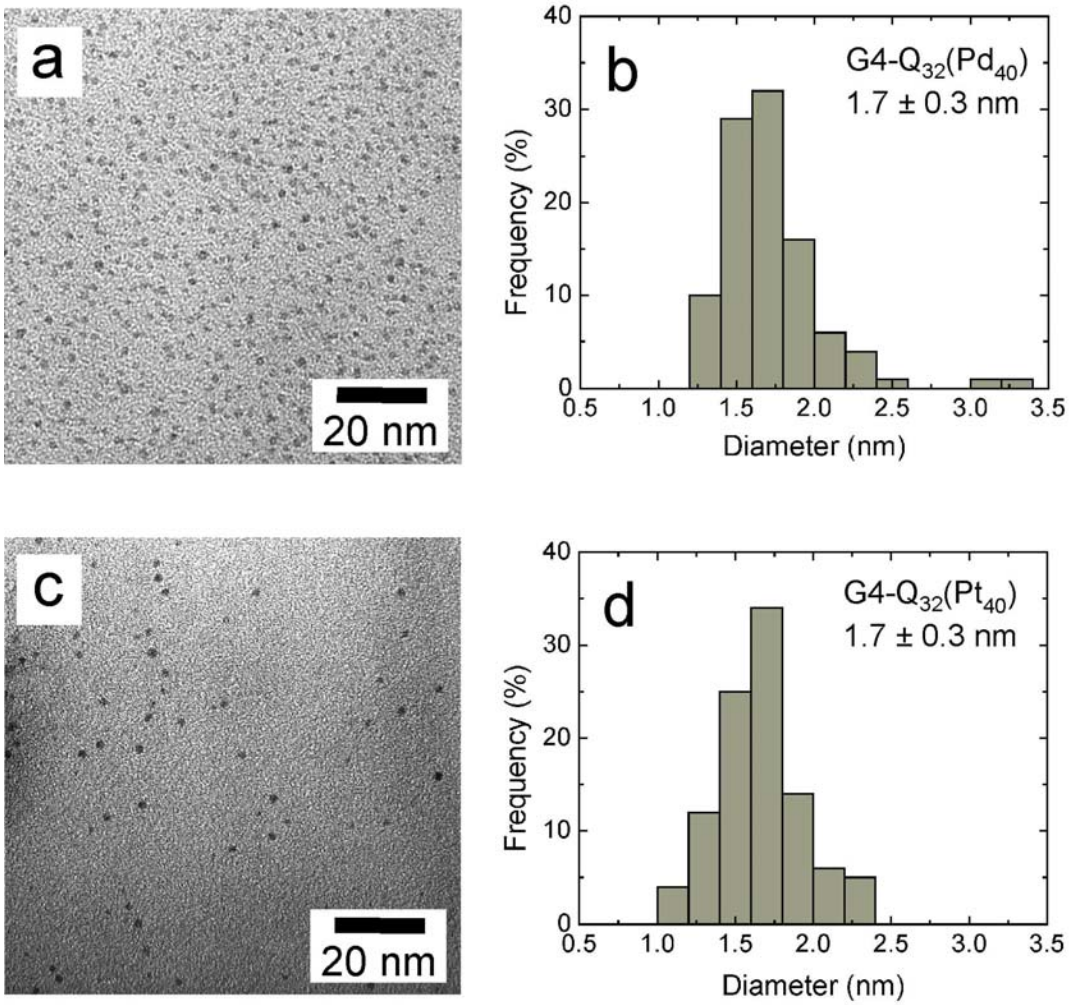

Figure 4.5. HRTEM images of (a) G4-$Q_{32}(Pd_{40})$ and (c) G4-$Q_{32}(Pt_{40})$ and corresponding particle size distributions of (b) G4-$Q_{32}(Pd_{40})$ and (d) G4-$Q_{32}(Pt_{40})$. The average particle size and distribution were determined by counting 100 metal particles.

Similarly, Li and El-Sayed prepared G4-OH(Pd_{10}) having 1.4 ± 0.4 nm in diameter.[74] Note that Au nanoparticles prepared in either G4-Q_{32} or G6-Q_{116} have sizes that correspond nearly exactly with expectations.[45] This suggests that there is something peculiar about Pt and Pd DENs that we do not understand at the present time.

Surface immobilization of polycationic, bifunctionalized DENs. Previous studies have shown that amine-terminated dendrimers can be easily covalently linked to Au surfaces via an intermediary SAM adhesion layer.[111,112] The method involves formation of a mercaptoundecanoic (MUA) SAM on an Au surface, activation of the distal carboxylic acid groups using ethyl chloroformate, and then reaction of this activated monolayer with primary amine groups on the dendrimer periphery. We thought it would be possible to use this same approach (Figure 4.6) to covalently link G4-Q_{32}(Pd_{40}) to Au surfaces, because G4-Q_{32} contains ~32 unfunctionalized primary amine groups at its periphery. The spectra shown in Figure 4.7 confirm this expectation. Spectrum ***a*** was obtained from the activated MUA SAM. The peaks at 1822 and 1746 cm^{-1} correspond to the anhydride carbonyl bands.[117] After reaction of the activated SAM with

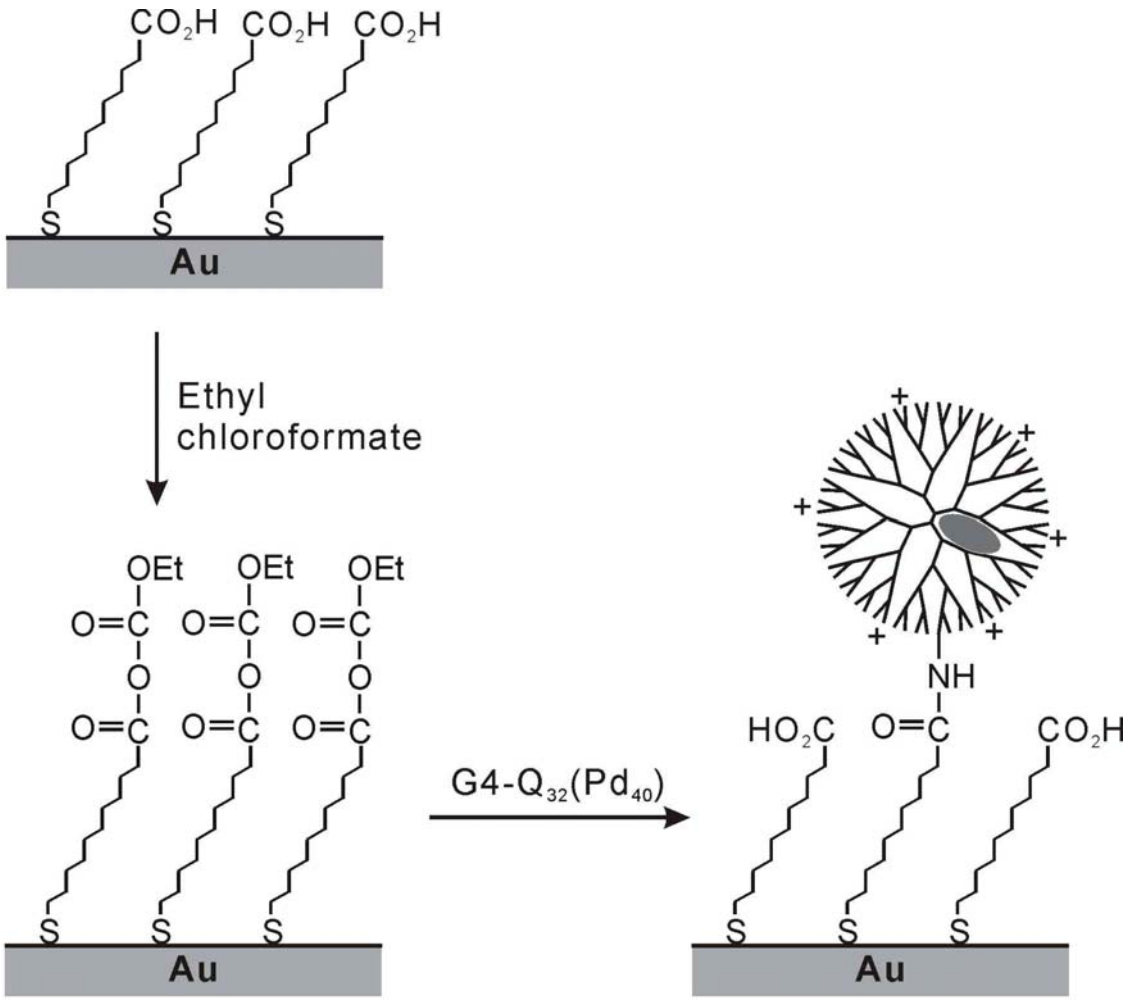

Figure 4.6. The procedures for the covalent attachment of amine-terminated dendrimer.

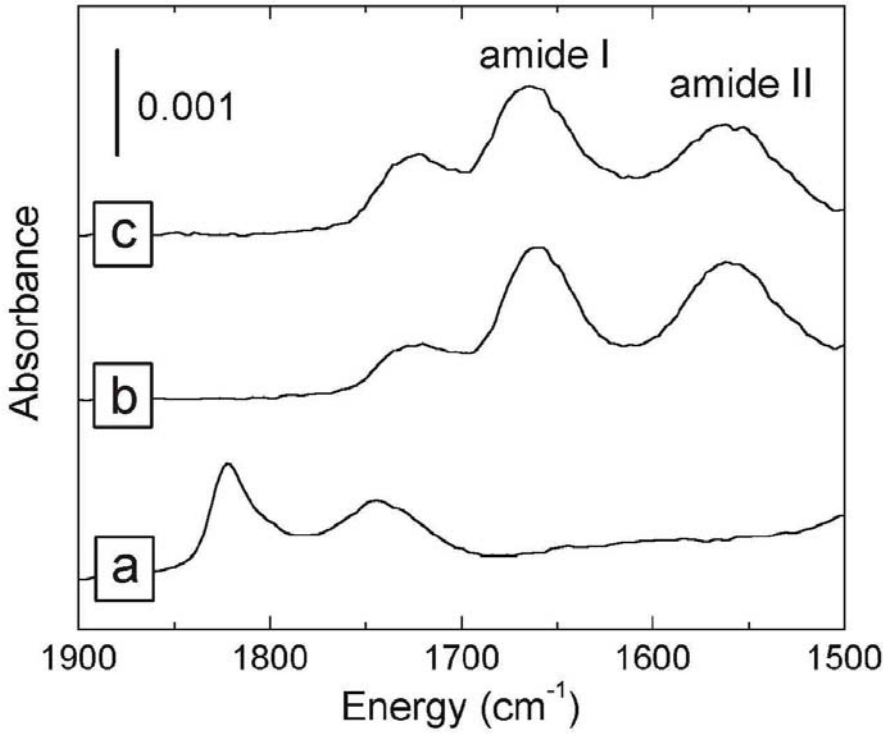

Figure 4.7. FTIR-ERS spectra of G4-$Q_{32}(Pd_{40})$ immobilized on anhydride-activated MUA SAMs. (a) An anhydride-activated MUA SAM. (b) A G4-$Q_{32}(Pd_{40})$ monolayer. (c) A G4-$Q_{32}(Pd_{40})$ monolayer after 20 continuous electrochemical scans between ± 0.6 V (vs. Ag/AgCl, 3 M NaCl). Cyclic voltammetric experiments were carried out in an aqueous electrolyte solution of 0.1 M Na_2SO_4 at 100 mV/s.

G4-$Q_{32}(Pd_{40})$ in water, these bands are replaced by three new peaks at 1723, 1661, and 1560 cm^{-1} (Spectrum ***b***). The peak at 1723 cm^{-1} arises from the carbonyl band of MUA, which is present as a consequence of partial hydrolysis of the activated monolayer.[112] The appearance of the amide I and II peaks at 1661 and 1560 cm^{-1}, respectively, arise from both the internal structure of G4-Q_{32} and the amide bonds formed by the reaction between the anhydride-activated SAM and the peripheral amines of G4-Q_{32}. It is possible to estimate the dendrimer coverage on the SAM surface by comparing the amide-band intensity to that of a full dendrimer monolayer physisorbed to a Au surface.[118] The results indicate that ~40% of maximum DEN coverage is attained in the experiment represented by Figure 4.7b.

The presence of metal nanoparticles on the MUA SAM was confirmed by X-ray photoelectron spectroscopy (XPS). The XPS analysis was carried out using G4-$Q_{32}(Pt_{40})$ instead of G4-$Q_{32}(Pd_{40})$, because the Pd($3d_{5/2}$) peak overlaps with the Au($4d_{5/2}$) substrate peak. The important point is that the XPS spectrum of G4-$Q_{32}(Pt)_{40}$ immobilized on an anhydride-activated MUA SAM provides clear evidence for the presence of zerovalent Pt in the monolayer (Figure 4.8).

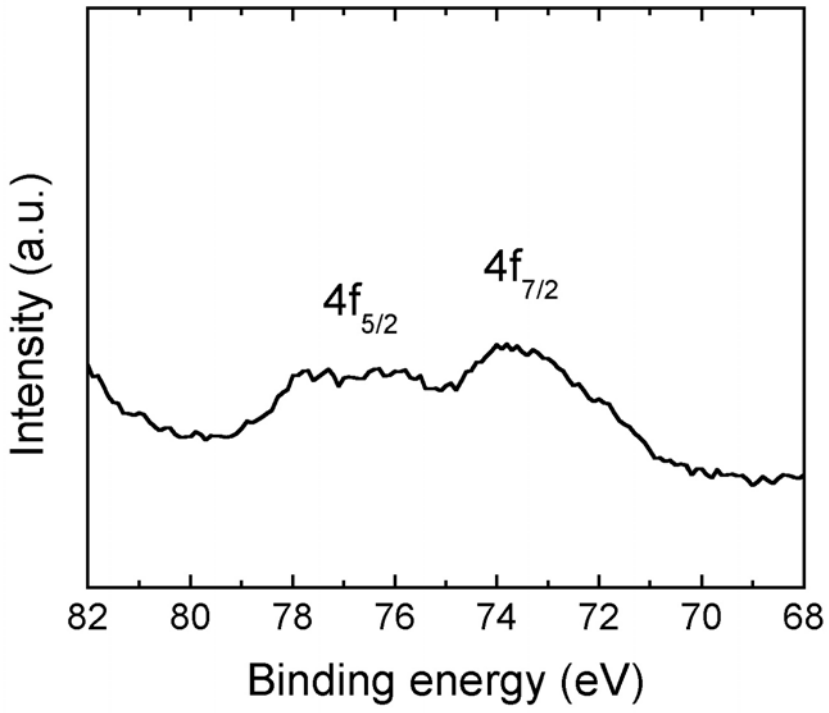

Figure 4.8. XPS spectrum of G4-$Q_{32}(Pt)_{40}$ immobilized on an anhydride-activated MUA SAM. XPS measurements were carried out using an Axis HSi 165 Ultra (Kratos Analytical, Manchester, UK) XPS spectrometer. The survey scan and Pt(4f) core level spectra were recorded with Al *K* radiation and the anode was operated at 15 mA and 15 kV. The XPS peak positions were referenced to the Au($4f_{7/2}$) peak at 83.8 eV. The Pt($4f_{7/2}$) peak is shifted 2.5 eV toward higher binding energy relative to that of bulk Pt (71.2 eV). The shift in the binding energy is likely related to the small size of the Pt nanoparticles and may also be a consequence of the presence of amine groups within the dendrimer interacting with the Pt surface (Eberhardt, W. ***et al. Phys. Rev. Lett.*** **1990**, *64*, 780-783; Fu, X. ***et al. J. Colloid Interface Sci.*** **2001**, *243*, 326-330).

To confirm covalent attachment of G4-$Q_{32}(Pd_{40})$ to the SAM, we carried out a series of experiments to test the stability of the DEN monolayers. First, because we are interested in using surfaces such as these for electrocatalysis, we investigated the effect of electrochemical potential on the stability of the monolayer. As shown Spectrum ***c*** in Figure 4.7, the magnitude of the amide I peak decreases by only ~10% even after 20 successive electrochemical scans between ±0.6 V (vs. Ag/AgCl, 3 M NaCl). This level of stability can be compared to our previous results involving monolayers of Pt DENs prepared within hydroxyl-terminated PAMAM dendrimers adsorbed to Au electrodes.[93] There, we observed that most of the DEN monolayer desorbed after only one voltammetric scan between −0.2 and +0.6 V.[119] The enhanced stability here is likely a consequence of the covalent attachment of G4-Q_{32} to the SAM.

In a second set of control experiments, we compared the stability of G4-$Q_{32}(Pd_{40})$ monolayers immobilized on both unactivated and anhydride-activated MUA SAMs. FTIR-ERS spectra ***a*** and ***b*** in Figure 4.9 were obtained from a G4-$Q_{32}(Pd_{40})$ monolayer on an anhydride-activated MUA SAM before and after, respectively, sonication in an aqueous HCl

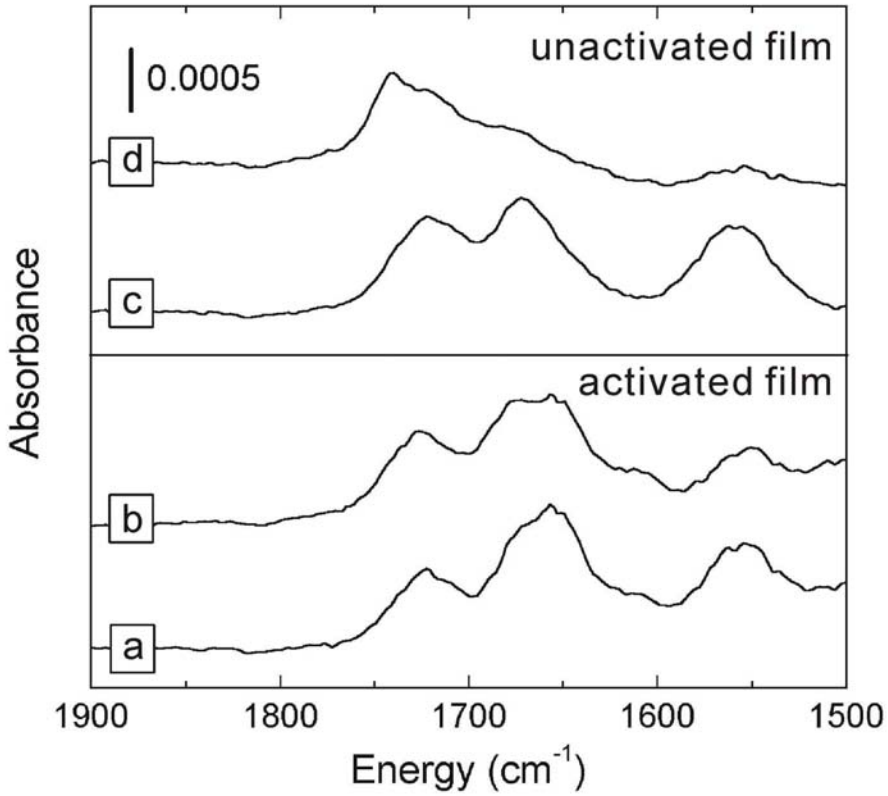

Figure 4.9. FTIR-ERS spectra of G4-$Q_{32}(Pd_{40})$ immobilized on (a and b) anhydride-activated MUA SAMs and (c and d) unactivated MUA SAMs (a and c) before and (b and d) after sonication in an aqueous HCl solution (pH = 2.0) for 5 min.

Table 4.1. Adsorption stability of G4-Q_{32}, G4-NH_2, and G4-OH monolayers immobilized on anhydride-activated MUA SAMs.

Treatment	Percentage decrease of amide I peak[a]		
	G4-Q_{32}	G4-NH_2	G4-OH
Sonication[b]	0.4	3.0	5.3
Sonication + Acid[c]	2.3	3.8	6.2
Voltametric scans[d]	9.0	13	41

[a]The percentage decrease is based on the relative intensity of the amide I peak before and after each treatment.
[b]Sonication in H_2O for 5 min.
[c]Sonication in an aqueous HCl solution (pH = 2.0) for 5 min.
[d]20 continuous electrochemical scans between ± 0.6 V (vs. Ag/AgCl, 3 M NaCl). The scan rate was 100 mV/s and the aqueous electrolyte solution contained 0.1 M Na_2SO_4.
[e]Not determined.

solution (pH = 2.0) for 5 min. The spectra show that ~85% of the amide bands at 1661 and 1560 cm^{-1} remain. In contrast, the intensity of the amide bands of a G4-Q_{32}(Pd_{40}) monolayer prepared on an unactivated MUA SAM (spectrum ***c*** in Figure 4.9) are almost entirely eliminated by the same acid treatment (spectrum ***d*** in Figure 4.9), suggesting that in this case G4-Q_{32}(Pd_{40}) is attached to the surface only by electrostatic interactions between the peripheral cationic groups of G4-Q_{32} and the carboxylate groups of the MUA SAM.

In a third set of control experiments, we compared the stability of a G4-Q_{32} monolayer to that of G4-NH_2 and G4-OH monolayers (Table 4.1). Because it was not possible to prepare Pt or Pd nanoparticles within the G4-NH_2 dendrimer, all of these data were obtained using metal-free dendrimers. The G4-NH_2 and G4-OH monolayers were prepared using the same activation procedure used for the preparation of the G4-Q_{32} monolayers, and the stability was judged by noting the change in the magnitude of the amide I bands before and after either sonication or electrochemical cycling. For G4-NH_2 monolayers, a high level of stability was observed due to covalent linking of the dendrimer to the MUA SAM via the peripheral primary amine groups.[111,112] Importantly, we found that stability of G4-Q_{32} monolayers is comparable to

that observed for G4-NH_2 monolayers. This provides additional support for our contention that it is covalently linked to the SAM. In the case of the G4-OH monolayers, however, 20 successive voltammetric scans results in a ~41% decrease in the intensity of amide peaks, which reflects poor adhesion of the dendrimer to the SAM. Taken together, these three spectroscopic and stability studies indicate that G4-$Q_{32}(Pd_{40})$ is covalently linked to the MUA SAM, and that this in turn leads to a robust G4-$Q_{32}(Pd_{40})$ monolayer.

4.4 Summary and Conclusions

We have described an approach for covalent immobilization of DENs on Au surfaces. This was accomplished by encapsulating Pt and Pd nanoparticles within dendrimers having a bifunctionalized periphery, and then reacting the dendrimer with an activated SAM. One component of the dendrimer periphery is designed to prevent agglomeration and precipitation during synthesis of the DEN, and the other component is used for linking the DEN to the SAM surface. These findings demonstrate that partially quaternized PAMAM dendrimers are a useful mediator for preparing robust, highly monodisperse metal nanoparticle arrays on surfaces. In a broader sense, it is clear that

multiple different functional groups appended onto the periphery of dendrimers can be used to multiplex chemical functionality. This has the potential to be an especially powerful property of dendrimers, because of the very large number of functional groups on their surface. At present we are examining the effectiveness of these surface-immobilized dendrimers for applications in heterogeneous catalysis. The results of those studies will be reported soon.

CHAPTER V

PREPARATION AND CHARACTERIZATION OF 1-2 NM DENDRIMER-ENCAPSULATED GOLD NANOPARTICLES HAVING VERY NARROW SIZE DISTRIBUTIONS*

5.1 Introduction

We report the synthesis of remarkably size-monodisperse Au nanoparticles prepared using a dendrimer templating approach.[10,11,13,14,92,102,120] Specifically, Au dendrimer-encapsulated nanoparticles (DENs) containing an average of 55 and 140 atoms and having sizes and size distributions of 1.3 ± 0.3 nm and 1.6 ± 0.3 nm, respectively, have been prepared within surface-functionalized poly(amidoamine) (PAMAM) dendrimers. For unpurified Au nanoparticles in this size range, this represents more than a 200% improvement compared to previously reported synthetic approaches where size distributions are reported.[13,35,38] Moreover, the nanoparticle synthesis is performed within a single aqueous phase and there are no variables in the synthesis that

---

* Reprinted with permission from Kim, Y.-G.; Oh, S.-K.; Crooks, R. M. *Chem. Mater.* **2004**, *16*, 167-172: copyright 2004 American Chemical Society.

require careful control or that are difficult to reproduce.

Metal nanoparticles <4 nm in diameter are interesting because of their inherent size-dependent optical, electrical, catalytic, and magnetic properties.[22,43,121-124] These materials have been integrated into new kinds of biosensors,[125] used to study the effects of particle size on heterogeneous catalytic reactions,[124,126] and used to fabricate nanometer-scale electronic devices, such as single-electron transistors,[127] supercapacitors,[128] and data storage devices.[129] Further development in these fields awaits better synthetic approaches for preparing nanomaterials. Here, 'better' means simpler syntheses that require minimal subsequent purification steps, more uniform particles having controllable architectures, higher levels of particle stability, particles having at least partially exposed surfaces, and simple linking chemistries that allow the particles to be attached to surfaces, polymers, and biomaterials without altering their physical and chemical properties.

A number of synthetic approaches have been used to improve the quality and control the physical properties of metal nanoparticles. These include stabilization of nanoparticles with micelles,[130] polymers,[131] and organic

ligands.[23,132] For example, Boyen and coworkers prepared stabilized Au nanoparticles in the 1-8 nm size range using block copolymers, and showed they self-assembled onto a variety of substrates.[133,134] Nanoparticles protected by organic ligands are particularly stable,[23] so quite a bit of effort has been focused on these materials. A major step forward in this regard is the phase-transfer synthetic approach for preparing monolayer-protected clusters (MPCs) first described by Brust,[24] and subsequently exploited by others for a variety of applications and fundamental studies.[34,35,38,135] MPCs typically have sizes ranging from 1.1 - 3.5 nm.[38,136] The size monodispersity is typically about ±1.0 nm, but it can be greatly improved by repeated fractional crystallization,[34] extraction and annealing,[33,43] or chromatography[32,34] into the range of ±0.2 to ±0.3 nm.

Dendrimers are good candidates for preparing metal nanoparticles, because they can act as structurally and chemically well-defined templates and robust stabilizers. In addition, encapsulated nanoparticle surfaces are accessible to substrates so that catalytic reactions can be carried out.[110] Moreover, the solubility and reactivity of DENs can be controlled by appropriate functionalization of

the peripheral groups. We and others have previously shown that metallic (Cu,[92] Pd,[73,137] Pt,[73,93,138] and Au[14,139]), bimetallic (Pd-Pt)[15], and semiconductor (CdS)[91] nanoparticles can be prepared within dendrimers. A typical synthesis is carried out by first sequestering metal ions within the dendrimer, and then chemically reducing the resulting inorganic/organic nanocomposite.[10,11] In most cases, hydroxyl-terminated PAMAM dendrimers (Gn-OH, where n represents the generation of the dendrimer) are used for this purpose, because dendrimers having metal-complexing ligands, such as amine groups, on their periphery usually (but not always)[100] crosslink and precipitate in the presence of metal ions such as Cu, Pd, and Pt.[94, 103] However, the synthesis of Au DENs within Gn-OH dendrimers is complicated by the fact that the Au precursor complex ($HAuCl_4$) is prematurely reduced by the peripheral hydroxyl groups.[139,140] This results in formation of large Au particles that are not encapsulated within a single dendrimer.

Dendrimers having functional groups on their surfaces other than hydroxyl groups have been used to prepare Au nanoparticles. Esumi *et al.* studied formation of Au nanoparticles within PAMAM dendrimers carrying amine,[141]

sugar,[140] methyl ester,[120] and alkyl groups[142] on their periphery. However, relatively large particles (2.1 nm – 12.8 nm) typically having broad size distributions were formed both in the interior and on the dendrimer exterior. Amis *et al.* reported the synthesis of Au nanoparticles synthesized using amine-terminated PAMAM dendrimers (Gn-NH_2).[14,143] They prepared relatively large Au nanoparticles (2.0 – 4.0 nm) using G2 – G10 dendrimers, but the size distributions determined by TEM were not clearly defined.[14] In addition, they reported that larger nanoparticles (4 nm) were obtained with G2 dendrimers than nanoparticles prepared in the presence of higher generations. This result indicates that low generation dendrimers act exclusively as surface stabilizers, similar to the *n*-alkanethiols used to prepare MPCs.

Recently, we described PAMAM dendrimers having both quaternary ammonium groups and primary amines on their periphery (Gn-Q_p, where *p* represents the number of quaternized peripheral groups) (Figure 2.1b).[44] We chose to use Gn-Q_p dendrimers as templates in this work for two reasons. First, Gn-Q_p dendrimers provide a synthetic handle (specifically, the unfunctionalized primary amines) for subsequent covalent attachment of the Au DENs to

surfaces and other molecules. Second, the quaternized amines provide a large positive charge on the dendrimer periphery and thereby reduce the likelihood of DEN agglomeration. For example, we previously showed that highly monodisperse Pd and Pt nanoparticles could be prepared within Gn-Q_p dendrimers and that the resulting composites could be covalently linked to a self-assembled monolayer (SAM).[44,116]

5.2 Experimental Section

Chemicals. Partially quaternized fourth- and sixth-generation dendrimers (G4-Q_{32} and G6-Q_{116}) were synthesized from fourth- and sixth-generation amine-terminated PAMAM dendrimers (G4-NH_2 and G6-NH_2) as previously reported.[44] G4-NH_2 and G6-NH_2 in methanol were obtained from Dendritech, Inc. (Midland, MI) and dried under vacuum to remove the solvent prior to use. $HAuCl_4$ and $NaBH_4$ were purchased from the Aldrich Chemical Co. (Milwaukee, WI) and used as received. NaOH was purchased from the EM science (Gibbstown, NJ) and 18 MΩ·cm Milli-Q water (Millipore, Bedford, MA) was used throughout.

DEN synthesis. 0.5 mL of a 10 μM Gn-Q_p aqueous solution and 55, 100, 140, or 300 equiv. of 2 mM $HAuCl_4$ in

water were mixed. This pale yellow solution was vigorously stirred for 20 min to provide enough time for $HAuCl_4$ to be extracted into the dendrimer interior. A 5-fold molar excess of $NaBH_4$ in 0.3 M NaOH was quickly added to this solution with stirring to reduce the Au complex to zerovalent Au, and immediately the color changed from yellow to brown. $NaBH_4$ was dissolved in 0.3 M NaOH, which helps to control the rate of reduction.[14] Following the synthesis, the total solution volume was 5 mL and the final concentration of DENs was 1 μM. G4-NH_2 dendrimers were also used to prepare Au DENs (G4-NH_2(Au_{55})) using the same method described for the synthesis of G4-Q_{32}(Au_{55}). All DENs were characterized without being purified.

Characterization. UV-vis absorbance spectra were obtained using quartz cells and a Hewlett-Packard 8453 UV-vis spectrometer system (Hewlett-Packard, Wilmington, DE) at 25 ± 2 °C. UV-vis spectra were obtained using 1 μM G6-Q_{116} and 140 μM $HAuCl_4$ aqueous solutions or 0.5 μM aqueous Au DEN solutions. High-resolution transmission electron microscopy (HRTEM) was performed using a JEOL 2010 electron microscope (JEOL USA Inc., Peabody, MA). Samples were prepared by placing 3 drops of 1 μM aqueous Au DEN

solutions on carbon-coated copper grids (EM science, Gibbstown, NJ) and allowing the solvent to evaporate in air.

5.3 Results and Discussion

Preparation of Au DENs. Au nanoparticles were prepared within fourth- and sixth-generation PAMAM dendrimers having about 50% of their peripheral amine groups modified with ammonium chloride (G4-Q_{32} and G6-Q_{116}, respectively, Figure 2.1b).[44] Because they are quaternized, Gn-Q_p dendrimers have permanent positive charges at their periphery. This high charge density minimizes the likelihood of dendrimer aggregation[14] and of multiple dendrimers stabilizing a single nanoparticle,[103,120] and it therefore enhances the probability of intradendrimer nanoparticle formation. Encapsulated Au nanoparticles were synthesized within quaternized dendrimers using a two-step process: extraction of aqueous $AuCl_4^-$ into the dendrimer interior, followed by reduction with $NaBH_4$ in 0.3 M NaOH solution.[14] Specifically, $HAuCl_4$ (55, 100, 140, or 300 equiv per dendrimer) was mixed with 0.5 mL of an aqueous 10 μM Gn-Q_p aqueous solution. This pale yellow solution was vigorously stirred for 20 min to provide enough time for

$HAuCl_4$ to be extracted into the dendrimer interior. Second, a 5-fold molar excess of $NaBH_4$ in 0.3 M NaOH was quickly added to this solution with stirring to reduce the Au complex to zerovalent Au. This resulted in conversion of the initially pale yellow solution to the characteristic brown color of Au nanoparticles (<2 nm).

UV-vis absorbance spectroscopy. Figure 5.1a shows UV-vis absorbance spectra of aqueous solutions containing $AuCl_4^-$, G6-Q_{116}, and G6-$Q_{116}(AuCl_4^-)_{140}$ before reduction with $NaBH_4$. The UV-vis spectrum of $AuCl_4^-$ reveals a strong absorption band at 220 nm and a shoulder at 290 nm. These bands were previously assigned as ligand-to-metal-charge-transfer (LMCT) transitions.[94] The spectrum of G6-Q_{116} is featureless, except for a rapidly increasing absorbance below about 230 nm. When G6-Q_{116} and $AuCl_4^-$ are mixed, the resulting spectrum, after subtraction of the G6-Q_{116} background, is different than the spectrum of a solution containing only $AuCl_4^-$. Specifically, the intensity of the band at 220 nm decreases and shifts to lower energy by 5 nm, while the intensity of the shoulder at 290 nm increases and broadens. The broad band centered around 290 nm is characteristic of ion-pair formation between $AuCl_4^-$ and G6-Q_{116}.[94]

Absorbance spectroscopy is useful for studying metal nanoparticles, because the peak positions and shapes are sensitive to particle size. For example, Au nanoparticles larger than 2 nm typically have a plasmon band in the range of 500 - 550 nm.[122,123] However, when the particle size is less than 2 nm the distinctive plasmon band is replaced by a featureless absorbance, which increases monotonically toward higher energies.[102, 144] This behavior is apparent in Figure 5.1b. There is no plasmon band apparent in spectra 2-4, which correspond to Au DENs containing an average of 140, 100, and 55 atoms, respectively. This result suggests that these particles are less than 2 nm in diameter. When the $[HAuCl_4]$:$[G6\text{-}Q_{116}]$ ratio increases to 300, however, a plasmon band appears as a broad and indistinct feature centered at 510 nm (Spectrum 1, Figure 5.1b).

High-resolution transmission electron microcopy. Figure 5.2 shows HRTEM images and size-distribution histograms for $G4\text{-}Q_{32}(Au_{55})$ and $G6\text{-}Q_{116}(Au_{55})$. The images reveal widely separated Au nanoparticles and little aggregation. This may be a consequence of the high charge density on the surface of the quaternized host dendrimers. The average sizes of the $G4\text{-}Q_{32}(Au_{55})$ and $G6\text{-}Q_{116}(Au_{55})$

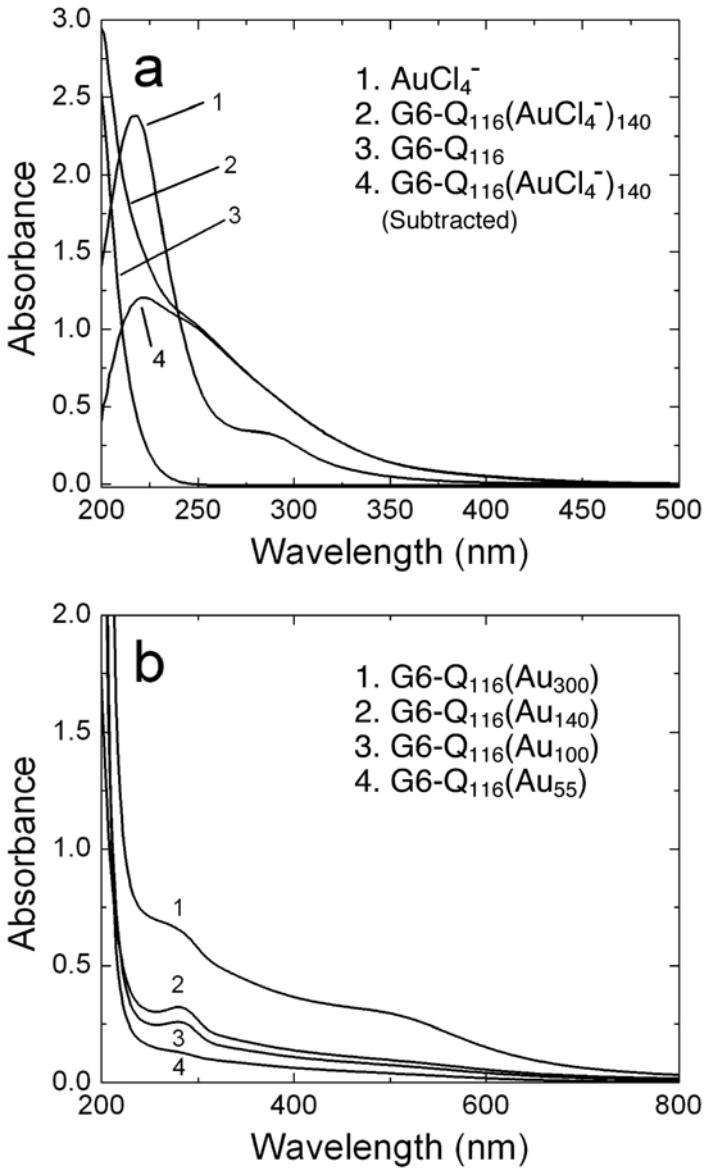

Figure 5.1. (a) UV-vis spectra of aqueous solutions of (1) $AuCl_4^-$; (2) G6-$Q_{116}(AuCl_4^-)_{140}$; and (3) G6-Q_{116} obtained using H_2O as a background spectrum. For comparison, spectrum 4 was obtained by subtracting spectrum 3 from spectrum 2. The spectra were obtained using solutions containing 1.0 μM G6-Q_{116} and 140 μM $AuCl_4^-$. (b) UV-vis spectra of aqueous solutions containing (1) G6-$Q_{116}(Au_{300})$; (2) G6-$Q_{116}(Au_{140})$; (3) G6-$Q_{116}(Au_{100})$; and (4) G6-$Q_{116}(Au_{55})$. The spectra were obtained from solutions containing 0.5 μM G6-Q_{116}.

DENs are 1.3 ± 0.4 nm and 1.3 ± 0.3 nm, respectively. A few particles having diameters larger than 2 nm are also present, but we suspect these arise from two or more overlapping small particles that appear in the two-dimensional HRTEM projection as a single larger particle. Note that the average size of the Au_{55} nanoparticles measured by HRTEM is very close to the value of 1.2 nm calculated by assuming that these materials are spherical in shape (Table 5.1).[145]

Figure 5.3 shows HRTEM images of G4-$Q_{32}(Au_{140})$ and G6-$Q_{116}(Au_{140})$ and corresponding histograms of particle size distributions. The measured diameters of G4-$Q_{32}(Au_{140})$ and G6-$Q_{116}(Au_{140})$ are 1.6 ± 0.4 nm and 1.6 ± 0.3 nm, respectively. As for the 55-atom DENs, these nanoparticles do not agglomerate and the average size (1.6 nm) is identical to the calculated value for particles containing this number of atoms. The measured diameters of Au nanoparticles from HRTEM images are compared to calculated values and summarized in Table 5.1.

An interesting conclusion that can be drawn from Figures 5.2 and 5.3 is that the size of the Au nanoparticles does not depend on the dendrimer generation,

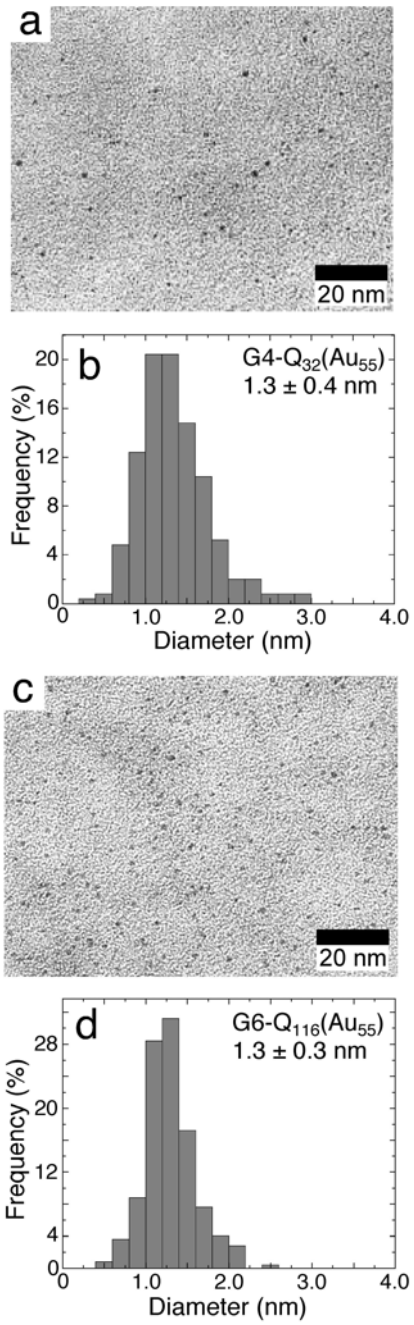

Figure 5.2. HRTEM images of (a) G4-$Q_{32}(Au_{55})$ and (c) G6-$Q_{116}(Au_{55})$ and corresponding particle size distributions (b and d, respectively). The average Au particle diameters are 1.3 ± 0.4 nm for G4-$Q_{32}(Au_{55})$ and 1.3 ± 0.3 nm for G6-$Q_{116}(Au_{55})$.

Table 5.1. Comparison between calculated and measured diameters of Au DENs.

DEN	Calculated diameter (nm)[a]	Measured diameter (nm)[b]
G4-Q_{32}(Au_{55})	1.2	1.3 ± 0.4
G6-Q_{116}(Au_{55})	1.2	1.3 ± 0.3
G4-Q_{32}(Au_{140})	1.6	1.6 ± 0.4
G6-Q_{116}(Au_{140})	1.6	1.6 ± 0.3
G6-Q_{116}(Au_{100})	1.4	1.4 ± 0.6

(a) Calculated using the equation: $n=4\pi(R-\delta)^3/3\nu_g$, where n is the number of Au atoms, R is radius of Au nanoparticle, δ is the length of the protecting ligands (in this case, δ = 0), and ν_g is the volume of one Au atom (17 Å^3).[145] (b) Measured from HRTEM images.

but rather only on the [$HAuCl_4$]:[Gn-Q_p] ratio.

In contrast, it has previously been reported that for amine-terminated PAMAM dendrimers the size of Au nanoparticles decreases as the dendrimer generation increases.[94,103,141] Although not conclusively demonstrated, the contention was that multiple low-generation dendrimers stabilize each nanoparticle, whereas for higher generations, smaller Au nanoparticles are encapsulated within individual dendrimers. That is, in the former case the nanoparticles are stabilized by primary amine peripheral groups rather than by true encapsulation within single dendrimers. Therefore, the observed independence of nanoparticle size on the dendrimer generation here provides evidence that the nanoparticles are truly templated by the interior of individual dendrimers.

It is also interesting to note that 140-atom DENs can be formed within the interior of the G4-Q_{32} dendrimer, which only contains 62 internal tertiary amine groups. With one exception,[146] previous reports from us[11] and others[14,138] have shown that the number of metal atoms that can be contained within a dendrimer is approximately equal to or less than the number of interior tertiary amines. This is because metal ion encapsulation of Cu, Pd, and Pt salts are driven

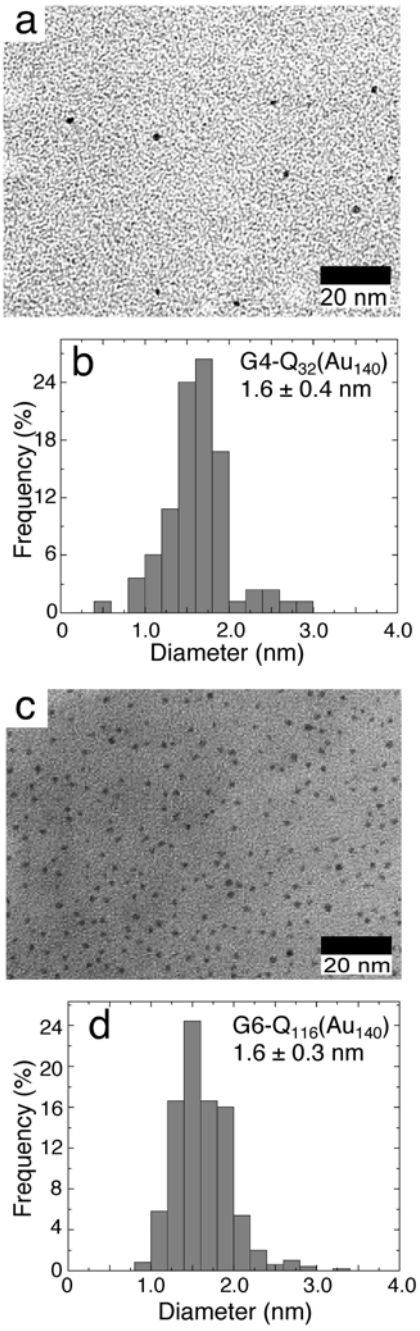

Figure 5.3. HRTEM images of (a) G4-$Q_{32}(Au_{140})$ and (c) G6-$Q_{116}(Au_{140})$ and corresponding particle size distributions (b and d, respectively). The average Au particle diameters are 1.6 ± 0.4 nm for G4-$Q_{32}(Au_{140})$ and 1.6 ± 0.3 nm for G6-$Q_{116}(Au_{140})$.

by specific interactions with these interior functional groups. In the one exception to this general finding the metal ions were driven into the dendrimer interior by differences in the dielectric strength of the solvent and dendrimer interior.[146] Taken together, these findings may suggest that $AuCl_4^-$ encapsulation within Gn-Q_p is driven by electrostatic interactions and perhaps also solubility differences of $AuCl_4^-$ in water compared to the dendrimer interior.[13,14] However, this is just speculation, and at the present time the driving force for $AuCl_4^-$ encapsulation is unknown.

The formation of the highly monodisperse Au nanoparticles reported here is possible in part because particular [$HAuCl_4$]:[Gn-Q_p] ratios were used to prepare them. Metal nanoparticles containing these "magic numbers" of atoms form energetically favorable, closed-shell crystals.[23] To verify that magic numbers of metal atoms are important for high monodispersity, we prepared Au nanoparticles using an intermediate [$HAuCl_4$]:[G6-Q_{116}] ratio of 100. Figure 5.4 shows the results of a HRTEM study of G6-Q_{116}(Au_{100}). The important observation is that the particle size distribution appears somewhat bimodal, and it is therefore not as narrow as for G6-Q_{116}(Au_{55}) or G6-Q_{116}(Au_{140}).

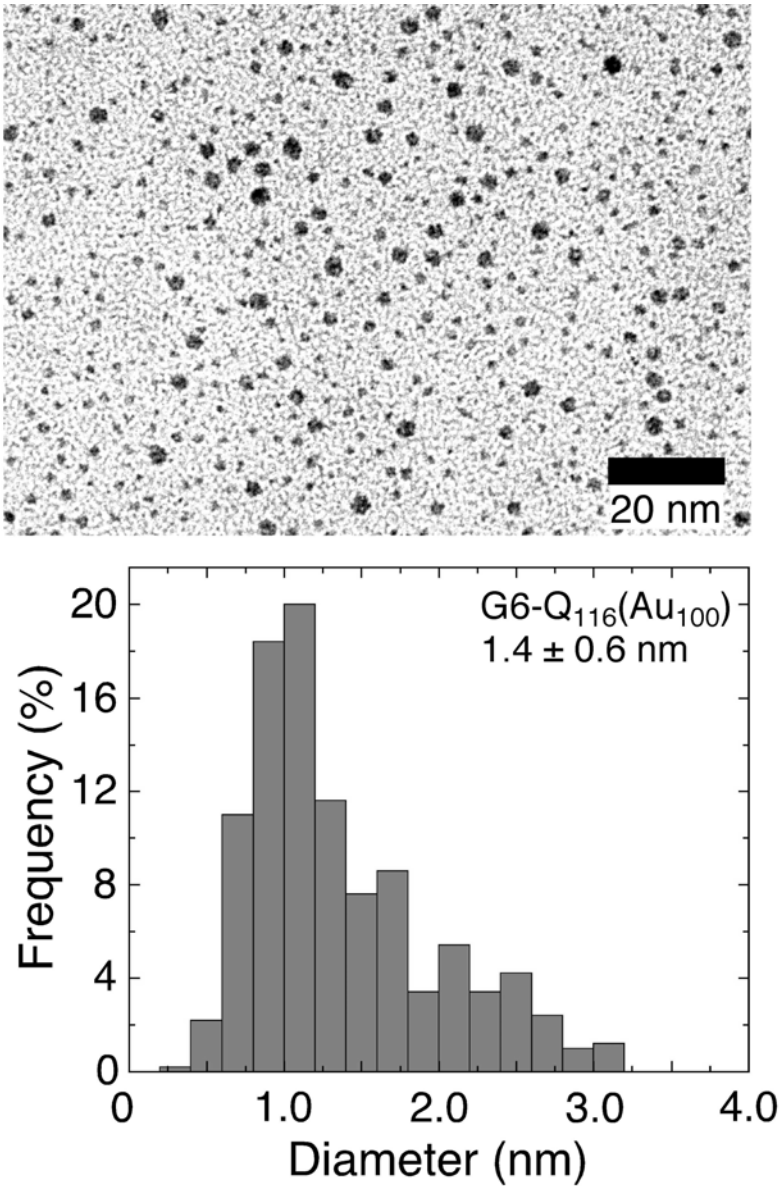

Figure 5.4. HRTEM image and corresponding particle size distribution for G6-$Q_{116}(Au_{100})$. The average Au particle diameter is 1.4 ± 0.6 nm.

Specifically, the average particle size for G6-$Q_{116}(Au_{100})$ is 1.4 ± 0.6 nm compared to 1.3 ± 0.3 nm and 1.6 ± 0.3 nm for G6-$Q_{116}(Au_{55})$ and G6-$Q_{116}(Au_{140})$, respectively.

To better understand the impact of the partially quaternized surface of G4-Q_{32} on the properties of encapsulated Au nanoparticles, we compared the average Au particle size and size distribution for nanoparticles prepared using G4-NH_2 and G4-Q_{32} templates. In both cases an [$HAuCl_4$]:[dendrimer] ratio of 55 was used. A HRTEM image of Au nanoparticles prepared within G4-NH_2 (Figure 5.5) reveals a slightly broader size distribution (1.3 ± 0.5 nm) compared to G4-$Q_{32}(Au_{55})$ (Figure 5.2a, 1.3 ± 0.4 nm). This result suggests that the main function of the quaternary amine groups is to prevent agglomeration of dendrimers, but that the charged surface exerts only a slight influence over the size of the encapsulated nanoparticles. This result is consistent with the dendrimer interior, rather than the periphery, controlling the size and size distribution of the particles. It may also suggest that factors other than electrostatic interactions control $AuCl_4^-$ encapsulation.

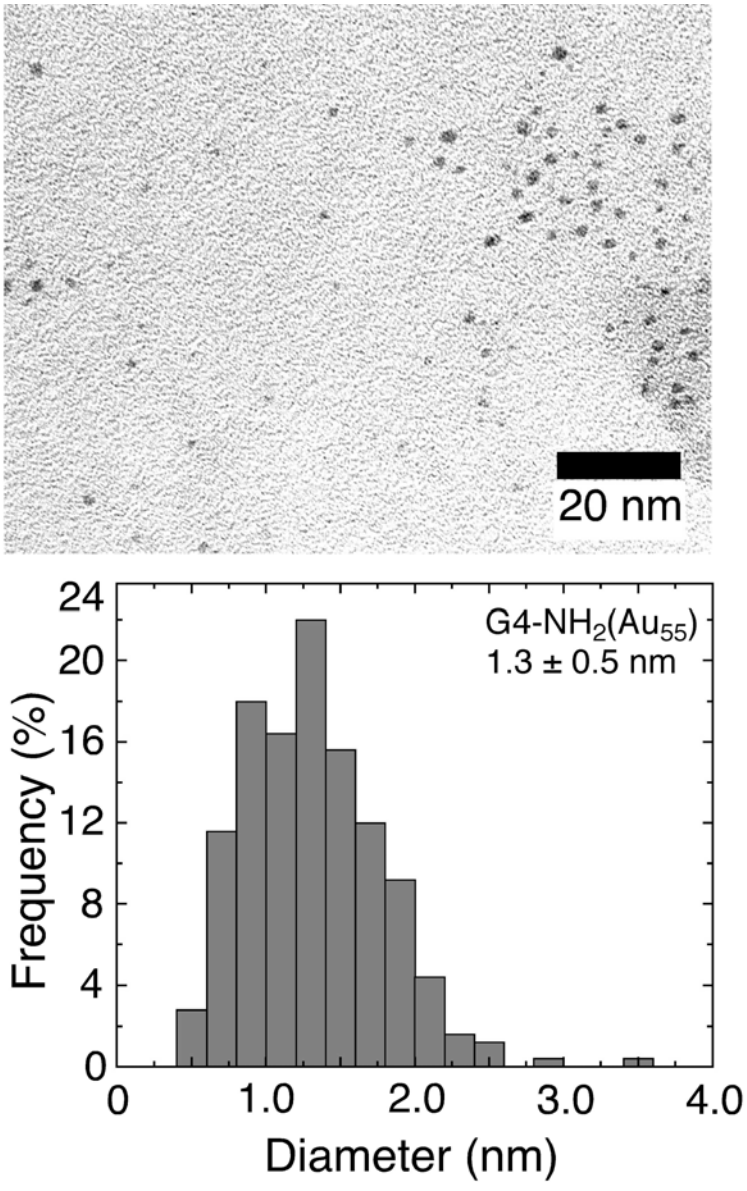

Figure 5.5. HRTEM image and corresponding particle size distribution for G4-NH_2(Au_{55}). The average Au particle diameter is 1.3 ± 0.5 nm.

5.4 Summary and Conclusions

The key result of this study is elucidation of a very simple, template-based approach for preparing size-monodisperse Au nanoparticles in the interesting size range of 1-2 nm. We believe the monodispersity of Au DENs prepared within Gn-Q_p is enhanced by three factors. First, because this is a template-based approach the variation of nanoparticle size that is inevitable for methods that rely on nucleation–and-growth phenomena is avoided. Second, the high permanent charge on the surface of the Gn-Q_p dendrimers lessens the likelihood of aggregation. Third, we chose to use "magic number"[23,147] ratios of [$HAuCl_4$]:[Gn-Q_p], because it has previously been shown that Au nanoparticles containing 55 or 140 atoms form energetically favorable structures.[38,148] When magic numbers of metal atoms were not used (e.g., [$HAuCl_4$]:[Gn-Q_p] = 100), the formation of significantly more polydisperse Au nanoparticles was observed.

Robust synthetic routes to monodisperse nanomaterials is an essential first step toward technologies that incorporate these materials, and there are some significant advantages of the approach described here for preparing Au nanoparticles. First, this approach is simple, highly

reproducible, and does not require careful control of experimental conditions. Second, a high level of monodispersity is attained without the need for subsequence purification. Third, as we have shown previously for Pd DENS,[73,110] the surface of the particles is accessible, and thus these materials can be used for catalysis. Fourth, the dendrimer itself provides a convenient means for linking DENs to other molecules or surfaces.[44] Finally, we have recently shown that both Pd and Au nanoparticles can be extracted from dendrimer templates with little or no change to their physical properties.[20] Our next step is to better understand the electronic and photonic properties of these materials,[33,149] and to further refine the synthesis with a view toward improving the size distribution to the resolution of available characterization methods, which seems to be limited to about ±0.15 nm.

CHAPTER VI

ELECTROCHEMICAL PROPERTIES OF MONOLAYER-PROTECTED Au AND Pd NANOPARTICLES EXTRACTED FROM WITHIN DENDRIMER TEMPLATES*

6.1 Introduction

In this chapter we describe the electrochemical properties of 1.2–1.9 nm-diameter Au and Pd nanoparticles prepared via a dendrimer-templating approach.[10-12,92] Specifically, we prepared Au and Pd dendrimer-encapsulated nanoparticles (DENs), and then extracted these into an organic phase using appropriate ligands. The properties of the resulting monolayer-protected clusters (MPCs)[22-25,150,151] could then be examined using electrochemical methods. The unpurified dendrimer-templated MPCs are sufficiently size-monodisperse that they exhibit well-defined quantized double-layer charging behavior. This is significant because DEN templating is one of the most versatile synthetic approaches for preparing nanoparticles having a high degree of size, compositional, and structural

---

* Reprinted with permission from Kim, Y.-G.; Garcia-Martinez, J. C.; Crooks, R. M. *Langmuir* **2005**, *21*, 5485-5491: copyright 2005 American Chemical Society.

uniformity.[10-12,92] This means that it will be possible to use electrochemical methods to characterize other interesting types of dendrimer-templated nanoparticles, including bimetallic alloys[15,18] and core/shell materials,[16, 19] which are difficult or impossible to prepare as MPCs using alternative synthetic strategies.[30,31]

We, and others, have previously reported the preparation of Ag,[152,153] Au,[13,14,21,45,102,120,139,142,154] Cu,[92,96] Pd,[20,44,73,100,110,116,137,154-158] Pt,[44,73,100,138,159] and bimetallic[15-19, 160] nanoparticles encapsulated within the interiors of dendrimers. DENs are prepared by first sequestering metal ions within the dendrimer interior, and then reducing them to yield a nanoparticle. This template-based approach has several desirable attributes.[10-12,92] First, the size distribution of the resulting nanoparticles is typically narrow, because the synthesis relies on kinetics rather than the thermodynamics of nucleation and growth. Second, nanoparticle size can be controlled by adjusting the metal-ion-to-dendrimer ratio and the size of the dendrimer template. Third, unpassivated nanoparticle surfaces are accessible to substrates, so that DENs can be used for catalytic reactions. For example, DENs have been used for hydrogenations,[15,16,73,110,137] electrochemical oxygen

reduction,[93,161] and Heck,[155,156] Suzuki,[158] and Stille[157] reactions.

Recently, our group reported that metal nanoparticles could be extracted from the interior of dendrimers as MPCs.[19-21,152] The extraction is carried out by mixing an aqueous DEN solution with an organic phase containing a suitable surfactant, such as an alkanethiol or alkanoic acid. We have proposed that the surfactant penetrates the dendrimer and adsorbs onto the surface of the nanoparticle when the two phases are mixed. This results in a hydrophobic nanoparticle that is subsequently extracted from the dendrimer interior and into the organic phase. Previous results have indicated that the extracted MPCs have the same chemical and physical properties as the original DENs, and therefore this method provides a general route to small quantities of highly monodisperse MPCs.

The most common alternative method for preparing MPCs involves reduction of metal complex ions, usually Au, in the presence of alkanethiols or other ligands that strongly complex with the growing metal nanoparticles.[23,24] MPCs prepared by this route have many desirable properties: they can be repeatedly isolated from and redissolved in common organic solvents without irreversible aggregation or

decomposition,[37] their surfaces can be functionalized with a vast range of modifiers,[162-164] and they can be linked to polymers, biomolecules, and monolithic surfaces.[23,25,151] A significant drawback of this synthetic approach is that it results in polydisperse size distributions of nanoparticles.[23,31,36,37,151,165-167] This is a consequence of the thermodynamics that govern the nucleation and growth of these materials. Importantly, however, purification of the crude reaction mixture can lead to large quantities of MPCs having narrow size distributions.[32-35,38,43]

The electrochemical properties of Au MPCs synthesized and purified as indicated above have been extensively studied by Murray[22,23,32,33,35,39,41,42,150,162,168,169] and others.[43, 170,171] The results indicate that MPCs in the size range of 1.1–4.6 nm act as capacitors that undergo quantized double-layer charging. On the basis of this model, it is possible to calculate the average size of MPCs from voltammetric measurements. Two additional points merit mention here. First, only been a few electrochemical studies of MPCs having cores other than Au have been reported.[26-29] This is apparently a consequence of the difficulty of preparing and purifying non-Au MPCs. Second, very small MPCs (<1.1 nm)

exhibit more complex electrochemical behavior that has been associated with molecule-like energetics.[41,42]

Here, we prepared Au DENs containing 140 or 225 atoms, and Pd DENs containing 40, 80, and 140 atoms. The DENs were then extracted into hexane using *n*-hexanethiol. The sizes of the resulting materials were evaluated using voltammetric data, and then the results were compared to the sizes of the particles measured by TEM and calculated from the average number of atoms per particle. All three methods were generally in good agreement, except TEM over-estimates the size of the smallest Pd nanoparticles. This correlation, coupled with the synthetic flexibility of the dendrimer-templating method, provides a basis for using electrochemical methods to study more complex types of nanoparticles in the future.

6.2 Experimental Section

Chemicals and materials. DENS were prepared within sixth-generation, amine-terminated poly(amidoamine) (PAMAM) dendrimers that were partially quaternized on their periphery. These materials are referred to as G6-Q_{116}, because 116 of the 256 peripheral primary amine groups were quaternized using a previously reported procedure.[44]

Fourth- and sixth-generation hydroxyl-terminated PAMAM dendrimers (G4-OH and G6-OH, respectively) were obtained as 10-25% aqueous solutions from Dendritech, Inc. (Midland, MI). P_2O_5, *n*-hexanethiol, $NaBH_4$, $HAuCl_4$, (Aldrich Chemical Co., Milwaukee, WI), K_2PdCl_4 (Strem Chemicals, Inc.), and Bu_4NPF_6 (Fluka, Milwaukee, WI) were used as received. HPLC grade hexane, and reagent grade ethanol, toluene, dichloromethane, and nitric acid, were purchased from EMD Chemicals Inc. (Gibbstown, NJ). 18 MΩ•cm Milli-Q water (Millipore, Bedford, MA) was used throughout.

Synthesis and extraction of the Au and Pd nanoparticles. The procedure used to prepare the Au^{45} and Pd^{73} DENs and then extract them as MPCs has been reported previously, but a short summary of the basic procedure follows.[20,21] For Au DENs 10.0 mL of an aqueous 10.0 μM G6-Q_{116} solution was mixed with either 140 or 225 equiv of an aqueous 2.00 mM $HAuCl_4$ solution to yield the corresponding dendrimer-encapsulated ions (G6-$Q_{116}(Au^{3+})_{140}$ or G6-$Q_{116}(Au^{3+})_{225}$, respectively). Next, these pale yellow solutions were vigorously stirred for 15 min and then reduced with a 5-fold molar excess of $NaBH_4$ in 0.30 M NaOH. This yields G6-$Q_{116}(Au_{140})$ and G6-$Q_{116}(Au_{225})$ DENs,

respectively. Slight deviations from this procedure were required to prepare Pd DENs. Specifically, 6.25 mL of an aqueous solution containing 0.10 mM G4-OH or G6-OH was mixed with 40, 80, or 140 equiv of an aqueous 5.00 mM K_2PdCl_4 solution. The solution was vigorously stirred for 5 min, and then a 10-fold molar excess of an aqueous $NaBH_4$ solution was added to yield G4-OH(Pd_{40}), G6-OH(Pd_{80}) or G6-OH(Pd_{140}), respectively.

The extraction was carried out by mixing together 10.0 mL of either an Au or Pd DEN aqueous solution and 10.0 mL of a hexane solution containing 50.0 mM *n*-hexanethiol. A 150-fold molar excess of $NaBH_4$ was added to the mixture[20, 21] and the vial was shaken. After settling, the hexane layer containing the *n*-hexanethiol-coated MPCs (MPC-6(Au_n) or MPC-6(Pd_n), where n is number of metal atoms) was transferred to a round-bottom flask and the solvent and excess *n*-hexanethiol were removed by evaporation under vacuum at 23 ± 2 °C. The dried MPC-6(Au_n) or MPC-6(Pd_n) were used for subsequent experiments without further purification.

Spectroscopic and microscopic characterization. UV-vis absorbance spectra were obtained at 23 ± 2 °C using

quartz cells and a Hewlett-Packard model 8453 UV-vis spectrometer system (Hewlett-Packard, Wilmington, DE). UV-vis spectra of 1.00 μM Au and 0.60 μM Pd DENs were collected using deionized water as the reference. The UV-vis spectra of the corresponding MPCs were obtained using toluene or hexane as the reference. Transmission electron microscopy (TEM) was performed using a JEOL 2010 electron microscope (JEOL USA Inc., Peabody, MA). Samples were prepared by placing 5 drops of the nanoparticle solution onto a 400-mesh, carbon-coated copper grid (EM science, Gibbstown, NJ) and allowing the solvent to evaporate in air. The microscope has a point-to-point resolution of 0.19 nm.

Electrochemical measurements. Differential pulse voltammetry (DPV) was performed in a 2 mL, single-compartment glass cell configured with a 1.0 mm-diameter Au disk working electrode, a Pt wire counter electrode, and a Ag wire quasi-reference electrode (QRE). The Au working electrode was successively polished with 1.00, 0.30, 0.05 μm alumina (Buehler, Lake Bluff, IL) and sonicated in Milli-Q water and ethanol. The counter electrode and QRE were cleaned in piranha solution (3:1 H_2SO_4/H_2O_2; caution: piranha reacts violently with organics and should be used

with care) before use, and the QRE was additionally soaked in HNO_3 for 5 min. Dichloromethane was purified by refluxing over P_2O_5 for 3 h and then distilling. Bu_4NPF_6 was used as received and stored in a N_2-purged drybox. The electrolyte solutions were prepared by dissolving Bu_4NPF_6 in dichloromethane in an Ar-purged vinyl bag. All DPV experiments were performed in the N_2-purged drybox. A model 760B electrochemical workstation (CH Instruments, Austin, TX) was used for all DPV experiments. The parameters used for DPV were: pulse amplitude, 50 mV; pulse width, 50 ms; pulse period, 200 ms; and sample width 17 ms.

6.3 Results and Discussion

Synthesis and characterization of Au and Pd nanoparticles. Au and Pd nanoparticles were prepared using the two-step procedure described in the Experimental Section. Briefly, Au DENs were prepared by sequestering $AuCl_4^-$ within the dendrimer template, and then reducing the composite with BH_4^-.[10-12,45,92] Partially quaternized, sixth-generation PAMAM dendrimers (G6-Q_{116}) were used to synthesize Au DENs. DENs are usually prepared using hydroxyl-terminated dendrimers, but gold complexes can be prematurely reduced by hydroxyl groups.[140] The resulting Au

DENs were extracted with *n*-hexanethiol to yield the corresponding dendrimer-templated MPCs.[20,21] These MPCs were characterized by UV-vis spectroscopy and TEM before and after extraction. The MPCs were not purified prior to characterization.

UV-vis spectra of aqueous G6-$Q_{116}(Au_{140})$ and G6-$Q_{116}(Au_{225})$ solutions are dominated by an increasing absorbance toward higher energy (Figure 6.1). A broad, weak plasmon band centered at ~520 nm is present in the spectrum of G6-$Q_{116}(Au_{225})$ but not in the spectrum of the smaller Au MPC. All of these observations are consistent with our previous reports.[45] After extraction, the UV-vis spectra of MPC-6(Au_{140}) and MPC-6(Au_{225}) were similar in both form and intensity to those of the aqueous-phase DENs (Figure 6.1).

The slight spectral variations that are present probably result from differences in the solvents used for DENs and MPCs (water and toluene, respectively).[21,172,173] TEM micrographs and size-distribution histograms before and after extraction of G6-$Q_{116}(Au_{140})$ and G6-$Q_{116}(Au_{225})$ confirm the spectroscopic results (Figures 6.2 and 6.3). Prior to extraction G6-$Q_{116}(Au_{140})$ and G6-$Q_{116}(Au_{225})$ have average diameters of 1.6 ± 0.3 nm and 1.8 ± 0.5 nm, respectively.

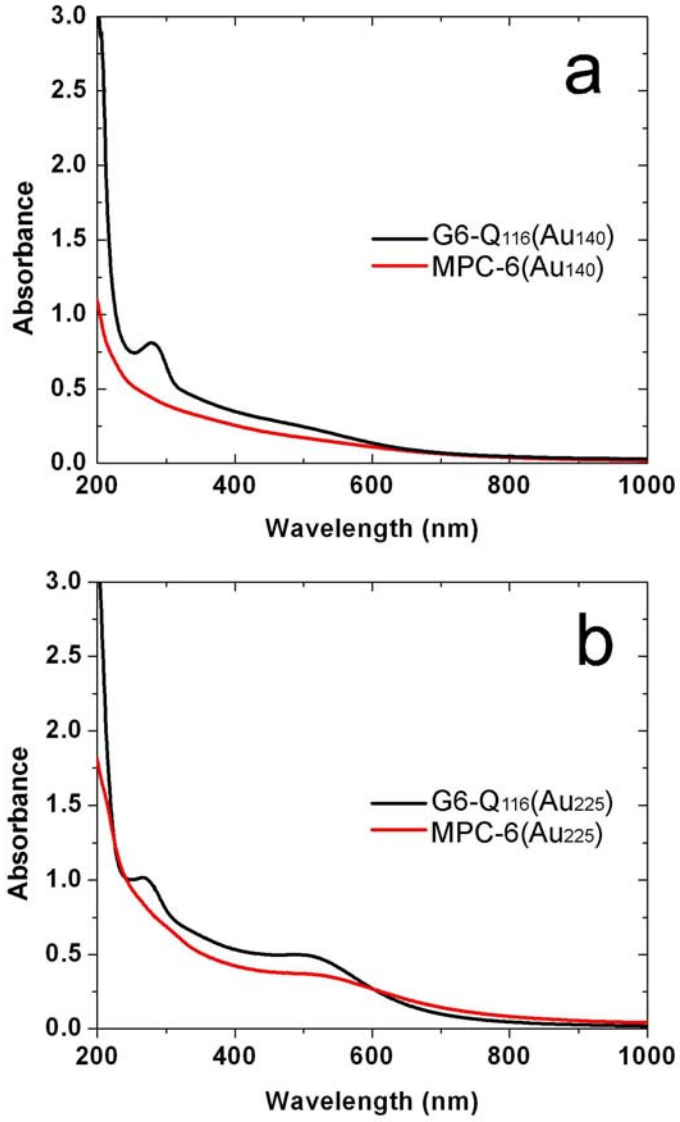

Figure 6.1. UV-vis spectra of (a) 1.00 μM G6-$Q_{116}(Au_{140})$ in water and 1.00 μM MPC-6(Au_{140}) in toluene. (b) 1.00 μM G6-$Q_{116}(Au_{225})$ in water and 1.00 μM MPC-6(Au_{225}) in toluene. The origin of the peak at about 270 nm is not clear. This peak was previously observed for Pt DENs and was thought to arise from unreduced Pt^{2+} within the dendrimers. However Esumi and coworkers observed this band when they prepared Au nanoparticles in the presence of PAMAM dendrimers by UV-irradiation. They assigned it to carbonyl bands in the dendrimer arising from photodecomposition. However there is still controversy.

These values are comparable to those calculated using the number of Au atoms present and assuming a spherical geometry (1.7 nm and 1.9 nm, respectively).[45,145] After extraction, the diameters of the corresponding MPCs were 1.6 ± 0.3 nm and 1.8 ± 0.4 nm, respectively. These results confirm our contention that the high degree of monodispersity inherent to the dendrimer templating method is retained in the extracted MPCs.[21]

Pd DENs were prepared within the interior of hydroxyl-terminated PAMAM dendrimers (G4-OH or G6-OH). These materials were prepared by addition of 40, 80, or 140 equiv of K_2PdCl_4 to an aqueous solution of the appropriate dendrimer followed by BH_4^- reduction. The DENs were subsequently extracted into hexane using *n*-hexanethiol to yield MPC-6(Pd_{40}), MPC-6(Pd_{80}), and MPC-6(Pd_{140}), respectively. Like the Au nanoparticles, TEM and UV- vis spectroscopic data indicate that the physical properties of the Pd DENs are preserved during extraction (Figures 6.4-6.7). For example, TEM data indicate that G4-OH(Pd_{40}) and MPC-6(Pd_{40}) have diameters of 1.6 ± 0.3 nm and 1.5 ± 0.4 nm, respectively; G6-OH(Pd_{80}) and MPC-6(Pd_{80}) have diameters of 1.4 ± 0.3 nm and 1.6 ± 0.4 nm, respectively; and G6-OH(Pd_{140}) and MPC-6(Pd_{140}) have diameters of 1.4 ± 0.3 nm and

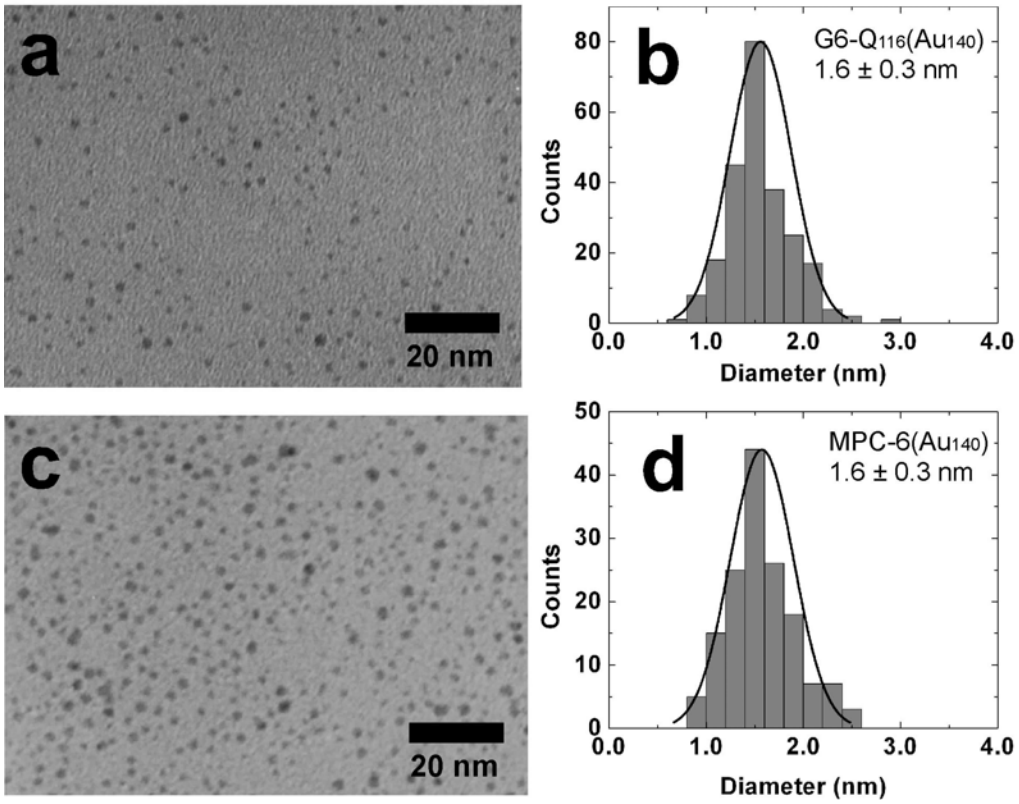

Figure 6.2. TEM micrographs of (a) G6-$Q_{116}(Au_{140})$ and (c) MPC-6(Au_{140}) and their corresponding size-distribution histograms (b and d, respectively).

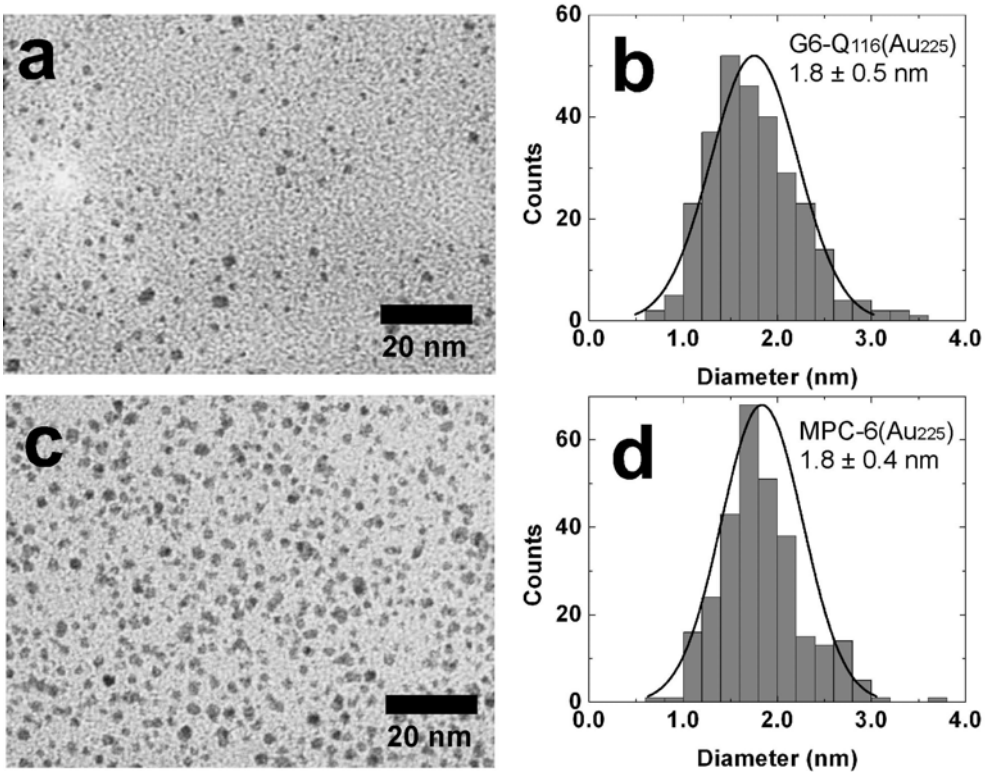

Figure 6.3. TEM micrographs of (a) G6-$Q_{116}(Au_{225})$ and (c) MPC-6(Au_{225}) and their corresponding size-distribution histograms (b and d, respectively).

1.6 ± 0.4 nm, respectively. Most of these values are larger than the sizes calculated from the number of atoms present in the particles. While we can't offer a conclusive explanation for this observation, it is highly reproducible[20,44,73,100,116] and has been observed by others.[158,174] This point will be addressed again later when we discuss the electrochemical data. The nanoparticle sizes discussed thus far are summarized in Table 6.1.

Electrochemical properties of extracted Au MPCs. The electrochemical properties of MPCs having a diameter greater than about 1.1 nm are similar to those of a metallic capacitor, and therefore quantized double-layer charging of MPCs is observed as peaks in voltammetric experiments.[22,23,28,29,32,33,35,36,43,72,150,165,170,171] The voltage between these peaks (ΔV) is inversely proportional to the nanoparticle capacitance (C_{CLU}), eq 1.[35,39] Here e is electronic charge.

$$\Delta V = e/C_{CLU} \qquad (1)$$

If the nanoparticle capacitor is assumed to have a spherical geometry, then eq 2 relates C_{CLU} to the dielectric

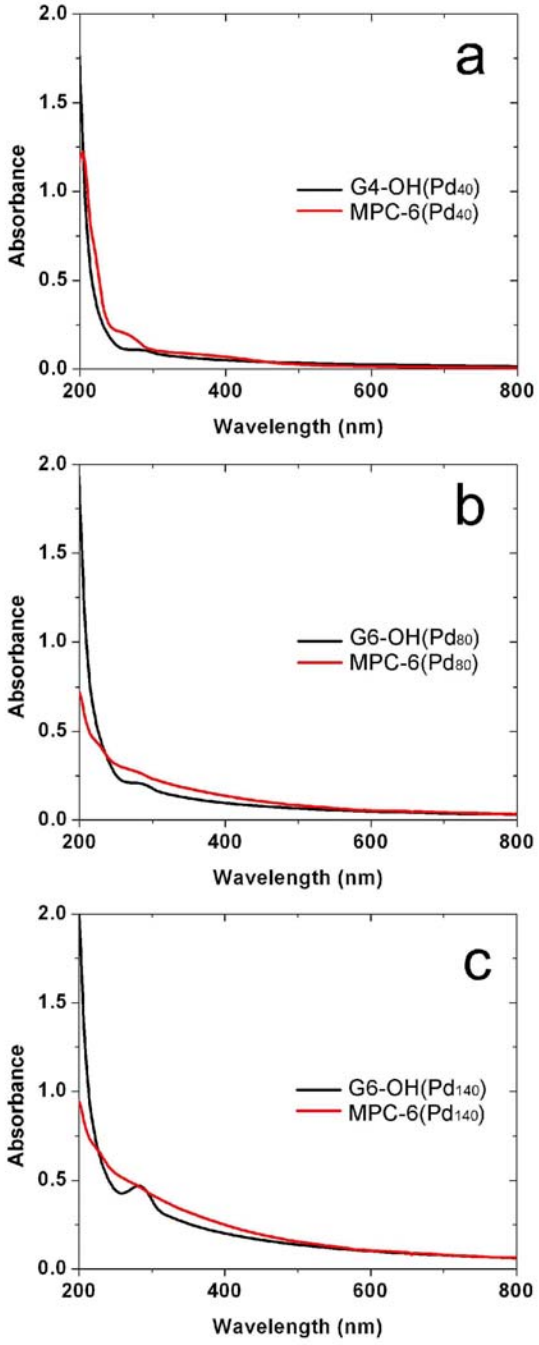

Figure 6.4. UV-vis spectra of (a) 0.60 µM G4-OH(Pd_{40}) in water and 0.60 µM MPC-6(Pd_{40}) in hexane; (b) 0.60 µM G6-OH(Pd_{80}) in water and 0.60 µM MPC-6(Pd_{80}) in hexane; and (c) 0.60 µM G6-OH(Pd_{140}) in water and 0.60 µM MPC-6(Pd_{140}) in hexane.

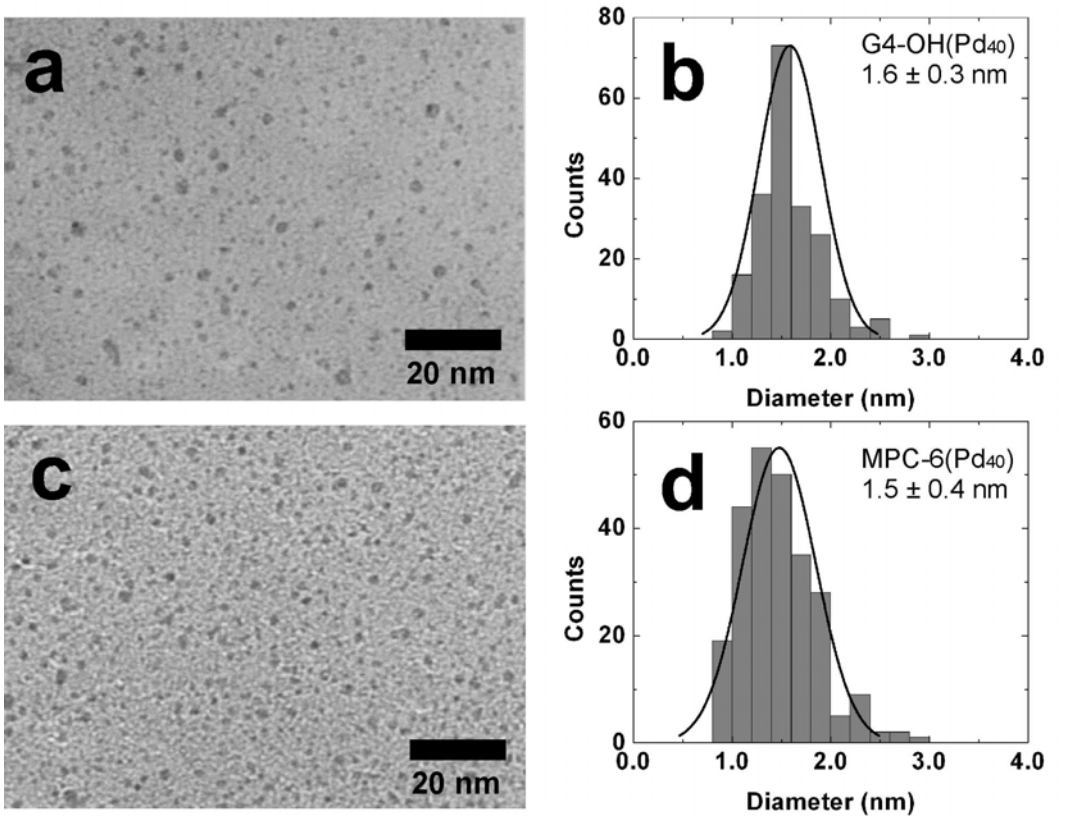

Figure 6.5. TEM micrographs of (a) G4-OH(Pd_{40}) and (c) MPC-6(Pd_{40}), and their corresponding size-distribution histograms (b and d, respectively).

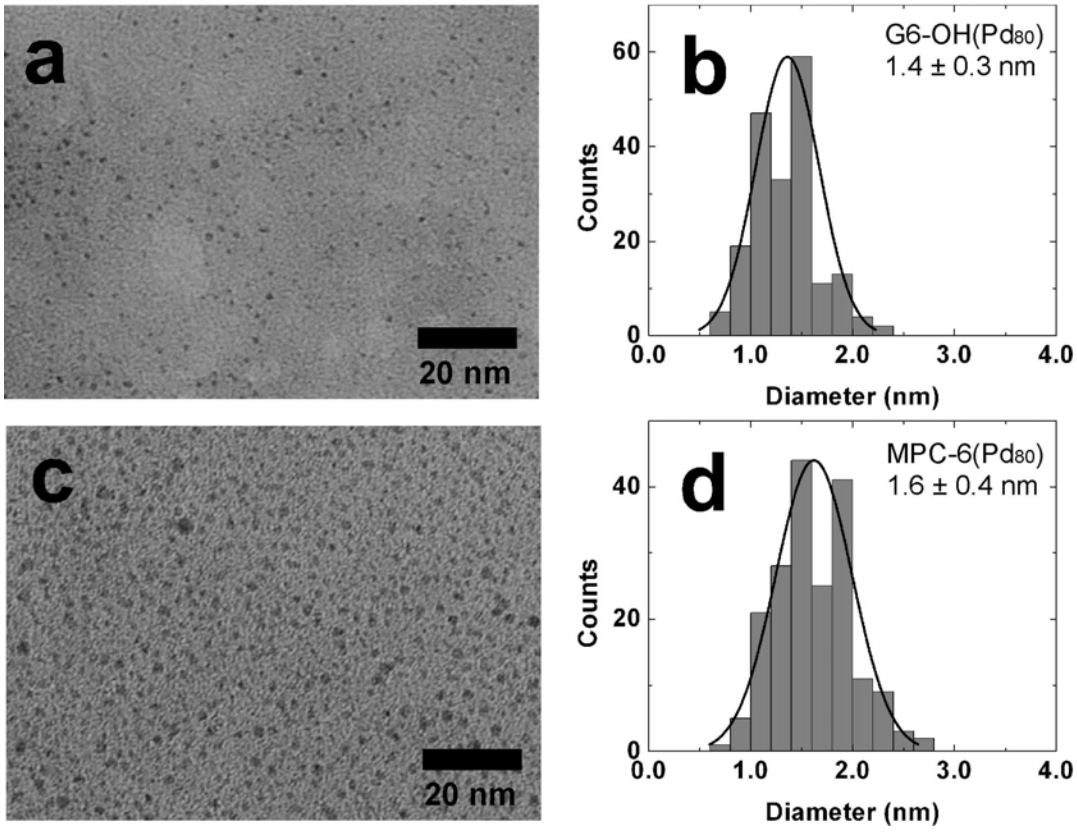

Figure 6.6. TEM micrographs of (a) G6-OH(Pd_{80}) and (c) MPC-6(Pd_{80}) and their corresponding size-distribution histograms (b and d, respectively).

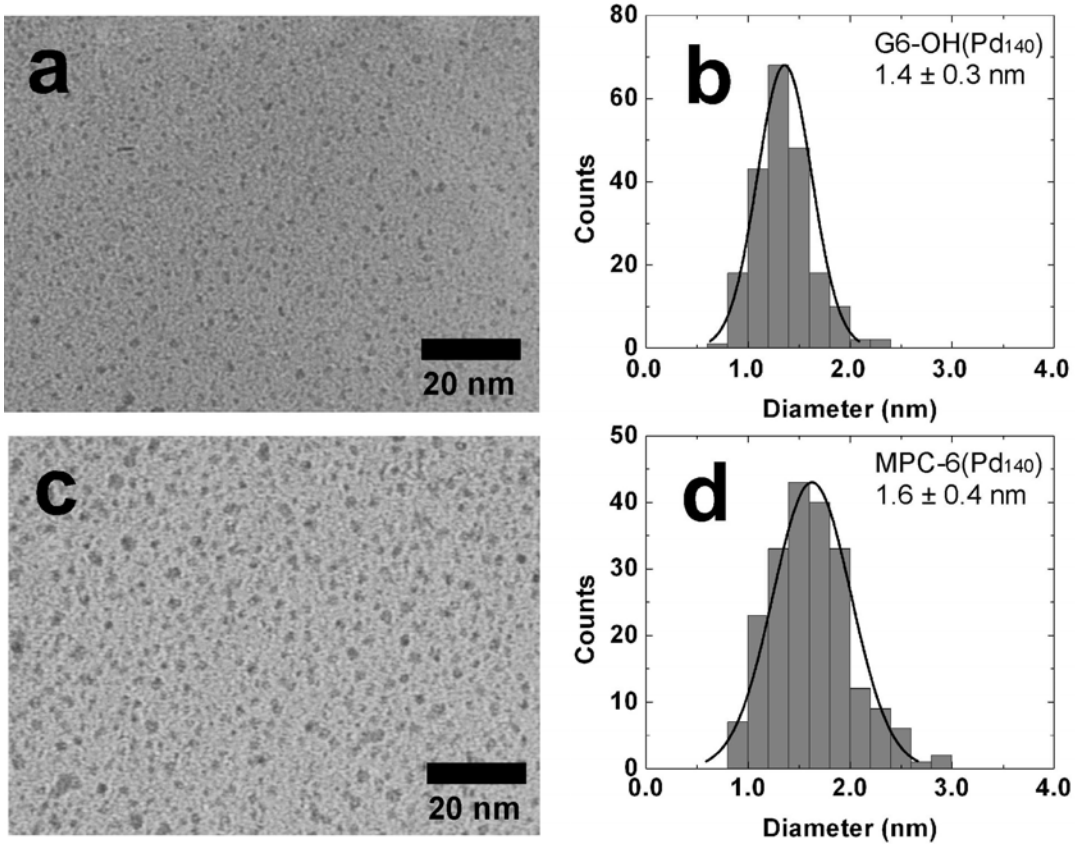

Figure 6.7. TEM micrographs of (a) G6-OH(Pd_{140}) and (c) MPC-6(Pd_{140}) and their corresponding size-distribution histograms (b and d, respectively).

Table 6.1. Comparison of Au and Pd nanoparticle diameters measured from TEM micrographs. The calculated diameters assumed close-paced atoms in a spherical nanoparticle.

Nanoparticle	Calculated diameter (nm)	DEN diameter (nm)	MPC-6 diameter (nm)
Au_{140}	1.7	1.6 ± 0.3	1.6 ± 0.3
Au_{225}	1.9	1.8 ± 0.5	1.8 ± 0.4
Pd_{40}	1.1	1.6 ± 0.3	1.5 ± 0.4
Pd_{80}	1.3	1.4 ± 0.3	1.6 ± 0.4
Pd_{140}	1.6	1.4 ± 0.3	1.6 ± 0.4

constant of the organic monolayer surrounding the metal core (ε = ~3 for *n*-alkanethiols), the radius of the nanoparticle (r), and the monolayer thickness (d = 0.77 nm for *n*-hexanethiol).[32,35]

$$C_{CLU} = 4\pi\varepsilon\varepsilon_0(r/d)(r+d) \quad (2)$$

If all of these assumptions are valid, then eqs 1 and 2 make it possible to calculate the average size of an ensemble of nanoparticles from ΔV data. It has been reported that Au MPCs smaller than ~1.1 nm exhibit molecule-like characteristics.[41,42] In voltammetric experiments this behavior is manifested as a departure from the predictions of the capacitor model, and a larger-than-anticipated ΔV between the -1/0 and 0/+1 charge states of the MPCs is observed. In this case, ΔV is thought to correlate to the energy of the HOMO-LUMO gap.[41] The magnitude of this energy is related to the size and composition of the metal core.[41]

DPV has been widely used to characterize the quantized double-layer charging of MPCs, because ΔV is usually better resolved compared to other electrochemical methods. Even

in this case, however, electrolyte solutions containing highly size-monodisperse MPCs are required to observe peaks that are sufficiently narrow for meaningful conclusions to be drawn.[23] Normally this is accomplished by using a two-phase synthesis followed by extensive purification.[32,34] However, the dendrimer templating/extraction method results in sufficiently pure MPCs that subsequent purification is not required. The DPV experiments described next were carried out using 0.05 M Bu_4NPF_6 in dichloromethane as the electrolyte solution, and they were carried out in a N_2-purged drybox at 23 ± 2 °C. Background voltammograms were obtained immediately prior to the addition of the MPCs to the electrolyte-only solutions. No peaks were observed in any of the background scans.

Figure 6.8a shows the DPV of MPC-6(Au_{140}) derived by extraction from G6-Q_{116}(Au_{140}). The presence of distinct peaks in these data indicates that the MPCs are quite monodisperse in size. The average peak spacing (ΔV) is 260 ± 10 mV, and as shown in Figure 6.8b there is a linear correspondence between the peak potential and the charge state. The capacitance of MPC-6(Au_{140}) obtained from the slope of the line in Figure 6.8b is 0.62 aF, and therefore

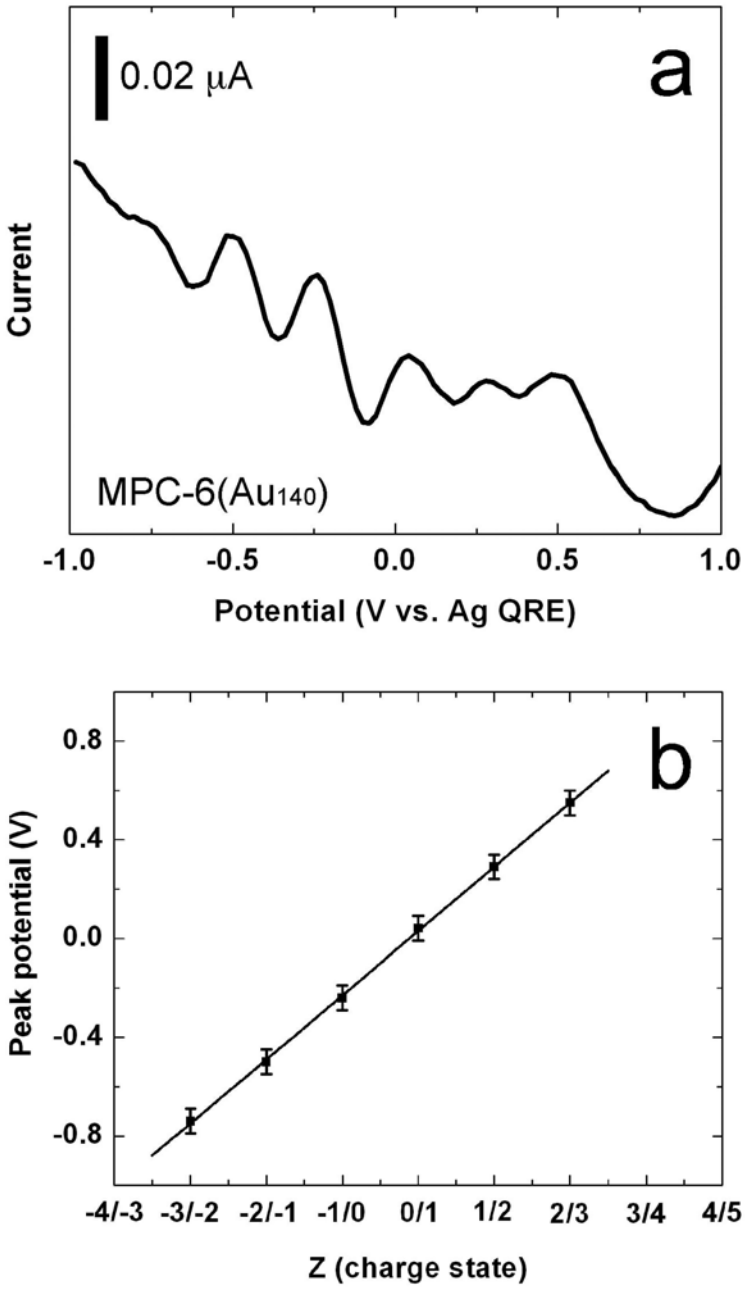

Figure 6.8. (a) DPV for a 0.18 mM MPC-6(Au_{140}) solution and (b) the relationship between the peak potentials in (a) and the charge state of the MPCs. The electrolyte solution consisted of 0.05 M Bu_4NPF_6 in dichloromethane. Other conditions used to obtain these data are provided in the Experimental Section.

the diameter ($2r$) of these nanoparticles calculated from eq 2 is 1.7 ± 0.1 nm. This value can be compared to that determined by TEM of G6-$Q_{116}(Au_{140})$ (1.6 ± 0.3 nm) and MPC-6(Au_{140}) (1.6 ± 0.3 nm), and to the value of 1.7 nm calculated assuming a 140-atom spherical Au nanoparticle. Note that particle-size data for all Au and Pd MPCs are collected in Table 6.1, and that TEM micrographs and size-distribution histograms for all the DENs and MPCs discussed in this paper are provided in the Figures 6.2, 6.3, and 6.5-6.7.

Figure 6.9a is the DPV of MPC-6(Au_{225}) extracted from G6-$Q_{116}(Au_{225})$, and Figure 6.9b is the corresponding plot of peak potential versus charge state. Peaks having a spacing of ΔV = 250 ± 50 mV are present, but the high standard deviation indicates that these larger MPCs are not as size-monodisperse as MPC-6(Au_{140}). The capacitance of MPC-6(Au_{225}) calculated from the slope of the line in Figure 6.9b is 0.65 aF, which correlates to a nanoparticle diameter of 1.8 ± 0.4 nm. The corresponding values obtained by TEM for G6-$Q_{116}(Au_{225})$ and MPC-6(Au_{225}) are 1.8 ± 0.5 nm and 1.8 ± 0.4 nm. Note that the ΔV and TEM data have nearly identical relative standard deviations,

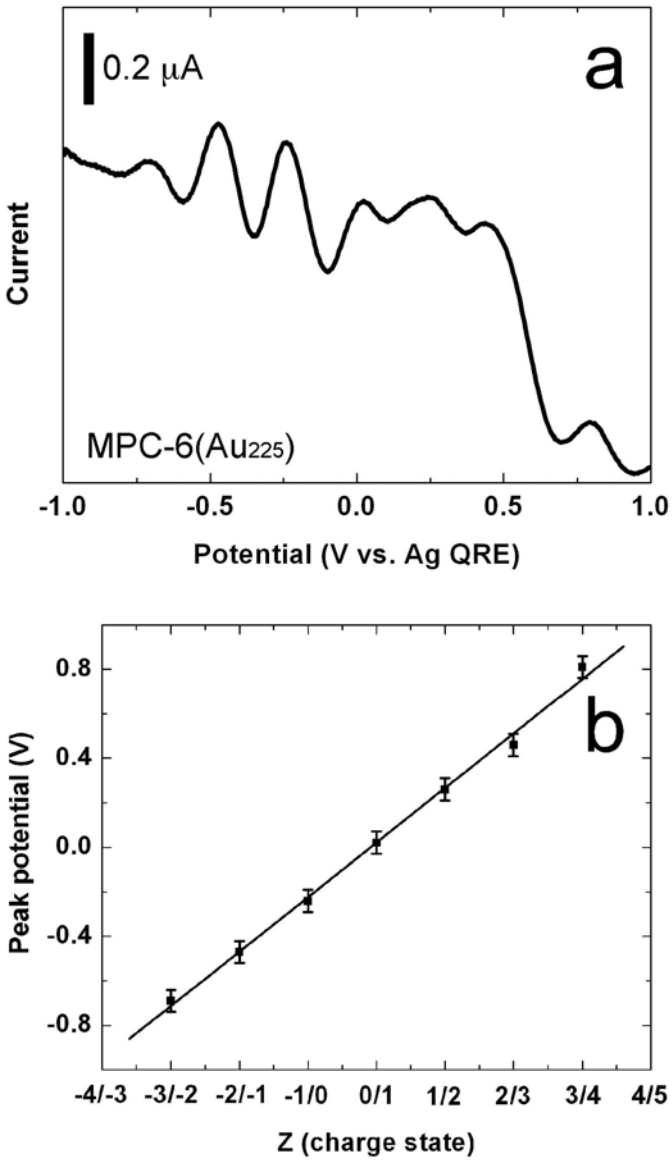

Figure 6.9. (a) DPV response of a 0.24 mM MPC-6(Au_{225}) solution and (b) the relationship between the peak potentials in (a) and the charge state of the MPCs. The electrolyte solution consisted of 0.05 M Bu_4NPF_6 in dichloromethane. Other conditions used to obtain these data are provided in the Experimental Section.

indicating the close agreement of these two methods. The calculated diameter for a close-packed 225-atom Au sphere is 1.9 nm.

Electrochemical properties of extracted Pd MPCs. There are only a few reports describing the electrochemical properties of Pd MPCs, and in all cases the signal-to-noise ratio is poor compared to Au MPCs.[29] This probably indicates that it is more difficult to synthesize and purify Pd MPCs compared to Au MPCs, but it might also be related to the propensity of Pd nanoparticles to partially oxidize in the presence of oxygen.[28,175] The DPV of MPC-6(Pd_{40}), obtained by extraction from G4-OH(Pd_{40}), is shown in Figure 6.10a. The presence of distinct peaks (ΔV = 460 ± 70 mV) indicates a fairly monodisperse distribution of particle sizes, but the standard deviation is rather large. The capacitance of MPC-6(Pd_{40}), calculated from the slope of the peak-potential-versus-charge data (Figure 6.11a) is 0.35 aF, which corresponds to a nanoparticle diameter of 1.2 ± 0.2 nm. This value is close to the theoretical value of 1.1 nm calculated for a sphere containing 40 Pd atoms.

The uniformity in the DPV peak spacing for MPC-6(Pd_{40}) is somewhat surprising, because it has previously been

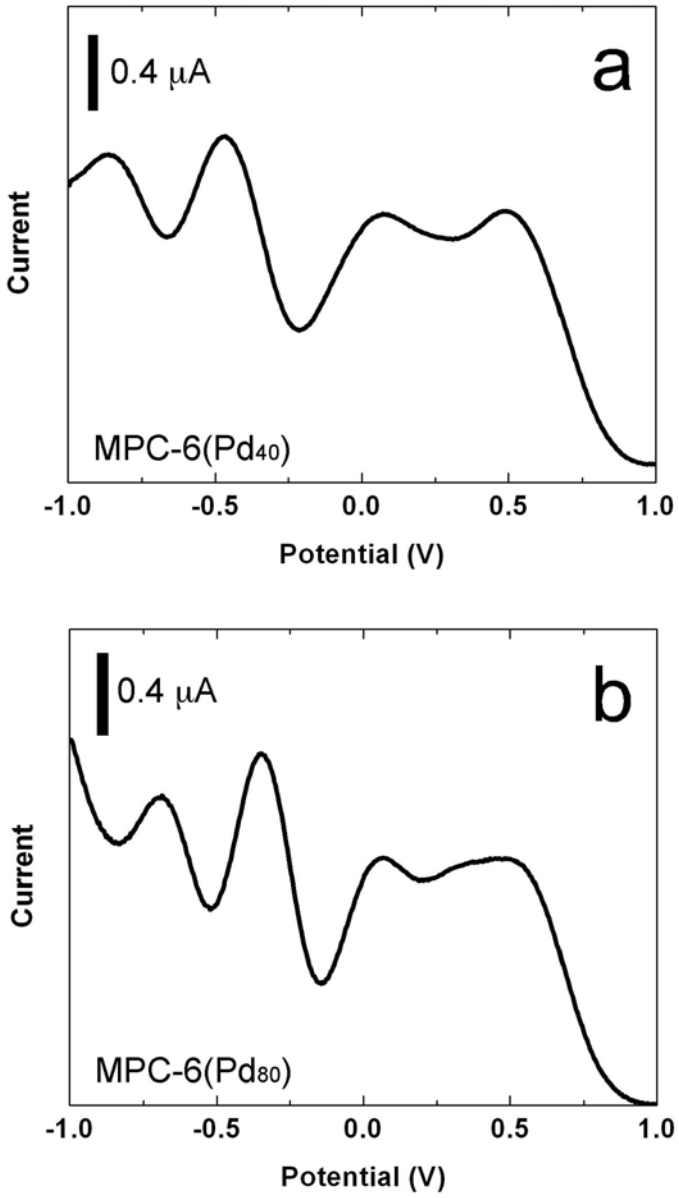

Figure 6.10. DPVs obtained for (a) 1.2 mM MPC-6(Pd_{40}) and (b) 1.1 mM MPC-6(Pd_{80}). The electrolyte solution consisted of 0.05 M Bu_4NPF_6 in dichloromethane. Other conditions used to obtain these data are provided in the Experimental Section.

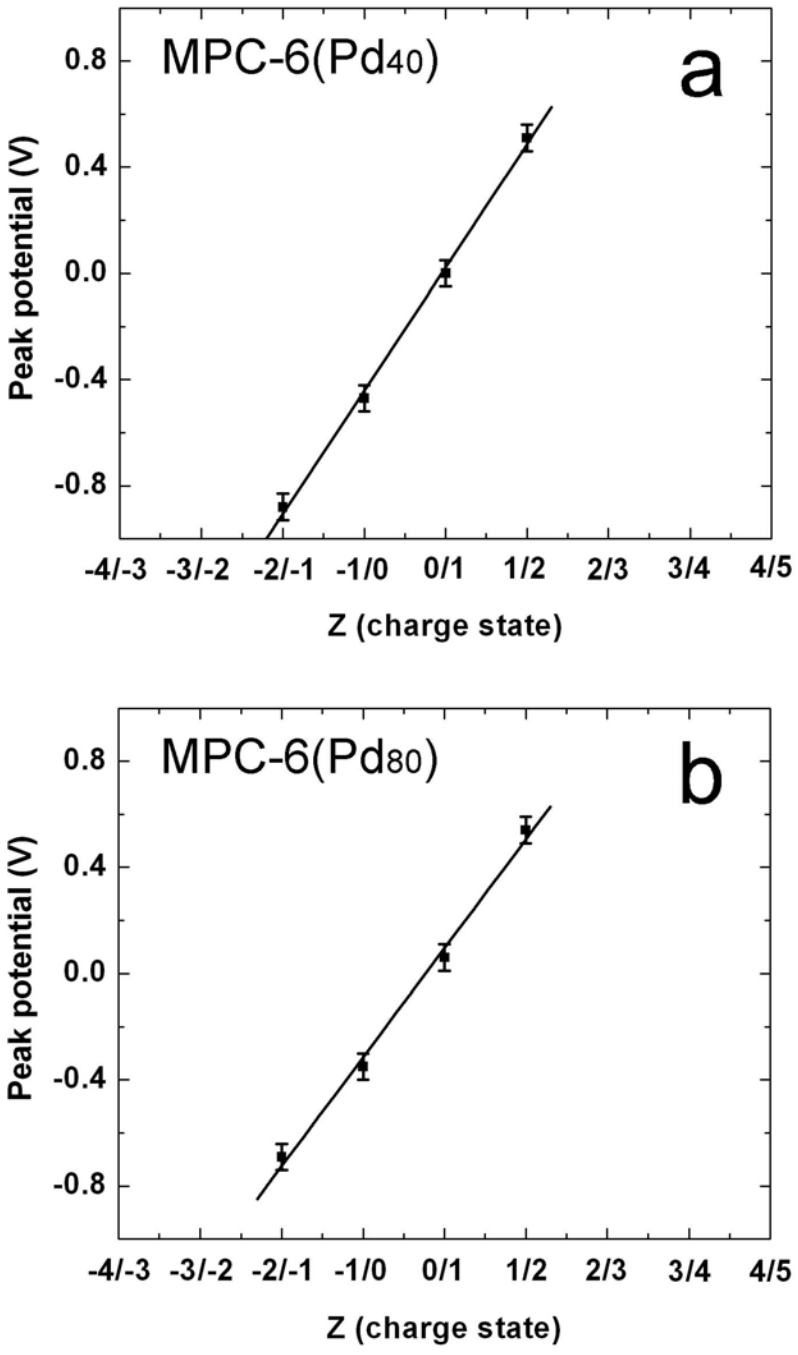

Figure 6.11. Plots of peak potential versus charge state for the indicated Pd MPCs. The data correspond to that shown in Figure 6.10.

shown that Au MPCs containing 38 atoms exhibit irregularly spaced peaks. The latter behavior has been attributed to the presence of a molecule-like electronic band structure these very small Au nanoparticles; that is, they are insufficiently large to have developed metal-like electronic characteristics.[41,42] If this explanation is correct, which seems likely, then the results reported here for MPC-6(Pd_{40}) imply that Pd nanoparticles possess more metal-like character than Au nanoparticles containing the same number of atoms. Such differences in electronic structure for different metals is to be expected.

We[20, 44, 73, 100, 116] and others[158,174] have previously reported a significant discrepancy between the size of Pd nanoparticles measured by TEM and their calculated sizes. For example, our results have shown that Pd_{40} DENs have measured diameters ranging from 1.4 ± 0.2 to 1.7 ± 0.4 nm. As mentioned earlier, the calculated diameter is 1.1 nm. TEM micrographs of the G4-OH(Pd_{40}) and MPC-6(Pd_{40}) nanoparticles used in this study indicate average particle sizes of 1.6 ± 0.3 nm and 1.5 ± 0.4 nm, respectively (Figure 6.5). The discrepancy between the calculated sizes and the diameters determined from TEM data has been rationalized in a number of ways. For example, Ploehn and

coworkers have attributed this effect to a change in nanoparticle structure arising from its interaction with a solid surfaces (for example, a TEM grid).[176] However, this argument seems unlikely to be correct, because it does not account for our finding that Au DENs of any size and larger Pd DENs (for example, G4-OH(Pd_{140})) have the expect size.

It is more likely that the disparity between the calculated and measured sizes of small Pd DENs and MPCs is a consequence of the finite resolution of the microscope used to generate size-distribution histograms. That is, because Pd particles having diameters of less than 1.0 nm are difficult to image, they are selectively omitted from the histograms. This effect is not too serious for larger Pd particles, such as the 140-atom nanoparticles used in this study, because the population of particles having diameters of less than 1 nm is not very big. However, for particles having an average diameter of around 1.2 nm there are likely to be a significant number of particles in the <1.0 nm range that are not properly counted. This is particularly true for the lighter transition metals like Pd, which offer poorer image contrast than Au.

Figure 6.12 shows size-distribution histograms for MPC-6(Pd_{40}), MPC-6(Pd_{80}), and MPC-6(Pd_{140}) determined by

counting particles in the corresponding TEM micrographs (Figure 6.5-6.7). The solid lines represent the Gaussian fits to the experimentally determined particle-size distributions, and the dashed lines represent Gaussian curves calculated for spherical Pd particles containing 40, 80, and 140 atoms. The standard deviations for the calculated histograms were assumed to be the same as those for the experimental data. The calculated (dashed) Gaussian for MPC-6(Pd_{40}) (Figure 6.12a) clearly anticipates the presence of nanoparticles <1.0 nm in diameter. However, as discussed earlier, particles in this size range are under-represented in the counting process, because they are not sufficiently well resolved. As the particle size increases (Figure 6.12b, MPC-6(Pd_{80})), the difference between the peaks in the calculated and experimental distributions decreases because there are less small particles unaccounted for. For larger particles (MPC-6(Pd_{140}), Figure 6.12c) the calculated and experimental Gaussian curves coincide, because nearly all particles present in the population are large enough to be counted.

Figure 6.10b shows the DPV for MPC-6(Pd_{80}) prepared by extraction from G6-OH(Pd_{80}). The voltammetry is qualitatively similar to that obtained for MPC-6(Pd_{40}), but

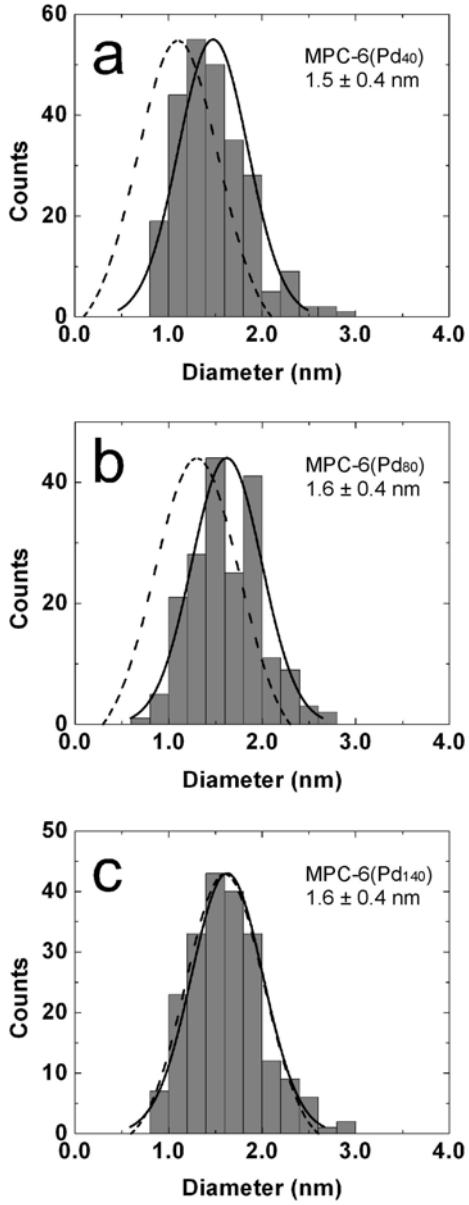

Figure 6.12. Size-distribution histograms for (a) MPC-6(Pd_{40}), (b) MPC-6(Pd_{80}), and (c) MPC-6(Pd_{140}) obtained from TEM data (micrographs are provided in the Supporting Information). The solid lines represent Gaussian fits to the experimentally determined data. The dashed lines correspond to Gaussians having the same standard deviation as the solid lines, but average values calculated by assuming spherical particles containing the indicated number of atoms. See Table 6.1.

the average peak spacing is a little smaller: ΔV = 410 ± 70 mV compared to ΔV = 460 ± 70 mV for MPC(Pd_{40}). The capacitance of MPC-6(Pd_{80}) calculated from the plot of peak potential versus charge state (Figure 6.11b) is 0.39 aF, which corresponds to a diameter of 1.3 ± 0.2 nm. This value is identical to the theoretical size of an 80-atom, spherical Pd nanoparticle, but it is smaller than the 1.6 nm diameter measured by TEM. As discussed in the previous paragraph, this is a consequence of smaller particles being under-represented in the counting process.

We examined the electrochemical properties of MPC-6(Pd_{140}), so that the results could be compared to that of MPC-6(Au_{140}), which has a similar theoretical size. Figure 6.13a shows the DPV for MPC-6(Pd_{140}) and the relationship between the peak potentials in these data and the charge state of the MPCs is shown in Figure 6.13b. The peaks in Figure 6.13a are narrow and better defined than for the smaller Pd MPCs, and this is reflected in the standard deviation of their width: ΔV = 270 ± 20 mV. The capacitance value obtained from slope of the line shown in Figure 6.13b is 0.59 aF, and the diameter calculated from this capacitance value is 1.7 ± 0.1 nm. In contrast to the

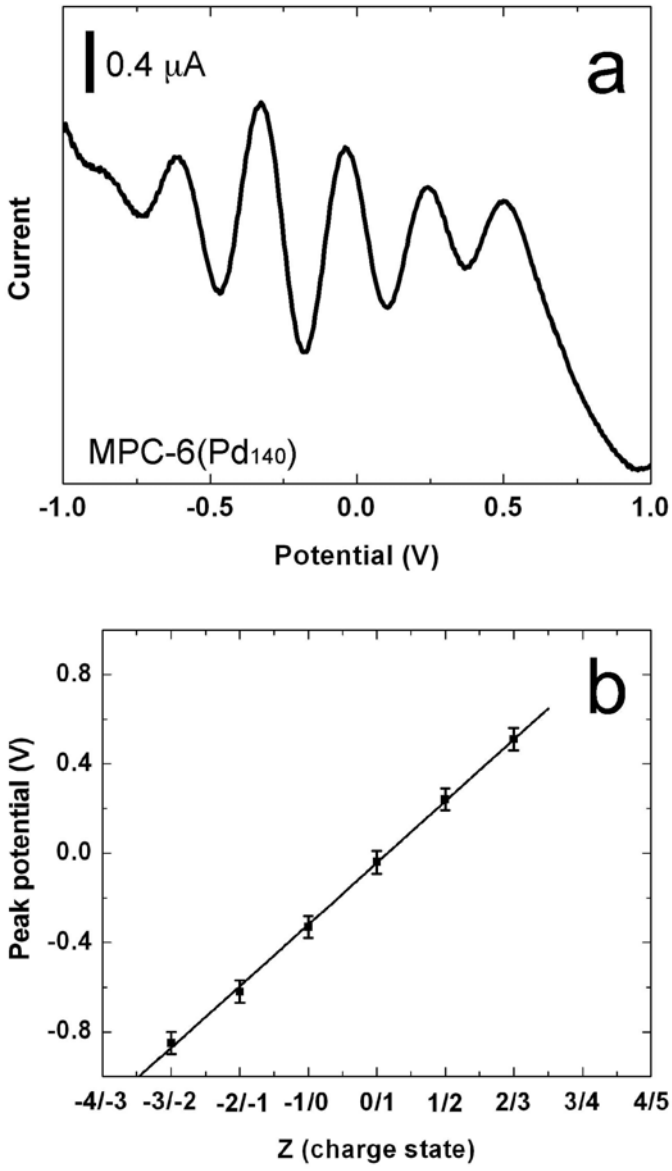

Figure 6.13. (a) DPVs obtained for a 1.1 mM MPC-6(Pd_{140}) solution and (b) the relationship between the peak potentials in (a) and the charge state of the MPCs. The electrolyte solution consisted of 0.05 M Bu_4NPF_6 in dichloromethane. Other conditions used to obtain these data are provided in the Experimental Section.

nanoparticles measured by DPV are identical (1.7 ± 0.1 nm, smaller Pd nanoparticles, this value is in accord with both the theoretical value (1.6 nm) and the diameter measured by TEM (1.6 ± 0.4 nm). This finding is consistent with the explanation offered earlier for the discrepancy between the TEM and electrochemical data. That is, the histogram for the 140-atom Pd nanoparticles (Figure 6.12c) is likely to better represent the population of particles present. Importantly, the diameters of the 140-atom Au and Pd Table 6.2), which provides evidence that these materials are acting as simple metallic capacitors whose properties do not depend on the identity of the metal core.

The data for Pd nanoparticles reported here can be compared to previous reports from others for related materials. For example, Zamborini and coworkers measured a DPV ΔV value of 450 mV for Pd particles coated with a hexanethiol monolayer.[29] The average diameter of these particles determined by TEM was 2.2 nm, but this ΔV value corresponds to a diameter of just 1.2 nm (this assumes that ε for the organic shell has the widely accepted value of 3).[29] They rationalized this finding by suggesting that the population of Pd MPCs giving rise to the DPV peaks was not

Table 6.2. Comparison of calculated nanoparticle diameters for MPCs to diameters measured experimentally by TEM and DPV.

MPC-6	Calculated particle size[a] (nm)	TEM particle size (nm)	Experimental peak spacing (mV)	DPV particle size[b] (nm)
Au_{140}	1.7	1.6 ± 0.3	260 ± 10	1.7 ± 0.1
Au_{225}	1.9	1.8 ± 0.4	250 ± 50	1.8 ± 0.4
Pd_{40}	1.1	1.5 ± 0.4	460 ± 70	1.2 ± 0.2
Pd_{80}	1.3	1.6 ± 0.4	410 ± 70	1.3 ± 0.2
Pd_{140}	1.6	1.6 ± 0.4	270 ± 20	1.7 ± 0.1

(a) Calculated using the equation: $n=4\pi r^3/3\nu_g$, where n is the number of Au or Pd atoms, r is radius of the Au or Pd nanoparticle, and ν_g is the volume of one Au (17 Å^3) or Pd (15 Å^3) atom.[145]
(b) This particle size was calculated from eqs 1 and 2 using the average peak spacing in the DPVs (Figure 6.8 – 6.10, 6.13).

well-represented by the TEM data or that the magnitude of for the adsorbed monolayer was different for Pd compared to Au. Chen and coworkers also reported DPV data for Pd MPCs.[28] In this case the average peak spacing was 210 mV, which corresponds to an average particle size of 2.0 nm (assuming $\varepsilon = 3$). However, the size determined by TEM (2.5 ± 0.3 nm) again over-estimates the average particle size.[28] This difference could arise from a dependence of ε on the size and composition of the metal nanoparticle.

Specifically, the authors concluded that the dielectric constant of the protecting hexanethiol monolayer was 2.1. This seems somewhat low given that the measured dielectric constant for a hexanethiol monolayer on a planar Au substrate is 2.4.[177] For reference, the dielectric constant of liquid hexanethiol is 4.3. It seems likely, therefore, that the dielectric constant of a hexanethiol monolayer on a small Pd cluster would be between 2.4 and 4.3. The point is that in both of these previous reports the TEM-derived histograms were assumed to be correct and the assumptions used to calculate the size of the particles from the electrochemical data were assumed to be wrong. In contrast, we think it more likely that the TEM data are less reliable than the electrochemical results. Note that

it is somewhat difficult to interpret the results in these prior studies, because it is not possible to calculate an anticipated particle size since there is no correlation between the amount of metal initially introduced into the synthesis and the particle size. In the dendrimer templating method, however, nanoparticle purification is not necessary, and therefore there is a direct relationship between particle size and the number of metal ions used for the synthesis. Because all of the metal is accounted for, it is possible to directly compare the electrochemical and TEM data to a calculated particle size.

6.4 Summary and Conclusions

There are two main conclusions from this paper. First, the nanoparticle extraction process does not result in a measurable change in the size of the precursor DENs, which is consistent with our previously reported spectroscopic and microscopic data.[20, 21] An important consequence of this finding is that it will now be possible to template, extract, and then electrochemically characterize MPCs having a wide variety of compositions and structures, including alloy and core/shell bimetallic nanoparticles. Second, electrochemical methods provide better agreement

with the calculated size of MPCs than do TEM data. This is particularly true for the smallest Pd nanoparticles, which are more poorly resolved by TEM than Au MPCs of the same size. We rationalize this finding by pointing out that size-distribution histograms are skewed in favor of larger particles for populations of nanoparticles having very small average sizes; this is particularly true for lighter transition elements like Pd. We are able to make this assertion because the average size of DENs is defined by the dendrimer-to-metal ratio used for the synthesis. This assumption is not valid for synthetic methods that result in loss of metal during purification steps.

At the present time we are examining the properties of MPCs that have not previously been characterized by electrochemical methods. This includes those prepared from Cu, Ag, and Pt, as well as both alloy and core/shell bimetallic nanoparticles. It will be interesting to see if, as predicted by the double-layer charging model, the electrochemical properties of MPCs are independent of their composition. Likewise, it should be enlightening to study the electrochemical properties of very small MPCs composed of different metals and correlate the results to the existing model that postulates molecule-like properties for

such materials.[41,42] The results of these studies will be reported shortly.

CHAPTER VII

ELECTROCHEMICAL PROPERTIES OF MONOLAYER-PROTECTED PdAu BIMETALLIC NANOPARTICLES EXTRACTED FROM WITHIN DENDRIMER TEMPLATES

7.1 Introduction

Here we report the synthesis and characterization of the electrochemical properties of dendrimer-templated PdAu bimetallic monolayer protected clusters (MPCs). Specifically, PdAu bimetallic dendrimer-encapsulated nanoparticles (DENs) were prepared in the interior of dendrimer and extracted by thiol ligands into an organic phase. These MPCs are sufficiently monodisperse enough to show a quantized double layer (QDL) charging behavior in the electrochemical studies without any purification steps. To our knowledge, QDL charging behavior has not been previously reported for bimetallic MPCs; this may be due to improper preparation or purification of bimetallic MPCs, which are relatively less stable than Au MPCs. In addition, this study demonstrated that the electrochemical method can be successfully applied to the characterization of DENs of varying compositions.

We have reported that size-monodisperse nanoparticles can be prepared within the interior of dendrimers,[10-12,92] and nanoparticle size can be precisely controlled by simply adjusting the [metal ion]:[dendrimer] ratios.[45] DENs are typically synthesized by first sequestering metal ions at the interior of a dendrimer and subsequently reducing them with a reducing agent. We and others previously reported that alloy and core/shell DENs could be prepared by co-complexation or sequential loading, respectively, and these DENs exhibited structure-dependent optical properties and catalytic activities.[15-19,160] For example, the PdAu core/shell DENs, G6-OH[Pd_{55}](Au_{255}) (brackets indicate the core metal and parentheses indicate the shell metal), showed a surface plasmon band at 520 nm in the UV-vis absorbance spectrum, which suggests the presence of an Au shell around a Pd core. However the surface plasmon band was not observed in the absorbance spectroscopy of PdAu alloy DENs (G6-OH($Pd_{55}Au_{255}$)).

Recently our group employed electrochemical methods to characterize DENs, in addition to the conventional methods (such as TEM and UV-vis spectroscopy).[46] Specifically, we characterized the electrochemical properties of dendrimer-templated MPCs prepared by the extraction method. The

extraction was carried out by mixing aqueous phase DENs with *n*-alkanethiols in the organic phase.[20,21] As a result, nanoparticles at the interior of the dendrimer were extracted into the organic phase as MPCs, without affecting the nanoparticle sizes. With these approaches, dendrimer-templated Au and Pd MPC sizes could be calculated by electrochemical methods and the calculated sizes were generally in good agreement with both the theoretical size and the sizes measured from TEM.[46]

The most common alternative way of preparing MPCs is a two-phase reaction first described by Brust, in which Au ion are reduced in the presence of alkanethol ligands.[23,24] MPCs are initially polydisperse because nanoparticles are prepared by a random nucleation and growth mechanism; however, the monodispersity can be improved by purification methods such as fractional precipitation,[34,38] HPLC,[32] and annealing.[33] MPCs can be prepared in large quantities and are stable during repeated dissolution and isolation due to their high air-stability.[23,25]

The electrochemical properties of MPCs have been extensively studied by Murray's group.[22,23,35,39,41,150,162] MPCs act as tiny capacitors, and QDL charging can be observed at room temperature ($\Delta V = e/C_{CLU}$) as a peak in the voltammogram

because of their small capacitances (~aF). The cluster capacitance is a function of particle size and it is therefore possible to calculate MPC sizes from the capacitance of MPCs.[22] Most research, however, is related to Au MPCs. Pd,[28,29] Cu,[27] and Ag[26] MPCs have been rarely reported due to difficulties in the preparation and purification.

The electrochemical responses of small Au MPCs (such as Au_{38}, ~1.1 nm) are different from those of large MPCs in which electrochemical responses can be explained by a simple metal-capacitor model.[41,42] In the voltammogram of Au_{38} MPCs, QDL charging peaks are irregularly spaced and large peak intervals between -1/0 and 0/+1 charge states of MPCs were observed. This molecular-like behavior originated from the opening of a HOMO-LUMO gap due to the very small particle size.

In this paper, we prepared dendrimer-templated Pd-Au bimetallic ($Pd_{70}Au_{70}$ and $Pd_{19}Au_{19}$) MPCs, that are difficult or impossible to prepare by other methods. The size of $Pd_{70}Au_{70}$ MPCs calculated from the electrochemical method agrees with the sizes measured from TEM and the theoretical values. However, electrochemical responses of $Pd_{19}Au_{19}$ MPCs differed from $Pd_{70}Au_{70}$ MPCs and showed a large central gap

between -1/0 and 0/+1 charge states in DPV due to the HOMO-LUMO gap energy. This band gap energy was between the values of Au_{38} and Pd_{40} MPCs.

7.2 Experimental Section

Chemicals and materials. DENs were prepared within sixth-generation, amine-terminated poly(amidoamine) (PAMAM) dendrimers that were partially quaternized on their periphery.[44] These materials are referred to as G6-Q_{116}, because 116 of the 256 peripheral primary amine groups were quaternized using a previously reported procedure. P_2O_5, *n*-hexanethiol, $NaBH_4$, $HAuCl_4$, (Aldrich Chemical Co., Milwaukee, WI), and K_2PdCl_4 (Strem Chemicals, Inc.) were used as received. Lithium tetrakis (pentafluorophenyl)borate etherate ($LiB(C_6F_5)_4O(CH_2CH_3)$, Boulder Scientific Co., Mead, CO) and bis(triphenylphosphoranylidene) ammonium chloride ($(C_6H_5)_3$ $P=N(Cl)=P(C_6H_5)_3$, Aldrich Chemical CO., Milwaukee, WI) were used as received. HPLC grade hexane, and reagent grade ethanol, toluene, dichloromethane, and nitric acid, were purchased from EMD Chemicals Inc. (Gibbstown, NJ). 18 MΩ•cm Milli-Q water (Millipore, Bedford, MA) was used throughout.

Synthesis and extraction of the PdAu bimetallic and Au nanoparticles. PdAu bimetallic DENs were prepared by following: 10.0 mL of a 10.0 μM G6-Q_{116} aqueous solution was mixed with 19, or 70 equiv of a 2.00 mM K_2PdCl_4 aqueous solution. 19 or 70 equiv of a 2.00 mM $HAuCl_4$ aqueous solution was added to the mixture after 30 min. The mixture was vigorously stirred for 10 min and then reduced with 10-fold molar excess of $NaBH_4$. This yields G6-$Q_{116}(Pd_{19}Au_{19})$ and G6-$Q_{116}(Pd_{70}Au_{70})$ DENs respectively. For the preparation of G6-$Q_{116}(Au_{38})$ DENs, 10.0 mL of an aqueous 10.0 μM G6-Q_{116} solution was mixed with either 38 equiv of an aqueous 2.00 mM $HAuCl_4$ solution to yield the corresponding dendrimer-encapsulated ions (G6-$Q_{116}(Au^{3+})_{38}$). Next, these pale yellow solutions were vigorously stirred for 15 min and then G6-$Q_{116}(Au_{38})$ is prepared by addition of a 5-fold molar excess of $NaBH_4$ in 0.30 M NaOH.

The extraction was carried out by mixing together 10.0 mL of either a PdAu DEN or Au DEN aqueous solution and 10.0 mL of a toluene solution containing 50.0 mM *n*-hexanethiol. A 150-fold molar excess of $NaBH_4$ was added to the mixture and the vial was shaken.[20, 21] After settling, the toluene layer containing the *n*-hexanethiol-coated MPCs (MPC-

6(Pd_nAu_n), where n is number of metal atoms) was transferred to a round-bottom flask and the solvent and excess *n*-hexanethiol were removed by evaporation under vacuum at 23 ± 2 °C. The dried MPC-6($Pd_{19}Au_{19}$), MPC-6($Pd_{70}Au_{70}$) and MPC-6(Au_{38}) were used for subsequent experiments without further purification. (* MPC-6($Pd_{19}Au_{19}$) is not so stable as larger MPC-6($Pd_{70}Au_{70}$). Therefore more efforts to minimize the exposure of MPC-6($Pd_{19}Au_{19}$) to air should be given compared to when MPC-6($Pd_{70}Au_{70}$) is used.)

Spectroscopic and microscopic characterization. UV-vis absorbance spectra were obtained at 23 ± 2 °C using quartz cells and a Hewlett-Packard model 8453 UV-vis spectrometer system (Hewlett-Packard, Wilmington, DE). UV-vis spectra of 1.00 μM PdAu and Au DENs were collected using deionized water as the reference. The UV-vis spectra of the corresponding MPCs were obtained using toluene as the reference. (* We could not observe some peaks due to discrete energy level from UV spectra of Au_{38} or $Pd_{19}Au_{19}$. This might be due to some polydispersity of small MPCs compared to large MPCs (Au_{140} or Au_{225}) as I mentioned earlier.) Transmission electron microscopy (TEM) was performed using a JEOL 2010 electron microscope (JEOL USA

Inc., Peabody, MA). Samples were prepared by placing 5 drops of the nanoparticle solution onto a 400-mesh, carbon-coated copper grid (EM science, Gibbstown, NJ) and allowing the solvent to evaporate in air. The microscope has a point-to-point resolution of 0.19 nm. Single-particle X-ray energy disperse spectroscopy (EDS) analysis was carried out at the university of Texas at Austin using a Philips CM200FEG 200 kV TEM equipped with an Oxford light element EDS detector and an EMiSPEC Vision data acquisition system.

Electrochemical measurements. Differential pulse voltammetry (DPV) was performed in a 2 mL, single-compartment glass cell configured with a 1.0 mm-diameter Au disk working electrode, a Pt wire counter electrode, and a Ag wire quasi-reference electrode (QRE). The Au working electrode was successively polished with 1.00, 0.30, 0.05 μm alumina (Buehler, Lake Bluff, IL) and sonicated in Milli-Q water and ethanol. The counter electrode and QRE were cleaned in piranha solution (3:1 H_2SO_4/H_2O_2; caution: piranha reacts violently with organics and should be used with care) before use, and the QRE was additionally soaked in HNO_3 for 5 min. Dichloromethane was purified by refluxing over P_2O_5 for 3 h and then distilling.

bis(triphenylphosphoranylidene) ammoniumtetrakis (pentafluorophenyl)borate was used as electrolytes. This salt is prepared by metathesis between lithium tetrakis(pentafluorophenyl)borate etherate and bis(triphenylphosphoranylidene)ammonium chloride.[43] The each solution was prepared by dissolving salts in water and methanol 1:2 mixture solution. The mixing of equimolar of each solution results in white precipitate immediately. This white precipitate filtered and recrystallized. Crystals dried in the oven at 130 °C for overnight and stored in the drybox. The electrolyte solutions were prepared by dissolving electrolyte in dichloromethane in an Ar-purged vinyl bag. All DPV experiments were performed in the N_2-purged drybox. A model 760B electrochemical workstation (CH Instruments, Austin, TX) was used for all DPV experiments. The parameters used for DPV were: pulse amplitude, 50 mV; pulse width, 50 ms; pulse period, 200 ms; and sample width 17 ms. (* Background was improved with this salt even though the potential window we can use is narrower than the literature. This may due to the residual water which could not be completely removed from glassware which contains MPCs. It is difficult to apply heat to dry

glass wares containing MPCs because MPCs are not stable at high temperature (> 40-50 °C).)

7.3 Results and Discussion

Synthesis and characterization of PdAu bimetallic and Au nanoparticles. PdAu bimetallic nanoparticles were prepared within six-generation PAMAM dendrimers, partially quaternized by ammonium chloride (G6-Q_{116}). Briefly, K_2PdCl_4 (19 and 70 equiv per dendrimer) aqueous solution was mixed with aqueous solution of G6-Q_{116}. Then, $PdCl_4^{2-}$ was sequestered into dendrimer interior for 30 minutes; the 19 and 70 equiv of $AuCl_4^-$ aqueous solution was added to the mixture. PdAu alloy DENs were synthesized by the reduction of metal ions with $NaBH_4$. For comparison, G6-$Q_{116}(Au_{38})$ was also prepared by the same method as described above with modifications. The corresponding MPCs were prepared by extracting nanoparticles with *n*-hexanethiol and employed to subsequent characterization without purification.

UV-vis absorbance spectra of aqueous PdAu alloy DEN and corresponding MPC are shown in Figure 7.1. Figure 7.1 shows featureless spectra in which the absorption band gradually increases toward the higher energy without plasmon bands. This observation was consistent with our

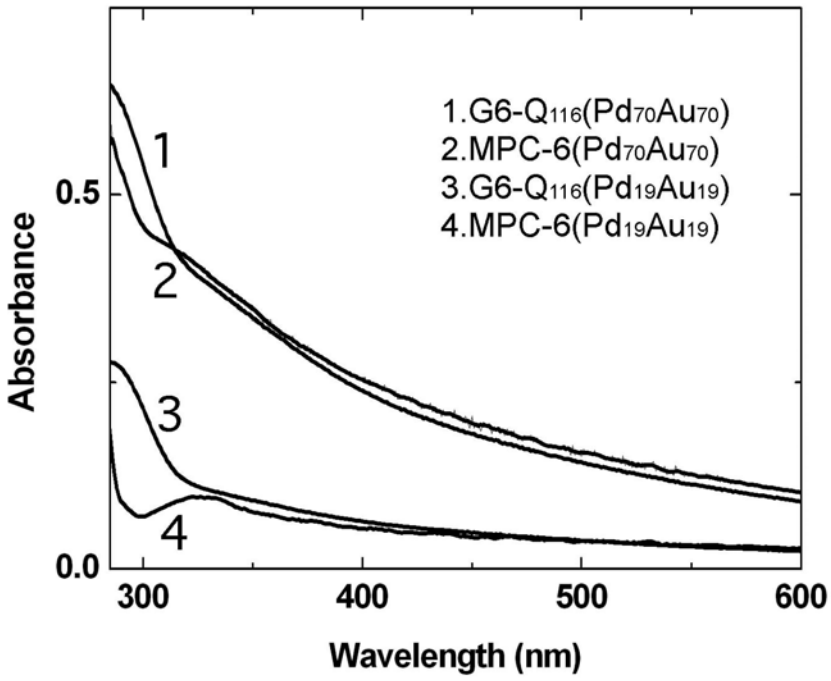

Figure 7.1. UV-vis spectra of (1) 1.00 µM G6-Q_{116}($Pd_{70}Au_{70}$) in water (2) 1.00 µM MPC-6($Pd_{70}Au_{70}$) in toluene (3) 1.00 µM G6-Q_{116}($Pd_{19}Au_{19}$) in water (4) 1.00 µM MPC-6($Pd_{19}Au_{19}$) in toluene.

previous reports on the PdAu DENs.[16] Previous studies showed that alloy PdAu bimetallic G6-$Q_{116}(Pd_nAu_{150-n})$ (25 < n < 150) did not show an absorption band in the UV-vis spectra. The absence of plasmon bands in the UV-vis spectra can be originated from the "damping effect" [123] in which the number of itinerary electrons decreases by interacting with neighboring atoms or a small size of nanoparticles containing a small number of electrons. Generally, UV-vis absorption spectra of MPCs are similar to spectra of DENs. The slight difference in the spectra might originate from the different solvent properties (water vs. toluene).[21,173] The overall shape of UV-vis spectra of G6-$Q_{116}(Pd_{19}Au_{19})$ and corresponding MPCs are similar to the spectra of G6-$Q_{116}(Pd_{70}Au_{70})$ and MPC-6($Pd_{70}Au_{70}$). A broad, weak plasmon band centered at 350 nm in the spectrum of MPC-6($Pd_{19}Au_{19}$) is attributed to discrete energy levels of small nanoparticles.[41]

TEM micrographs and size-distribution histograms before and after extraction of G6-$Q_{116}(Pd_{70}Au_{70})$ are shown in Figure 7.2. TEM micrographs revealed widely separated PdAu nanoparticles with little aggregation. The average particle size of the G6-$Q_{116}(Pd_{70}Au_{70})$ was 1.4 ± 0.3 nm, and this value is comparable to the theoretically calculated

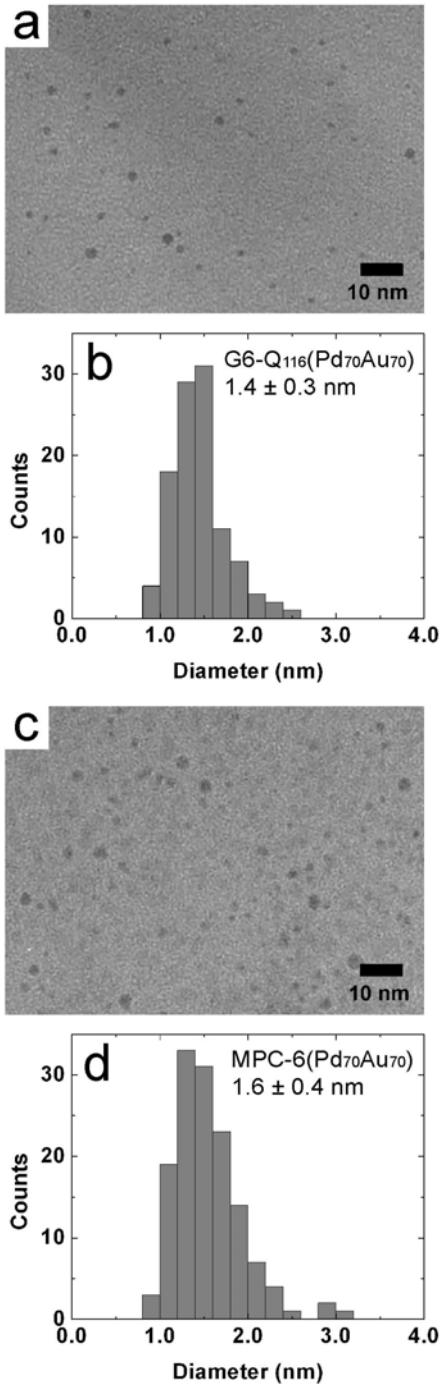

Figure 7.2. TEM micrographs of (a) G6-Q_{116}($Pd_{70}Au_{70}$) and (c) MPC-6($Pd_{70}Au_{70}$) and their corresponding size-distribution histograms (b and d, respectively).

value (1.6 nm) by assuming that these materials are spherical in shape. After extraction, the diameters of corresponding MPCs were 1.6 nm ± 0.4 nm (Figure 7.2c and 7.2d). These results confirm our previous findings that nanoparticle sizes are not altered after extraction.[20, 21] The compositions of G6-$Q_{116}(Pd_{70}Au_{70})$ and MPC-6$(Pd_{70}Au_{70})$ were confirmed by a single-particle EDS measurement. The EDS analysis of five particles demonstrated that bimetallic DENs and MPCs were successfully synthesized. An average composition of Pd was 41 ± 19% and an average composition of Au was 59 ± 19% for the PdAu DENs. These values agree with stoichiometric expectation from the composition of G6-$Q_{116}(Pd_{70}Au_{70})$. In addition, the composition of DENs was not modified after extraction (Pd, 47 ± 23%; Au, 53 ± 23%). Figures 7.3a and 7.3b show TEM micrograph and the size distribution histogram of G6-$Q_{116}(Pd_{19}Au_{19})$. The measured diameter of G6-$Q_{116}(Pd_{19}Au_{19})$ was 1.1 ± 0.3 nm, and this value is identical to the theoretical value (1.1 nm). The TEM micrograph and size-distribution histogram of MPC-6$(Pd_{19}Au_{19})$ are shown in Figures 7.3c and 7.3d. The average diameter of MPC-6$(Pd_{19}Au_{19})$ is 1.2 ± 0.3 nm; this value is close to the theoretical value and the diameter of G6-$Q_{116}(Pd_{19}Au_{19})$. The TEM micrographs and corresponding

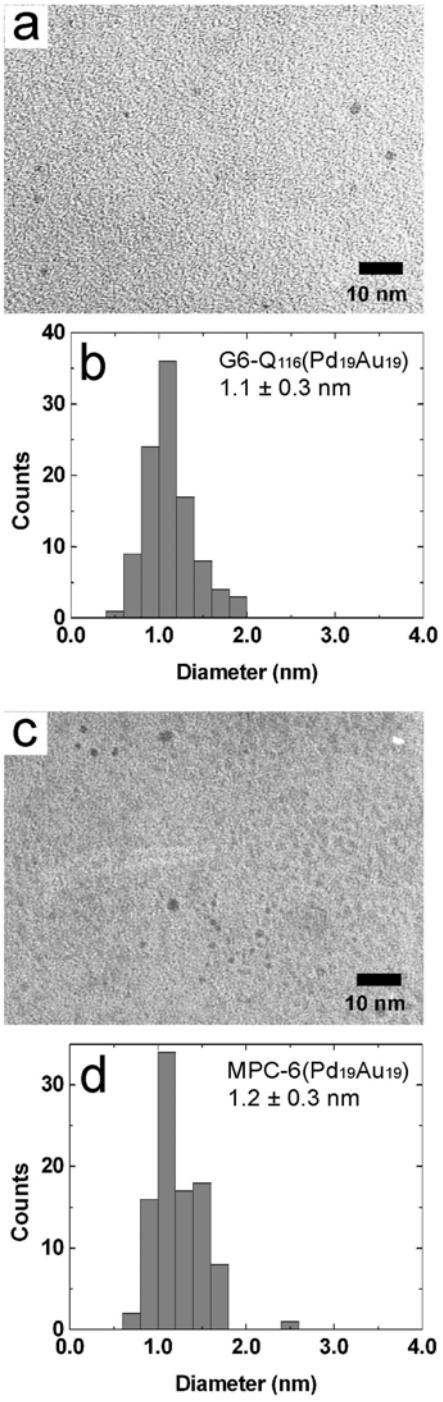

Figure 7.3. TEM micrographs of (a) G6-$Q_{116}(Pd_{19}Au_{19})$ and (c) MPC-6($Pd_{19}Au_{19}$) and their corresponding size-distribution histograms (b and d, respectively).

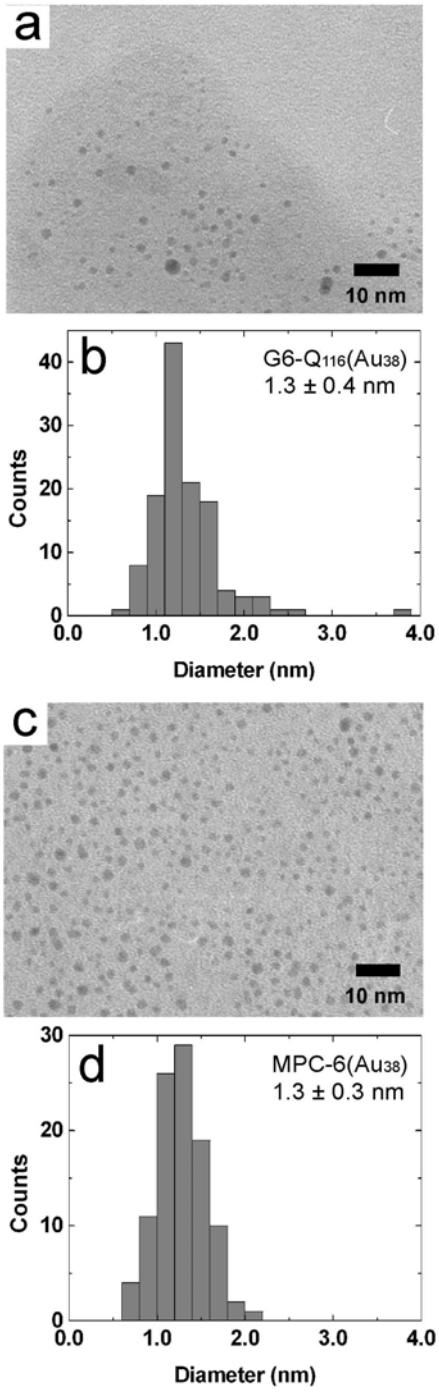

Figure 7.4. TEM micrographs of (a) G6-Q_{116}(Au_{38}) and (c) MPC-6(Au_{38}) and their corresponding size-distribution histograms (b and d, respectively).

histograms of G6-$Q_{116}(Au_{38})$ and MPC-6(Au_{38}) are shown in Figure 7.4. The average particle sizes of G6-$Q_{116}(Au_{38})$ and MPC-6(Au_{38}) were 1.3 ± 0.4 nm and 1.3 ± 0.3 nm, respectively. These sizes are slightly larger than the theoretical value (1.1 nm). UV-vis spectroscopy and TEM results confirm our previous findings that size-monodisperse nanoparticles can be prepared by dendrimer-templating method and after the extraction, sizes of nanoparticles and the high degree of monodispersity are retained.

Electrochemical properties of extracted PdAu and Au MPCs. The QDL charging behavior of Au MPCs can be observable as a peak in the voltammogram at room temperature due to the small capacitance (~aF) of MPCs. The average peak spacing (ΔV) is inversely proportional to the nanoparticle capacitance (C_{CLU}) by eq 1.[22,35]

$$\Delta V = e/C_{CLU} \quad (1)$$

The nanoparticle capacitance is a function of particle size(r), protecting ligand length (d), and dielectric constant(ε) (eq. 2).[42,35]

$$C_{CLU} = 4\pi\varepsilon\varepsilon_0(r/d)(r+d) \quad (2)$$

Therefore it is possible to calculate nanoparticle size by using eq. 1 and eq. 2 from average peak spacing. However, MPCs should be size-monodisperse to show QDL charging peaks in the voltammogram, otherwise the peaks are not well defined and smeared.[23] We recently reported that dendrimer-templated Pd and Au MPCs are sufficiently size monodisperse enough to show QDL charging in voltammograms without purification.[46] Nanoparticle sizes of Pd and Au MPCs with a size range of 1.2–1.9 nm can be precisely calculated by electrochemical methods. The calculated value was in good agreement with the corresponding value obtained by TEM and the theoretically calculated size.

Figure 7.5a shows the DPV of MPC-6($Pd_{70}Au_{70}$) extracted from G6-Q_{116}($Pd_{70}Au_{70}$) and Figure 7.5b corresponds the plot of peak potential versus the MPC charge state. The presence of well defined peaks indicates that the extracted MPCs are size monodisperse enough to show QDL charging peaks in the voltammograms. The capacitance calculated from the slope of the line in Figure 7.5b was 0.49 aF, and corresponding diameter of MPC was 1.5 ± 0.4 nm. This value

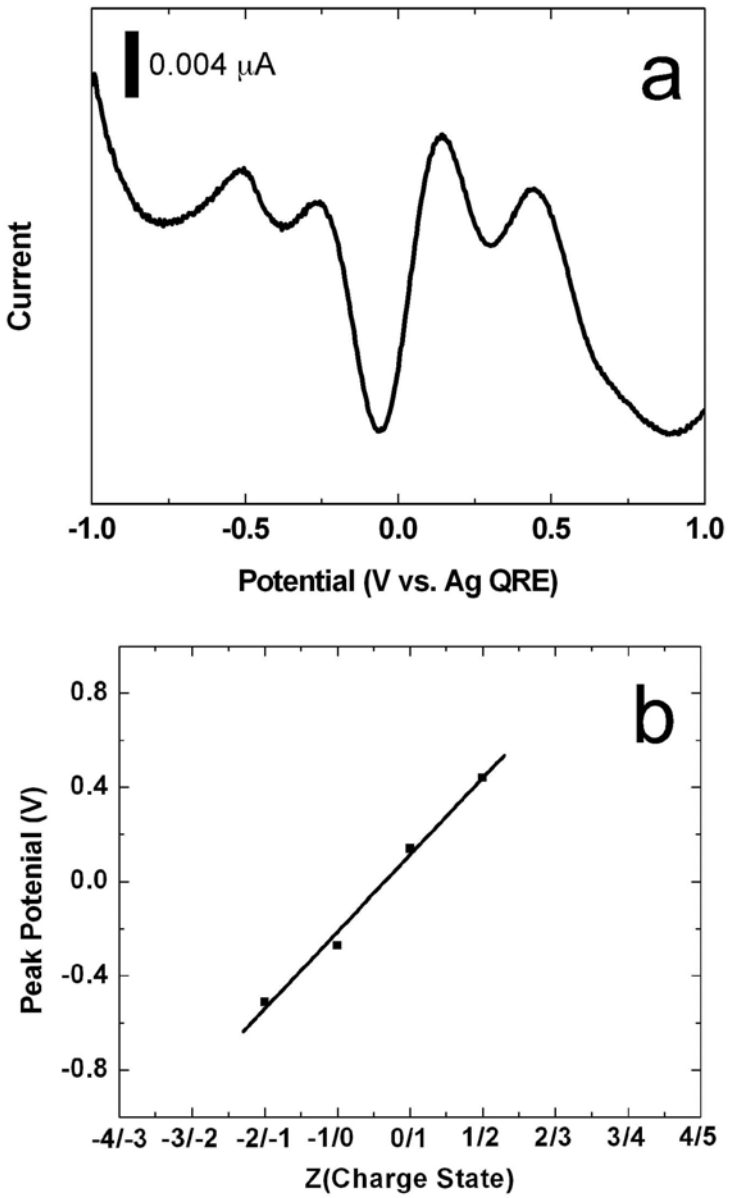

Figure 7.5. (a) DPV for a 0.1 mM MPC-6($Pd_{70}Au_{70}$) solution and (b) the relationship between the peak potentials in (a) and the charge state of the MPCs.

is comparable to the theoretical value (1.6 nm) and the value obtained by TEM of MPC-6($Pd_{70}Au_{70}$) (1.6 nm ± 0.4 nm). The result indicates that MPC-6($Pd_{70}Au_{70}$) can be considered as a metal capacitor and the size can be precisely calculated by electrochemical measurement.

Previous study of Au_{38} MPCs (~1.1 nm) revealed that the DPV of Au_{38} MPCs was different from DPVs of larger size MPCs due to the molecular-like energetics.[41-43] Peaks are irregularly spaced, and large peak spacing was present between the -1/0 and 0/+1 charge state of MPCs. This originates from the emergency of the HOMO-LUMO band gap and band gap energy can be calculated from this peak interval. However, this band gap was not observed for the Pd_{40} MPCs, even though the nanoparticle size is comparable to Au_{38} MPCs.[46] We believe this indicates Pd_{40} MPCs has more metallic characters than Au_{38} MPC.[178] Therefore, we tested the electrochemical properties of MPC-6($Pd_{19}Au_{19}$) containing a similar number of atoms to MPC-6(Au_{38}) and MPC-6(Pd_{40}).

The DPV of MPC-6($Pd_{19}Au_{19}$) is shown in Figure 7.6a. The voltammogram shows that two adjacent peaks with 0.31 V peak spacing and a third peak separated by 0.80 V. The presence of large central gap indicates that the HOMO-LUMO band gap energy was included besides charging energy (0.31 V). The

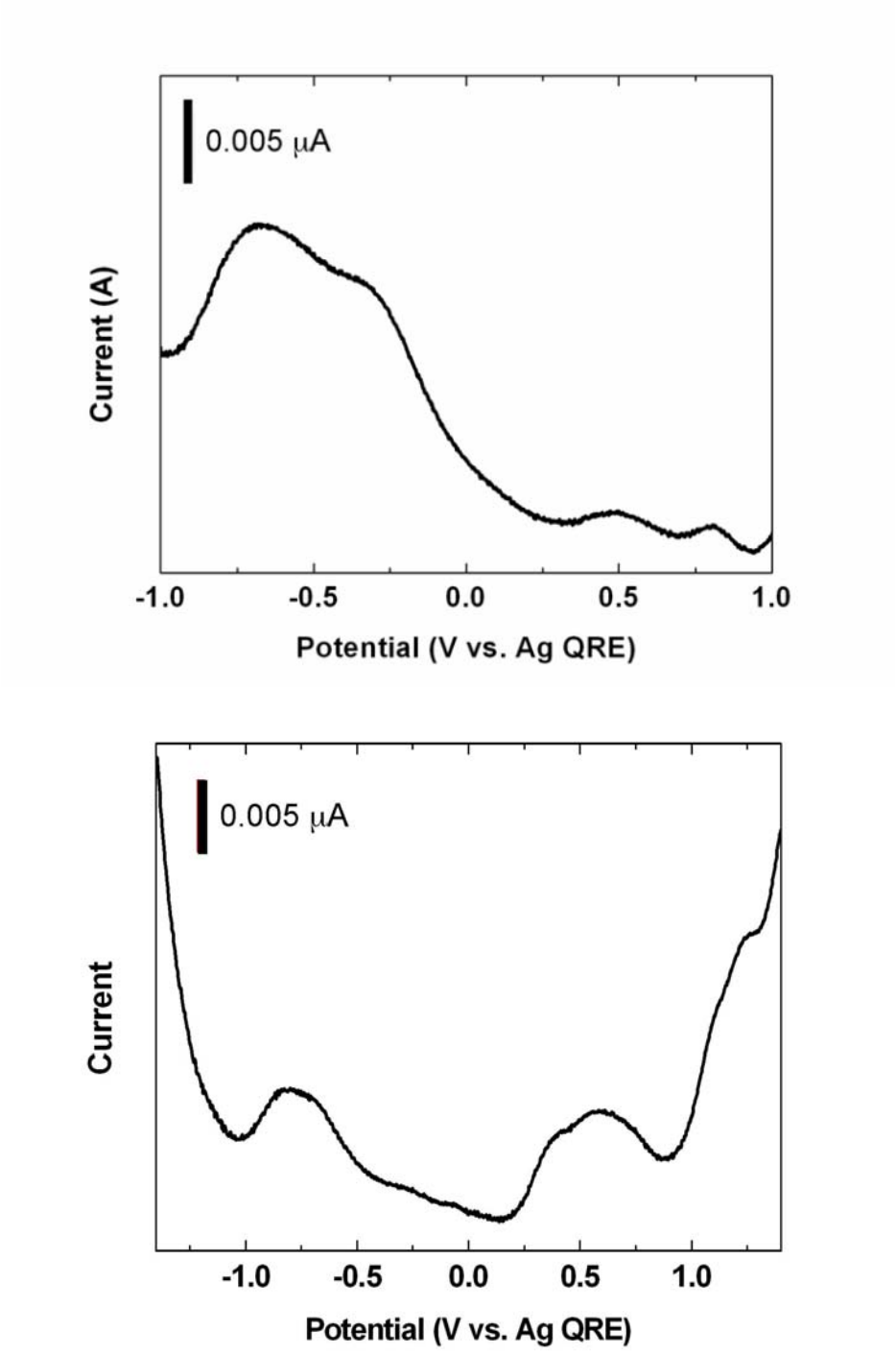

Figure 7.6. DPVs obtained for (a) 0.2 mM MPC-6($Pd_{19}Au_{19}$) and (b) 0.2 mM MPC-6(Au_{38}).

estimated HOMO-LUMO gap energy, by subtracting charging energy from a large energy gap, is 0.49 V and this value is neither that of Au_{38} or Pd_{40} MPCs. For the comparison, the DPV of MPC-6(Au_{38}) was also studied (Figure 7.6b). In the voltammogram, the first oxidation and first reduction peaks were separated by 1.10 V, and the first and second oxidation peaks were separated by 0.22 V. These values are consistent with the previously reported value.[43] The spacing between first oxidation and first reduction peaks was same as MPC-6($Pd_{19}Au_{19}$); however, the HOMO-LUMO gap energy calculated by allowing charging energy (0.22 V) is 0.98 V. This value is larger than the HOMO-LUMO gap energy of MPC-6($Pd_{19}Au_{19}$). The observation is reasonable because MPC-6($Pd_{19}Au_{19}$) has more metal-like characters than MPC-6 (Au_{38}). These results indicate that bimetallic nanoparticle is successfully synthesized, instead of individual nanoparticles separately formed and MPC-6($Pd_{19}Au_{19}$) has the mixed properties of Pd_{40} and Au_{38} MPCs.

7.4 Summary and Conclusions

The main conclusions of this paper are: First, highly monodisperse bimetallic MPCs can be prepared by dendrimer-templated method. This result is consistent to our

previous results that dendrimer-templated MPCs are monodisperse. Second, MPCs with various compositions can be characterized by electrochemical methods. Bimetallic MPCs could be characterized by electrochemical method and MPC size calculated by electrochemical method was consistent with sizes measured by TEM and theoretical values. Third, HOMO-LUMO gap energy of bimetallic nanoparticles can be calculated by electrochemical method and the value is different from monometallic Au or Pd MPCs. This result indicates that PdAu bimetallic MPCs are successfully prepared and HOMO-LUMO band gap energy of PdAu bimetallic MPCs differed from the values of Au_{38} and Pd_{40} MPCs. We are currently examining other type of bimetallic nanoparticles such as Au-Ag and Pt-Pd to extend our knowledge on the structure-sensitive electrochemical properties of bimetallic nanoparticles.

CHAPTER VIII

SUMMARY AND CONCLUSION

First, it was demonstrated that covalently linked films up to six monomer units in length can be prepared on a solid support using vapor-phase reactions. We have shown that a number of reactions routinely used in liquid-phase synthesis are also effective for vapor-phase reactions. These include reactions between acid chlorides and both aliphatic and aromatic amine, hydrolysis reactions, anhydride activation, and reactions between anhydrides and primary amines. Finally, we demonstrated that homobifunctionalized monomers, react primarily via a single functional group rather than cross coupling on the reactive surface. This approach for preparing organic thin films may find use in some technological applications where the trade-off between film quality and convenience is positive.

DENs could be covalently immobilized on Au surfaces. This was accomplished by encapsulating Pt and Pd nanoparticles within dendrimers having a bifunctionalized periphery (Gn-Q_p), and then reacting the dendrimer with an activated SAM. One component of the dendrimer periphery is designed to prevent agglomeration and precipitation during

synthesis of the DEN, and the other component is used for linking the DEN to the SAM surface. These findings demonstrate that partially quaternized PAMAM dendrimers are a useful mediator for preparing robust, highly monodisperse metal nanoparticle arrays on surfaces.

Size-monodisperse Au nanoparticles in the interesting size range of 1-2 nm were synthesized by a very simple, template-based approach using Gn-Q_p. There are some significant advantages of the approach described here for preparing Au nanoparticles. First, this approach is simple, highly reproducible, and does not require careful control of experimental conditions. Second, a high level of monodispersity is attained without the need for subsequence purification. Third, as we have shown previously for Pd DENS, the surface of the particles is accessible, and thus these materials can be used for catalysis. Fourth, the dendrimer itself provides a convenient means for linking DENs to other molecules or surfaces.

Dendrimer-templated Pd, Au, and PdAu MPCs were studied using electrochemical methods. There are two main conclusions from this part of my work: First, the nanoparticle extraction process does not result in a measurable change in the size of the precursor DENs, which

is consistent with our previously reported spectroscopic and microscopic data. Second, MPCs with various compositions can be characterized by electrochemical methods. Monometallic and bimetallic MPCs could be characterized by electrochemical method and MPC size calculated by electrochemical method was consistent with sizes measured by TEM and theoretical values. This finding is important because it will now be possible to template, extract, and then electrochemically characterize MPCs having a wide variety of compositions and structures.

REFERENCES

1. Chailapakul, O.; Sun, L.; Xu, C.; Crooks, R. M. *J. Am. Chem. Soc.* **1993**, *115*, 12459-12467.
2. Xu, C.; Sun, L.; Kepley, L. J.; Crooks, R. M.; Ricco, A. J. *Anal. Chem.* **1993**, *65*, 2102-2107.
3. Yang, H. C.; Dermody, D. L.; Xu, C.; Ricco, A. J.; Crooks, R. M. *Langmuir* **1996**, *12*, 726-735.
4. Sun, L.; Thomas, R. C.; Crooks, R. M. *J. Am. Chem. Soc.* **1991**, *113*, 8550-8552.
5. Himmel, H.-J.; Weiss, K.; Jager, B.; Dannenberger, O.; Grunze, M.; Woll, C. *Langmuir* **1997**, *13*, 4943-4947.
6. Sabapathy, R. C.; Crooks, R. M. *Langmuir* **2000**, *16*, 1777-1782.
7. Sabapathy, R. C.; Crooks, R. M. *Langmuir* **2000**, *16*, 7783-7788.
8. Tomalia, D. A.; Baker, H.; Dewald, J.; Hall, M.; Kallos, G.; Martin, S.; Roeck, J.; Ryder, J.; Smith, P. *Macromolecules* **1986**, *19*, 2466-2468.
9. Watkins, D. M.; Sayed-Sweet, Y.; Klimash, J. W.; Turro, N. J.; Tomalia, D. A. *Langmuir* **1997**, *13*, 3136-3141.
10. Crooks, R. M.; Lemon, B. I.; Sun, L.; Yeung, L. K.; Zhao, M. *Top. Curr. Chem.* **2001**, *212*, 81-135.

11. Crooks, R. M.; Zhao, M.; Sun, L.; Chechik, V.; Yeung, L. K. *Acc. Chem. Res.* **2001**, *34*, 181-190.

12. Scott, R. W. J.; Wilson, O. M.; Crooks, R. M. *J. Phys. Chem. B.* **2005**, *109*, 692 -704.

13. Michels, J. J.; Huskens, J.; Reinhoudt, D. N. *J. Chem. Soc., Perkin Trans 2* **2002**, 102-105.

14. Gröhn, F.; Bauer, B. J.; Akpalu, Y. A.; Jackson, C. L.; Amis, E. J. *Macromolecules* **2000**, *33*, 6042-6050.

15. Scott, R. W. J.; Datye, A. K.; Crooks, R. M. *J. Am. Chem. Soc.* **2003**, *125*, 3708-3709.

16. Scott, R. W. J.; Wilson, O. M.; Oh, S.-K.; Kenik, E. A.; Crooks, R. M. *J. Am. Chem. Soc.* **2004**, *126*, 15583-15591.

17. Scott, R. W. J.; Sivadinarayana, C.; Wilson, O. M.; Yan, Z.; Goodman, D. W.; Crooks, R. M. *J. Am. Chem. Soc.* **2005**, *127*, 1380-1381.

18. Lang, H.; Maldonado, S.; Stevenson, K. J.; Chandler, B. D. *J. Am. Chem. Soc.* **2004**, *126*, 12949-12956.

19. Wilson, O. M.; Scott, R. W. J.; Garcia-Martinez, J. C.; Crooks, R. M. *J. Am. Chem. Soc.* **2005**, *127*, 1015-1024.

20. Garcia-Martinez, J. C.; Scott, R. W. J.; Crooks, R. M. *J. Am. Chem. Soc.* **2003**, *125*, 11190-11191.

21. Garcia-Martinez, J. C.; Crooks, R. M. *J. Am. Chem. Soc.* **2004**, *126*, 16170-16178.

22. Chen, S.; Ingram, R. S.; Hostetler, M. J.; Pietron, J. J.; Murray, R. W.; Schaaff, T. G.; Khoury, J. T.; Alvarez, M. M.; Whetten, R. L. *Science* **1998**, *280*, 2098-2101.

23. Templeton, A. C.; Wuelfing, W. P.; Murray, R. W. *Acc. Chem. Res.* **2000**, *33*, 27-36.

24. Brust, M.; Walker, M.; Bethell, D.; Schiffrin, D. J.; Whyman, R. *J. Chem. Soc., Chem. Commun.* **1994**, 801-802.

25. Brust, M.; Kiely, C. J. *Colloids Surf., A* **2002**, *202*, 175-186.

26. Cheng, W.; Dong, S.; Wang, E. *Electrochem. Commun.* **2002**, *4*, 412-416.

27. Chen, S.; Sommers, J. M. *J. Phys. Chem. B* **2001**, *105*, 8816-8820.

28. Chen, S.; Huang, K.; Stearns, J. A. *Chem. Mater.* **2000**, *12*, 540-547.

29. Zamborini, F. P.; Gross, S. M.; Murray, R. W. *Langmuir* **2001**, *17*, 481-488.

30. Hostetler, M. J.; Zhong, C.-J.; Yen, B. K. H.; Anderegg, J.; Gross, S. M.; Evans, N. D.; Porter, M.; Murray, R. W. *J. Am. Chem. Soc.* **1998**, *120*, 9396-9397.

31. Shon, Y.-S.; Dawson, G. B.; Porter, M.; Murray, R. W. *Langmuir* **2002**, *18*, 3880-3885.

32. Jimenez, V. L.; Leopold, M. C.; Mazzitelli, C.; Jorgenson, J. W.; Murray, R. W. *Anal. Chem.* **2003**, *75*, 199-206.

33. Hicks, J. F.; Miles, D. T.; Murray, R. W. *J. Am. Chem. Soc.* **2002**, *124*, 13322-13328.

34. Schaaff, T. G.; Shafigullin, M. N.; Khoury, J. T.; Vezmar, I.; Whetten, R. L.; Cullen, W. G.; First, P. N.; Gutiérrez-Wing, C.; Ascensio, J.; Jose-Yacamán, M. J. *J. Phys. Chem. B* **1997**, *101*, 7885-7891.

35. Hicks, J. F.; Templeton, A. C.; Chen, S.; Sheran, K. M.; Jasti, R.; Murray, R. W.; Debord, J.; Schaaf, T. G.; Whetten, R. L. *Anal. Chem.* **1999**, *71*, 3703-3711.

36. Chen, S.; Templeton, A. C.; Murray, R. W. *Langmuir* **2000**, *16*, 3543-3548.

37. Hostetler, M. J.; Wingate, J. E.; Zhong, C.-J.; Harris, J. E.; Vachet, R. W.; Clark, M. R.; Londono, J. D.; Green, S. J.; Stokes, J. J.; Wignall, G. D.; Glish, G. L.; Porter, M. D.; Evans, N. D.; Murray, R. W. *Langmuir* **1998**, *14*, 17-30.

38. Whetten, R. L.; Khoury, J. T.; Alvarez, M. M.; Murthy, S.; Vezmar, I.; Wang, Z. L.; Stephens, P. W.;

Cleveland, C. L.; Luedtke, W. D.; Landman, U. *Adv. Mater.* **1996**, *8*, 428-433.

39. Chen, S.; Murray, R. W.; Feldberg, S. W. *J. Phys. Chem. B* **1998**, *102*, 9898-9907.

40. Guo, R.; Georganopoulou, D.; Feldberg, S. W.; Donkers, R.; Murray, R. W. *Anal. Chem.* **2005**, *77*, 2662-2669.

41. Lee, D.; Donkers, R. L.; Wang, G.; Harper, A. S.; Murray, R. W. *J. Am. Chem. Soc.* **2004**, *126*, 6193-6199.

42. Jimenez, V. L.; Georganopoulou, D. G.; White, R. J.; Harper, A. S.; Mills, A. J.; Lee, D.; Murray, R. W. *Langmuir* **2004**, *20*, 6864-6870.

43. Quinn, B. M.; Liljeroth, P.; Ruiz, V.; Laaksonen, T.; Kontturi, K. *J. Am. Chem. Soc.* **2003**, *125*, 6644-6645.

44. Oh, S.-K.; Kim, Y.-G.; Ye, H.; Crooks, R. M. *Langmuir* **2003**, *19*, 10420-10425.

45. Kim, Y.-G.; Oh, S.-K.; Crooks, R. M. *Chem. Mater.* **2004**, *16*, 167-172.

46. Kim, Y.-G.; Garcia-Martinez, J. C.; Crooks, R. M. *Langmuir* **2005**, *21*, 5485-5491.

47. Kim, T.; Ye, Q.; Sun, L.; Chan, K. C.; Crooks, R. M. *Langmuir* **1996**, *12*, 6065-6073.

48. Zhu, P.; Kang, H.; Facchetti, A.; Evmenenko, G.; Dutta, P.; Marks, T. J. *J. Am. Chem. Soc.* **2003**, *125*, 11496-11497.

49. Jung, G.-Y.; Li, Z.; Wu, W.; Chen, Y.; Olynick, D. L.; Wang, S.-Y.; Tong, W. M.; Williams, R. S. *Langmuir* **2005**, *21*, 1158-1161.

50. Ferguson, M. K.; Low, E. R.; Morris, J. R. *Langmuir* **2004**, *20*, 3319-3323.

51. Sun, L.; Crooks, R. M.; Ricco, A. J. *Langmuir* **1993**, *9*, 1775-1780.

52. Wells, M.; Dermody, D. L.; Yang, H. C.; Kim, T.; Crooks, R. M.; Ricco, A. J. *Langmuir* **1996**, *12*, 1989-1996.

53. Sun, L.; Kepley, L. J.; Crooks, R. M. *Langmuir* **1992**, *8*, 2101-2103.

54. Dermody, D. L.; Crooks, R. M.; Kim, T. *J. Am. Chem. Soc.* **1996**, *118*, 11912-11917.

55. Hayes, W. A.; Shannon, C. *Langmuir* **1996**, *12*, 3688-3694.

56. Bruening, M. L.; Zhou, Y.; Aguilar, G.; Agee, R.; Bergbreiter, D. E.; Crooks, R. M. *Langmuir* **1997**, *13*, 770-778.

57. Tsao, M.-W.; Hoffmann, C. L.; Rabolt, J. F.; Johnson, H. E.; Castner, D. G.; Erdelen, C.; Ringsdorf, H. *Langmuir* **1997**, *13*, 4317-4322.

58. Colthup, N. B., Daly, L. H., Wiberley, S. E. *Introduction to Infrared and Raman Spectroscopy*. Academic Press: Boston, MA, 1990.

59. Major, J. S.; Blanchard, G. J. *Chem. Mater.* **2002**, *14*, 2574-2581.

60. Porter, M. D.; Bright, T. B.; Allara, D. L.; Chidsey, C. E. D. *J. Am. Chem. Soc.* **1987**, *109*, 3559 - 3568.

61. Vallant, T.; Brunner, H.; Mayer, U.; Hoffmann, H. *Langmuir* **1998**, *14*, 5826-5833.

62. Kepley, L. J.; Crooks, R. M.; Ricco, A. J. *Anal. Chem.* **1992**, *64*, 3191-3193.

63. Kang, J. F.; Ulman, A.; Jordan, R.; Kurth, D. G. *Langmuir* **1999**, *15*, 5555-5559.

64. Clegg, R. S.; Hutchison, J. E. *J. Am. Chem. Soc.* **1999**, *121*, 5319 - 5327.

65. Tam-Chang, S.-W.; Biebuyck, H. A.; Whitesides, G. M.; Jeon, N.; Nuzzo, R. G. *Langmuir* **1995**, *11*, 4371 - 4382.

66. Yan, L.; Marzolin, C.; Terfort, A.; Whitesides, G. M. *Langmuir* **1997**, *13*, 6704-6712.

67. Yan, L.; Huck, W. T. S.; Zhao, X.-M.; Whitesides, G. M. *Langmuir* **1999**, *15*, 1208-1214.

68. Aspnes, D. E.; Theeten, J. B.; Hottier, F. *Phys. Rev. B* **1979**, *20*, 3292-3302.

69. Murray, C. B.; Kagan, C. R.; Bawendi, M. G. *Annu. Rev. Mater. Sci.* **2000**, *30*, 545-610.

70. Shenhar, R.; Rotello, V. M. *Acc. Chem. Res.* **2003**, *36*, 549-561.

71. Roucoux, A.; Schulz, J.; Patin, H. *Chem. Rev.* **2002**, *102*, 3757-3778.

72. Bonnemann, H.; Richards, R. M. *Eur. J. Inorg. Chem.* **2001**, 2455-2480.

73. Zhao, M.; Crooks, R. M. *Angew. Chem. Int. Ed.* **1999**, *38*, 364-366.

74. Li, Y.; El-Sayed, M. A. *J. Phys. Chem. B* **2001**, *105*, 8938-8943.

75. Teranishi, T.; Miyake, M. *Chem. Mater.* **1999**, *11*, 3414-3416.

76. Kiely, C. J.; Fink, J.; Brust, M.; Bethell, D.; Schiffrin, D. J. *Nature* **1998**, *396*, 444-446.

77. Klein, D. L.; Roth, R.; Lim, A. K. L.; Alivisatos, A. P.; McEuen, P. L. *Nature* **1997**, *389*, 699-701.

78. Taton, T. A.; Mucic, R. C.; Mirkin, C. A.; Letsinger, R. L. *J. Am. Chem. Soc.* **2000**, *122*, 6305-6306.

79. Templeton, A. C.; Zamborini, F. P.; Wuelfing, W. P.; Murray, R. W. *Langmuir* **2000**, *16*, 6682-6688.

80. Schmid, G.; Baumle, M.; Beyer, N. *Angew. Chem., Int. Ed.* **2000**, *39*, 181-183.

81. Malynych, S.; Luzinov, I.; Chumanov, G. *J. Phys. Chem. B* **2002**, *106*, 1280-1285.

82. Freeman, R. G.; Grabar, K. C.; Allison, K. J.; Bright, R. M.; Davis, J. A.; Guthrie, A. P.; Hommer, M. B.; Jackson, M. A.; Smith, P. C.; Walter, D. G.; Natan, M. J. *Science* **1995**, *267*, 1629-1632.

83. Musick, M. D.; Pena, D. J.; Botsko, S. L.; McEvoy, T. M.; Richardson, J. N.; Natan, M. J. *Langmuir* **1999**, *15*, 844-850.

84. Brust, M.; Bethell, D.; Kiely, C. J.; Schiffrin, D. J. *Langmuir* **1998**, *14*, 5425-5429.

85. Hu, K.; Brust, M.; Bard, A. J. *Chem. Mater.* **1998**, *10*, 1160-1165.

86. Cassagneau, T.; Mallouk, T. E.; Fendler, J. H. *J. Am. Chem. Soc.* **1998**, *120*, 7848-7859.

87. Sarathy, K. V.; Thomas, P. J.; Kulkarni, G. U.; Rao, C. N. R. *J. Phys. Chem. B* **1999**, *103*, 399-401.

88. Musick, M. D.; Keating, C. D.; Lyon, L. A.; Botsko, S. L.; Pena, D. J.; Holliway, W. D.; McEvoy, T. M.; Richardson, J. N.; Natan, M. J. ***Chem. Mater.*** **2000**, ***12***, 2869-2881.

89. Harnisch, J. A.; Pris, A. D.; Porter, M. D. ***J. Am. Chem. Soc.*** **2001**, ***123***, 5829-5830.

90. Chan, E. W. L.; Yu, L. P. ***Langmuir*** **2002**, ***18***, 311-313.

91. Lemon, B. I.; Crooks, R. M. ***J. Am. Chem. Soc.*** **2000**, ***122***, 12886-12887.

92. Zhao, M.; Sun, L.; Crooks, R. M. ***J. Am. Chem. Soc.*** **1998**, ***120***, 4877-4878.

93. Zhao, M.; Crooks, R. M. ***Adv. Mater.*** **1999**, ***11***, 217-220.

94. Esumi, K.; Suzuki, A.; Yamahira, A.; Torigoe, K. ***Langmuir*** **2000**, ***16***, 2604-2608.

95. Esumi, K.; Hosoya, T.; Suzuki, A.; Torigoe, K. ***J. Colloid Interface Sci.*** **2000**, ***226***, 346-352.

96. Balogh, L.; Tomalia, D. A. ***J. Am. Chem. Soc.*** **1998**, ***120***, 7355-7356.

97. Recently, we found that Au nanoparticles with improved monodispersity can be prepared in either Gn-Qp or Gn-NH_2 dendrimers by using magic number ratios of $[HAuCl_4]$:[dendrimer].

98. Manna, A.; Imae, T.; Aoi, K.; Okada, M.; Yogo, T. *Chem. Mater.* **2001**, *13*, 1674-1681.

99. Chechik, V.; Zhao, M.; Crooks, R. M. *J. Am. Chem. Soc.* **1999**, *121*, 4910-4911.

100. Ye, H.; Scott, R. W. J.; Crooks, R. M. *Langmuir* **2004**, *20*, 2915-2920.

101. Quinn, M.; Mills, G. *J. Phys. Chem.* **1994**, *98*, 9840-9844.

102. Zheng, J.; Petty, J. T.; Dickson, R. M. *J. Am. Chem. Soc.* **2003**, *125*, 7780-7781.

103. Garcia, M. E.; Baker, L. A.; Crooks, R. M. *Anal. Chem.* **1999**, *71*, 256-258.

104. Sun, L.; Crooks, R. M. *Langmuir* **2002**, *18*, 8231-8236.

105. He, J. A.; Valluzzi, R.; Yang, K.; Dolukhanyan, T.; Sung, C. M.; Kumar, J.; Tripathy, S. K.; Samuelson, L.; Balogh, L.; Tomalia, D. A. *Chem. Mater.* **1999**, *11*, 3268-3274.

106. Gröhn, F.; Gu, X. H.; Grull, H.; Meredith, J. C.; Nisato, G.; Bauer, B. J.; Karim, A.; Amis, E. J. *Macromolecules* **2002**, *35*, 4852-4854.

107. Choi, H. C.; Kim, W.; Wang, D. W.; Dai, H. J.. *J. Phys. Chem. B* **2002**, *106*, 12361-12365.

108. Won, J.; Ihn, K. J.; Kang, Y. S. *Langmuir* **2002**, *18*, 8246-8249.

109. Sayed-sweet, Y.; Hedstrand, D. M.; Spinder, R.; Tomalia, D. A. *J. Mater. Chem.* **1997**, *7*, 1199-1205.

110. Niu, Y.; Yeung, L. K.; Crooks, R. M. *J. Am. Chem. Soc.* **2001**, *123*, 6840-6846.

111. Wells, M.; Crooks, R. M. *J. Am. Chem. Soc.* **1996**, *118*, 3988-3989.

112. Tokuhisa, H.; Crooks, R. M. *Langmuir* **1997**, *13*, 5608-5612.

113. Fink, J.; Kiely, C. J.; Bethell, D.; Schiffrin, D. J. *Chem. Mater.* **1998**, *10*, 922-926.

114. Zheng, J.; Stevenson, M. S.; Hikida, R. S.; Van Patten, P. G. *J. Phys. Chem. B* **2002**, *106*, 1252-1255.

115. PdCl42- and PtCl42- complex ions can exist in multiple displaced-ligand forms in water and within the dendrimer. Because we don't always know which form is present, we choose to denote all possible complex ions as Pd2+ or Pt2+ to minimize confusion.

116. Scott, R. W. J.; Ye, H.; Henriquez, R. R.; Crooks, R. M. *Chem. Mater.* **2003**, *15*, 3873-3878.

117. Lin-Vien, D.; Colthup, N. B.; Fateley, W. G.; Grasseli, J. G. *Infrared and Raman Characteristic Frequencies of Organic Molecules*. Academic Press: San Diego, CA, 1991.

118. Tokuhisa, H.; Zhao, M.; Baker, L. A.; Phan, V. T.; Dermody, D. L.; Garcia, M. E.; Peez, R. F.; Crooks, R. M.; Mayer, T. M. *J. Am. Chem. Soc.* **1998**, *120*, 4492-4501.

119. Zhao, M.; Crooks, R. M. **1999**, unpublished data, Department of Chemistry, Texas A&M University.

120. Esumi, K.; Kameo, A.; Suzuki, A.; Torigoe, K. *Colloids Surf., A* **2001**, *189*, 155-161.

121. Suzdalev, I. P.; Suzdalev, P. I. *Russ. Chem. Rev.* **2001**, *70*, 177-210.

122. Rao, C. N. R.; Kulkarni, G. U.; Thomas, P. J.; Edwards, P. P. *Chem.-Eur. J.* **2002**, *8*, 29-35.

123. Alvarez, M. M.; Khoury, J. T.; Schaaff, T. G.; Shafigullin, M. N.; Vezmar, I.; Whetten, R. L. *J. Phys. Chem. B* **1997**, *101*, 3706-3712.

124. Valden, M.; Lai, X.; Goodman, D. W. *Science* **1998**, *281*, 1647-1650.

125. Wang, J.; Xu, D. K.; Kawde, A. N.; Polsky, R. *Anal. Chem.* **2001**, *73*, 5576-5581.

126. Li, Y.; Boone, E.; El-Sayed, M. A. *Langmuir* **2002**, *18*, 4921-4925.

127. Kastner, M. A. *Rev. Mod. Phys.* **1992**, *64*, 849-858.

128. Kötz, R.; Carlen, M. *Electrochim. Acta* **2000**, *45*, 2483-2498.

129. Jensen, T. R.; Malinsky, M. D.; Haynes, C. L.; Van Duyne, R. P. *J. Phys. Chem. B* **2000**, *104*, 10549-10556.

130. Veisz, B.; Kiraly, Z. *Langmuir* **2003**, *19*, 4817-4824.

131. Walker, C. H.; St John, J. V.; Wisian-Neilson, P. *J. Am. Chem. Soc.* **2001**, *123*, 3846-3847.

132. Wang, Y. A.; Li, J. J.; Chen, H. Y.; Peng, X. G. *J. Am. Chem. Soc.* **2002**, *124*, 2293-2298.

133. Boyen, H.-G.; Kastle, G.; Weigl, F.; Koslowski, B.; Dietrich, C.; Ziemann, P.; Spatz, J. P.; Riethmuller, S.; Hartmann, C.; Moller, M.; Schmid, G.; Garnier, M. G.; Oelhafen, P.. *Science* **2002**, *297*, 1533-1536.

134. Spatz, J. P.; Mössmer, S.; Hartmann, C.; Möller, M.; Herzog, T.; Krieger, M.; Boyen, H.-G.; Ziemann, P.; Kabius, B. *Langmuir* **2000**, *16*, 407-415.

135. Chen, S.; Pei, R. J. *J. Am. Chem. Soc.* **2001**, *123*, 10607-10615.

136. Lee, D.; Donkers, R. L.; DeSimone, J. M.; Murray, R. W. *J. Am. Chem. Soc.* **2003**, *125*, 1182-1183.

137. Ooe, M.; Murata, M.; Mizugaki, T.; Ebitani, K.; Kaneda, K. *Nano Lett.* **2002**, *2*, 999-1002.

138. Esumi, K.; Nakamura, R.; Suzuki, A.; Torigoe, K. *Langmuir* **2000**, *16*, 7842-7846.

139. West, R.; Wang, Y.; Goodson III, T. *J. Phys. Chem. B* **2003**, *107*, 3419-3426.

140. Esumi, K.; Hosoya, T.; Suzuki, A.; Torigoe, K. *Langmuir* **2000**, *16*, 2978-2980.

141. Esumi, K.; Torigoe, K. *Progr. Colloid. Polym. Sci.* **2001**, *117*, 80-87.

142. Esumi, K.; Hosoya, T.; Suzuki, A.; Torigoe, K. *J. Colloid Interface Sci.* **2000**, *229*, 303-306.

143. Gröhn, F.; Kim, G.; Bauer, A. J.; Amis, E. J. *Macromolecules* **2001**, *34*, 2179-2185.

144. Roldughin, V. I. *Russ. Chem. Rev.* **2000**, *69*, 821-843.

145. Leff, D. V.; Ohara, P. C.; Heath, J. R.; Gelbart, W. M. *J. Phys. Chem.* **1995**, *99*, 7036-7041.

146. Niu, Y.; Crooks, R. M. *Chem. Mater.* **2003**, *15*, 3463-3467.

147. Mottet, C.; Tréglia, G.; Legrand, B. *Surf. Sci.* **1997**, *383*, L719-L727.

148. Schmid, G. *Chem. Rev.* **1992**, *92*, 1709-1727.

149. Hicks, J. F.; Zamborini, F. P.; Osisek, A. J.; Murray, R. W. *J. Am. Chem. Soc.* **2001**, *123*, 7048-7053.

150. Ingram, R. S.; Hostetler, M. J.; Murray, R. W.; Schaaff, T. G.; Khoury, J. T.; Whetten, R. L.; Bigioni, T. P.; Guthrie, D. K.; First, P. N. *J. Am. Chem. Soc.* **1997**, *119*, 9279-9280.

151. Whetten, R. L.; Shafigullin, M. N.; Khoury, J. T.; Schaaff, T. G.; Vezmar, I.; Alvarez, M. M.; Wilkinson, A. *Acc. Chem. Res.* **1999**, *32*, 397-406.

152. Wilson, O. M.; Scott, R. W. J.; Garcia-Martinez, J. C.; Crooks, R. M. *Chem. Mater.* **2004**, *16*, 4202-4204.

153. Zhao, M.; Crooks, R. M. *Chem. Mater.* **1999**, *11*, 3379-3385.

154. Scott, R. W. J.; Wilson, O. M.; Crooks, R. M. *Chem. Mater.* **2004**, *16*, 5682-5688.

155. Yeung, L. K.; Crooks, R. M. *Nano Lett.* **2001**, *1*, 14-17.

156. Rahim, E. H.; Kamounah, F. S.; Frederiksen, J.; Christensen, J. B. *Nano Lett.* **2001**, *1*, 499 -501.

157. Garcia-Martinez, J. C.; Lezutekong, R.; Crooks, R. M. *J. Am. Chem. Soc.* **2005**, *127*, 5097-5103.

158. Narayanan, R.; El-Sayed, M. A. *J. Phys. Chem. B* **2004**, *108*, 8572-8580.

159. Lang, H.; May, R. A.; Iversen, B. L.; Chandler, B. D. *J. Am. Chem. Soc.* **2003**, *125*, 14832-14836.

160. Chung, Y. M.; Rhee, H. K. *Catal. Lett.* **2003**, *85*, 159-164.

161. Ye, H.; Crooks, R. M. *J. Am. Chem. Soc.* **2005**, *127*, 4930-4934.

162. Templeton, A. C.; Hostetler, M. J.; Kraft, C. T.; Murray, R. W. *J. Am. Chem. Soc.* **1998**, *120*, 1906-1911.

163. Templeton, A. C.; Cliffel, D. E.; Murray, R. W. *J. Am. Chem. Soc.* **1999**, *121*, 7081-7089.

164. Wang, G.; Zhang, J.; Murray, R. W. *Anal. Chem.* **2002**, *74*, 4320-4327.

165. Chen, S.; Murray, R. W. *Langmuir* **1999**, *15*, 682-689.

166. Cliffel, D. E.; Zamborini, F. P.; Gross, S. M.; Murray, R. W. *Langmuir* **2000**, *16*, 9699-9702.

167. Kohlmann, O.; Steinmetz, W. E.; Mao, X.-A.; Wuelfing, W. P.; Templeton, A. C.; Murray, R. W.; Johnson, C. S., Jr. *J. Phys. Chem. B* **2001**, *105*, 8801-8809.

168. Song, Y.; Heien, M. L.; Jimenez, V.; Wightman, R. M.; Murray, R. W. *Anal. Chem.* **2004**, *76*, 4911-4919.

169. Brennan, J. L.; Branham, M. R.; Hicks, J. F.; Osisek, A. J.; Donkers, R. L.; Georganopoulou, D. G.; Murray, R. C. *Anal. Chem.* **2004**, *76*, 5611 -5619.

170. Yang, Y.; Pradhan, S.; Chen, S. *J. Am. Chem. Soc.* **2004**, *126*, 76-77.

171. Chaki, N. K.; Kakade, B.; Vijayamohanan, K. P. *Electrochem. Commun.* **2004**, *6*, 661-665.

172. Mulvaney, P. *Langmuir* **1996**, *12*, 788-800.

173. Templeton, A. C.; Pietron, J. J.; Murray, R. W.; Mulvaney, P. *J. Phys. Chem. B* **2000**, *104*, 564-570.

174. Pittelkow, M.; Moth-Poulsen, K.; Boas, U.; Christensen, J. B. *Langmuir* **2003**, *19*, 7682-7684.

175. Murayama, H.; Narushima, T.; Negishi, Y.; Tsukuda, T. *J. Phys. Chem. B* **2004**, *108*, 3496-3503.

176. Gu, Y.; Xie, H.; Gao, J.; Liu, D.; Williams, C. T.; Murphy, C. J.; Ploehn, H. J. *Langmuir* **2005**, *21*, 3122-3131.

177. Cheng, Q.; Brajter-Toth, A. *Anal. Chem.* **1995**, *67*, 2767-2775.

178. Efremenko, I.; Sheintuch, M. *Surf. Sci.* **1998**, *414*, 148-158.

VITA

Name: Yong-Gu Kim

Address: 98-32 Nokbun Eunpyung Samsung Billate 202

Seoul, South Korea

E-mail address: ykim@mail.chem.tamu.edu

Objective: Research and development of materials based on a broad background in materials chemistry, surface chemistry, electrochemistry and analytical chemistry.

Education:

Ph.D. / Analytical Chemistry

Texas A&M University, College Station, TX

Dissertation title: "Synthesis and electrochemical characterization of highly monodisperse dendrimer-templated monolayer protected clusters."

Advisor : Prof. Richard M. Crooks

M.S. / Applied Chemistry

Ajou University, Suwon, South Korea (1999)

Thesis title: "Size selective molecular recognition from monolayers of beta-cyclodextrin and p-tert-butylcalix[4]arene."

Advisor: Prof. Jae-Ho Kim

B.S. / Applied Chemistry

Ajou University, Suwon, South Korea (1997)